ST. ANTHONY FALLS HYDRAULIC LABORATORY
UNIVERSITY OF MINNESOTA

Project Report No. 45

A SLOTTED-WALL TEST SECTION FOR A WATER TUNNEL

Submitted by
LORENZ G. STRAUB
Director

Prepared by
REUBEN M. OLSON

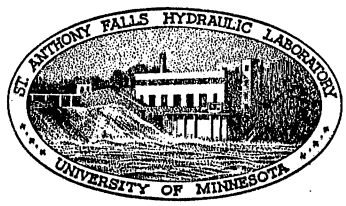

February, 1955

Prepared for
DAVID TAYLOR MODEL BASIN
Department of the Navy
Washington, D.C.

Office of Naval Research Contract Nonr-710(08)

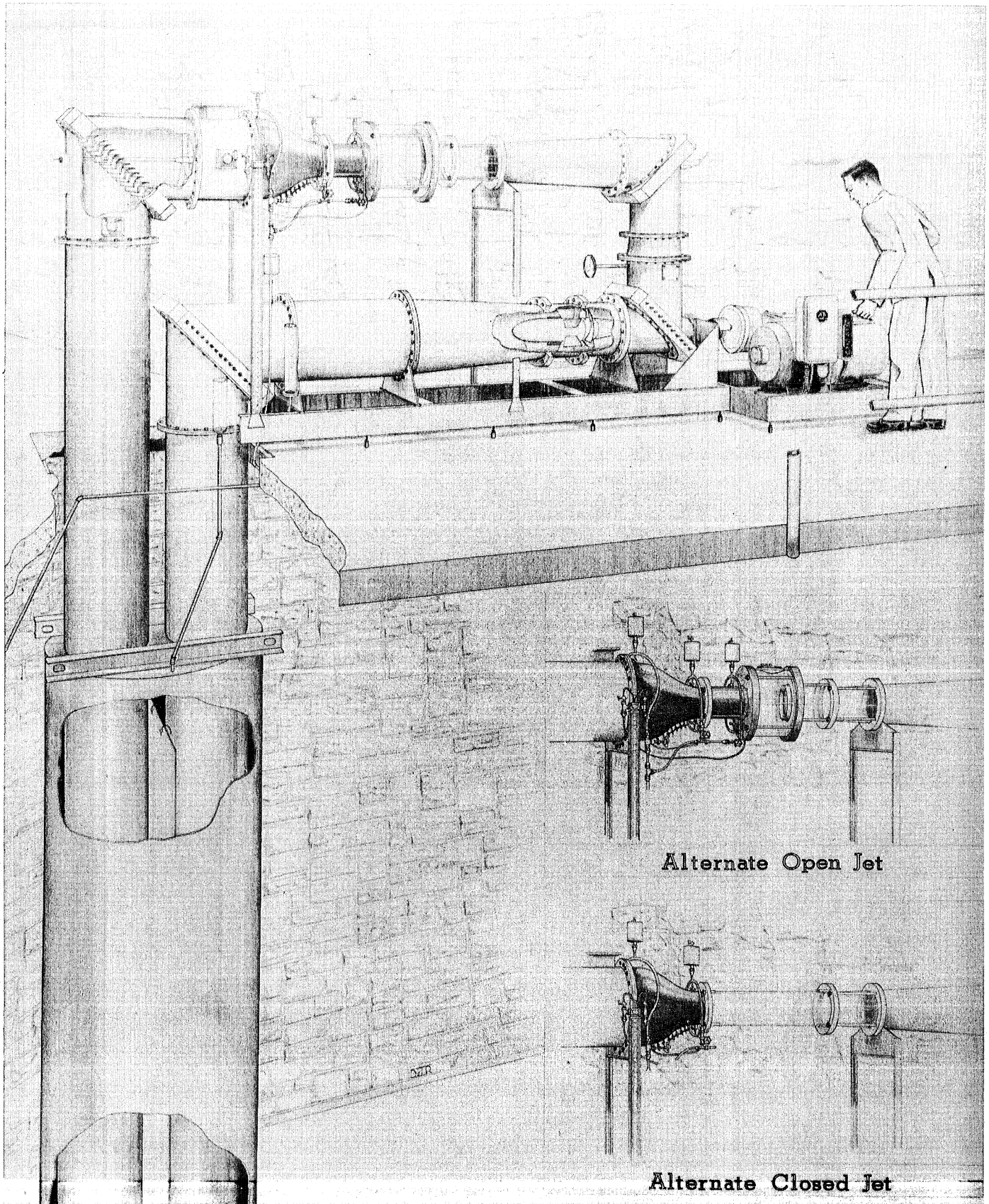

Alternate Open Jet

Alternate Closed Jet

ST. ANTHONY FALLS
MODEL WATER TUNNEL

P R E F A C E

Contract Nonr-710(08) between the University of Minnesota St. Anthony Falls Hydraulic Laboratory and the Department of the Navy, David Taylor Model Basin provided for model tests of a slotted-wall test section which could be incorporated into the design of a proposed 36-in. water tunnel. This report gives the analytical and experimental results of these tests.

The program has been under the general direction of Dr. Lorenz G. Straub, Director of the Laboratory, and was supervised by R. M. Olson. Most of the experimental work was done by R. S. Dart, A. G. Mercer, D. W. Rolschau, R. P. Wengler, and N. R. Ziemke. The report was reviewed by J. F. Ripken and was prepared for publication by L. A. Johnson and Mrs. Marie Berg.

A B S T R A C T

Studies have been under way at the St. Anthony Falls Hydraulic Laboratory to investigate the possibility of including an alternate slotted-wall test section in a proposed 36-in. water tunnel for the David Taylor Model Basin. The experimental program was conducted in a 6-in. model water tunnel previously used in design studies for the 36-in. tunnel, and in a 10-in. free-jet tunnel at the Laboratory.

Tests were run on slotted-wall test sections 2.18 and 2.38 test-section diameters in length and indicated that perhaps 2.5 diameters would be the maximum length possible without altering the diffuser following the test section. Axial pressures uniform within 1/2 per cent of the free stream dynamic pressure were obtained for a length of 2 test-section diameters. Velocity profiles in the test section compared favorably with those for a closed-jet test section, being flat within 1 per cent over 90 per cent of the diameter in the upstream portion, and over 80 per cent in the downstream portion of the useful test-section length. It was estimated that the energy losses for this slotted-wall test section would be about 10 per cent greater than for the shorter open-jet test section which will be included in the 36-in. tunnel. The cavitation characteristics were not as good as those for an open-jet tunnel, incipient cavitation occurring at an index of about 0.6 to 0.9; below 0.5 the reservoir chamber became cloudy. A minimum of optical distortion is expected to result if slots are omitted from the slotted-wall cylinder near the axis on the viewing side and if flat windows are used for the reservoir barrel. Tests on a hemispherical-nosed body indicated that the 2.4-diameter length was shorter than would be desired for testing bodies whose diameters are one-third the test-section diameter and more than two or three body-diameters in length.

C O N T E N T S

LIST OF ILLUSTRATIONS

LIST OF SYMBOLS

a - Axial distance from intersection of test-section axis and camera axis.

A_o - Cross-sectional area of upstream end of test section in square feet.

A_5 - Cross-sectional area at measuring station at downstream end of main diffuser in square feet.

d - Diameter of hemispherical head form.

D_o - Diameter of upstream end of test section.

g - Acceleration of gravity in feet per second squared.

h - Piezometric head on test body, guide bar, or contraction surface.

h_o - Piezometric head at upstream end of test section in feet of water.

h_5 - Piezometric head at downstream end of main diffuser in feet of water.

h_8 - Piezometric head upstream of pump impeller in feet of water.

h_9 - Piezometric head downstream of pump impeller in feet of water.

h_f - Head loss due to friction in feet of water.

h_x - Piezometric head along axis of test section in feet of water.

K_o - Form loss coefficient in terms of test-section velocity head.

M_a - Axial magnification; ratio of axial apparent to actual length.

M_r - Radial magnification; ratio of radial apparent to actual length.

n_{a-m} - Index of refraction of a material with respect to air.

n_{a-p} - Index of refraction of Plexiglas with respect to air.

n_{a-w} - Index of refraction of water with respect to air.

r - Radial distance from axis to a point in the flow stream.

r_c - Distance from camera or observer to the test-section axis.

r_r - Normal distance from test-section axis to outer flat face of the reservoir viewing window.

R - Radius of tunnel component.

s - Distance aft of nose of hemispherical head form measured along the surface.

t_m - Thickness of a material in an optical path.

V - Mean temporal axial velocity at a point in feet per second.

$\overline{V}$ or V_{av} - Mean bulk-flow velocity at any cross section in feet per second.

V_{max} - Maximum mean temporal axial velocity in a cross section in feet per second.

V_o - Mean bulk-flow velocity at the upstream end of the test section (bare test section without dynamometer shaft housings) in feet per second.

x - Distance downstream of beginning of test section.

α - Kinetic-energy correction factor, the ratio of true kinetic energy to that based on the mean bulk-flow velocity at a cross section.

α_o - Kinetic-energy correction factor at upstream end of test section.

α_5 - Kinetic-energy correction factor at downstream end of main diffuser.

σ_o - Cavitation index at the upstream end of the test-section axis based on vapor pressure, h_v:

$$\sigma_o = \frac{h_o - h_v}{V_o^2/2g}$$

A SLOTTED-WALL TEST SECTION FOR A WATER TUNNEL

I. INTRODUCTION

Two common types of test sections for water tunnels are the open-jet and the closed-jet. The open-jet test section has a relatively short useful working length because of the rapid decrease in velocity with increasing length together with a flow instability in the region of the jet pickup. This instability increases as the jet velocity and length increase. For these reasons the open jet is used for relatively low speeds and for tests of short bodies such as propellers. However, relatively large propellers are tested. The closed jet produces a stable flow, and high speeds may be used. One disadvantage, however, is due to the interference effects of the wall and large corrections must often be made.

A third type of test section is the free-jet [1],* where the tunnel interference corrections are either very small or negligible. Pressure gradients are essentially nonexistent, and very low pressures may be attained for cavitation testing. The chief disadvantages are from the turbulent mixing of the jet with the surrounding air which results in a dissolution of the jet and entrainment of air into the test stream. This limits the length of the working section and makes recirculation difficult.

A fourth type of test section, the slotted-wall, has been suggested [2, 3, and 4]. This can be considered as an open jet wherein the jet is guided by longitudinal bars or rods, or as a closed jet wherein the walls are slotted and a cage placed around the slotted section to provide a reservoir of constant pressure. It was believed that the wall interference would be minimized in this configuration.

Studies have been under way at the St. Anthony Falls Hydraulic Laboratory to determine reasonably optimum geometries of a slotted-wall test section for a water tunnel; and to determine the flow quality in the test section, the energy losses in this type of tunnel, its cavitation characteristics, and the ability of the slotted-wall test section to produce an essentially infinite-field flow stream about a test body. Consideration has also

---

*Numbers in brackets refer to the Bibliography on p. 27.

been given to problems incident to making the test-section region transparent for viewing and photographic purposes. The test program has been directed toward a study of a slotted-wall test section which can be incorporated into the design of the proposed 36-in. water tunnel at the David Taylor Model Basin, rather than a study of slotted-wall test sections in general [5]. This report summarizes the work done on the project.

II. TEST FACILITIES AND ASSEMBLIES

A. Test Facilities

The slotted-wall test-section assemblies were tested in the 6-in. model water tunnel at the Laboratory. This tunnel is shown in the frontispiece and in Fig. 1. It is a 1/6-scale model of the proposed 36-in. water tunnel for the David Taylor Model Basin and was used in previous design studies of this tunnel [6, 7]. Test-section velocities ranged up to 50 fps and were varied by means of a mechanical transmission with an electrically driven speed-changing system. Test-section pressures were varied by means of a pressure-control system with an open surface which could be moved from 2 ft above to 18 ft below the test-section centerline. The pressure-control system was connected to the upstream end, center, or downstream end of the contraction which precedes the test section, or to the test-section reservoir itself. Thus, the pressure in the test section was, in the first two instances, determined not only by the setting of the pressure-control system, but also by the pressure drop through the contraction, and was, therefore, not entirely independent of velocity.

The 10-in. free-jet water tunnel at the Laboratory [1] was used to measure the pressure distribution along a hemispherical head form for a comparison with similar measurements in both a diverging closed-jet as well as a slotted-wall test section.

B. Test Assemblies

The slotted-wall test sections were preceded by a conventional axisymmetric contraction for producing a uniform test stream and were followed by a diffuser for recovering the kinetic energy of the test stream. It is customary to provide a flow easement called a diffuser transition between the test section and diffuser proper, and in the present tests this was a parabolic

curve, ranging in length from 0.24 to 0.83 test-section diameters (D_o). The basic geometry is shown in Fig. 2. Since the slotted wall was to be incorporated into the proposed 36-in. water tunnel at the David Taylor Model Basin, the length of the model test section and diffuser transition was limited to a maximum of 20.625 inches in order to match fixed end points of the removable open- and closed-jet test sections in the 36-in. tunnel. Permissible test-section lengths, diffuser entrance diameters, and diffuser transition lengths are interrelated and are not independent of one another. In general, as the diffuser entrance is enlarged, the test-section length can become greater. The longest length physically possible would be desirable, although this is a function of the required or limiting diffuser entrance diameter.

The slotted walls were surrounded by a closed reservoir, cylindrical except for the pick-up cones at the downstream end, which was 2.5 or, in two tests, 1.75 D_o in diameter.

The test-stream guide bars were made from Plexiglas cylinders with 1/2-in. walls and were mounted between aluminum flanges at each end of the test section. Five types of slotted walls were used, designated as Types A, B, C, D, and E. These are shown in Figs. 3 to 10. The total slot width was 18 per cent of the test-section circumference, except for Type B which had 36 per cent at the downstream end, and Type E which had two of the sixteen slots omitted on one side to reduce the open portion to about 16 per cent. The slots were cut horizontally and vertically, as shown in Figs. 3 to 10, rather than radially in order to minimize optical distortion. The tapered end of Type C was shortened in 1/2-in. steps in order to vary the gap between the end of the guide bars and the diffuser entrance. By lengthening the reservoir 1.25 in., and by providing a 1/4-in. spacer at the upstream flange, gaps of 0, 0.5, 0.75, 1.0, 2.0, and 2.25 in. were obtained. The cantilevered guide bars for Types C and E were supported by the method indicated in Figs. 2, 8, 9, 10, and 12.

In order to direct the flow back from the reservoir into the main stream, various forms of contractions were placed in the downstream end of the reservoir. These are referred to as pick-up cones, and are shown in Fig. 11. Types I and II were of spun aluminum, Types III, IV, and V were accurately machined from aluminum plate, and Type VI was machined from a Plexiglas ring. The first five types were similar to the types which have been used in

TABLE I

SLOTTED-WALL TEST ASSEMBLIES

Assembly	Slotted Wall	Pick-up Cone Type	Pick-up Cone Space, in.†	Guide-Bar Gap, in.††	Diffuser Entrance Diameter, in.	Reservoir Diameter, in.	Diffuser Transition Length, in.
1	A	none	--	--	6.000	15	3.00
2	A	I	--	--	6.000	15	3.00
3	B	none	--	--	6.000	15	3.00
4	B	I	--	--	6.000	15	3.00
5	C	IV	--	0	6.000	15	3.00
6	C	III	--	0	6.120	15	4.96
7	C	III	--	0.5	6.120	15	4.96
8	C	III	--	1.0	6.120	15	4.96
9	C	III	--	2.25	6.120	15	2.45
10	C	II	--	2.25	6.120	15	2.45
11	C	none	--	2.25	6.120	15	2.45
12	C*	III	--	2.25	6.120	15	2.45
13	C	V	--	2.25	6.180	15	2.45
14	C	V	--	0.75	6.180	15	3.94
15	C	V	--	0.75	6.180	10.5	3.94
16	C	VI	0	0.75	6.180	15	3.94
17	C	VI	0	2.0	6.180	15	1.44
18	C	VI	0.25	2.0	6.180	15	1.44
19	C	VI	0.25	1.0	6.180	15	3.94
20	C	VI	0.50	1.0	6.180	15	3.94
21	D	**	--	--	6.180	15	3.94
22	E	VI	0.50	1.0	6.180	15	1.44
23	E	VI	0.50	1.0	6.180	10.5	1.44

* Guide bars converged to $0.98\ D_o$ at downstream end

** Fig. 9 shows downstream contour of slots

† Applies only to Type VI pick-up cone

†† Applies only to types C and E slotted walls

wind- and water-tunnel studies for slotted-wall water-tunnel designs [2, 3, and 4], while Type VI was similar to a conventional pick-up cone for an open-jet test section and to types used in investigations for slotted-wall wind-tunnel designs [8, 9].

A view of Assembly 2 (Type A-I) mounted in the water tunnel is shown in Fig. 12, the mechanical assembly of Type C in Fig. 13, and Assembly 22 (Type E-VI) mounted in the tunnel in Fig. 14. Figure 1 shows Assembly 7 (Type C-III) in the 6-in. water tunnel.

A total of 23 different assemblies were tested. These are listed in Table I and are shown schematically in Figs. 15 to 36.

III. AXIAL PRESSURE MEASUREMENTS

One desirable characteristic of a test section for a water tunnel is that there be a uniform axial pressure. Some effort was directed toward obtaining a geometry which would result in a constant axial pressure over as great a portion of the test section as possible. This was considered especially important because of the relatively short test-section length to which the design was restricted.

The axial pressure was measured by means of an extension to the upstream dynamometer shaft housing for most of the tests, and an extension to a diffuser dynamometer shaft housing for later tests. This extension was 0.542 inch in diameter with a 0.312-in. bore. Piezometer holes were drilled every 0.5 in. through both walls of this tube, and a piston with rubber O-rings was moved along the inside of the tube to transmit the pressure at each set of holes to an external manometer through a smaller tube inside the entire length of the dynamometer shaft housing. Pressure measurements were made with respect to a constant reference at about 30 and 48 fps, and the results are shown dimensionlessly in Figs. 15 to 36.

A. Type A Assemblies

The axial pressure gradient was about $0.02\ V_o^2/2g$ per diameter throughout most of the test-section length, and the actual pressure head decreased to $-0.8\ V_o^2/2g$ in the diffuser entrance (Fig. 15). The effect of the Type I pick-up cone was to decrease the pressure drop in the upstream portion of the test section, but the low pressure in the diffuser entrance remained about the same (Fig. 16).

B. Type B Assemblies

The effect of increasing the slot area at the downstream end of the test section was measured after Type A was modified to Type B. The pressure gradient was even greater than for Type A (Fig. 17), and the effect of adding the Type I pick-up cone was the same as for the Type A, namely, to reduce the pressure gradient in the upstream portion of the test section (Fig. 18). The low pressure head in the diffuser entrance region remained about the same, about $-0.10\ V_o^2/2g$ below that at the beginning of the test section.

Both Types A and B slotted walls had poor cavitation characteristics (p. 15), and the Type C slotted wall was intended as an improved form in this respect as well as for the axial pressures.

C. Type C Assemblies

The first Type C slotted wall was tested with a Type IV pick-up cone. The axial pressure gradient was of the same order as for Types A and B (Fig. 19). The low pressures in the diffuser entrance region indicated that the entrance area was too small, and it was increased 4 per cent (2 per cent increase in diameter). Tests with the larger diffuser entrance and with the larger-radius Type III pick-up cone indicated a smaller pressure drop (Fig. 20), but it was still considered too large.

The effects of increasing the gap between the end of the guide bars and the point of minimum area in the pick-up region from zero to 2.25 in. are shown in Figs. 21 to 23. The larger gaps produced a greater pressure rise near the end of the slots. The position of the maximum pressure hump moved downstream with an increase in the gap, thus indicating that the stagnation pressure field of the downstream end of the reservoir was being reflected upstream. The Type II pick-up cone, similar to Type III except for a rounded outer portion, produced results essentially identical to those for Type III with a 2.25-in. gap (Figs. 24 and 23). The low pressures in the diffuser entrance region with no pick-up cone (Fig. 25) probably resulted from a contraction of the flow in this entrance. The same pressure hump from the pressure field of the downstream end of the reservoir is indicated.

Converging the guide bars to give a 4 per cent reduction in area along their length had no measurable effect (compare Fig. 26 with Fig. 24). Increasing the diffuser entrance area to 6 per cent over that of the test-section entrance (3 per cent increase in diameter) reduced the pressure drop slightly, but also increased the pressure rise slightly (Figs. 27 and 23) for a 2.25-in. gap. Reducing the gap from 2.25 to 0.75 in. with the enlarged diffuser entrance diameter (1.03 D_o) resulted in a uniform axial pressure head for 2.1 diameters (uniform within $0.005\ V_o^2/2g$) as shown in Fig. 28. The axial pressures shown in Fig. 28 for Assembly 14 were more uniform than those for an open-jet and a cylindrical closed-jet test section, and were nearly as uniform as those for a diverging closed-jet test section for a length of 2.0 test-section diameters [9].

The tests thus far discussed (Assemblies 1 to 14) were made with a reservoir diameter 2.5 times the test-section diameter. Reducing this to 1.75 had a negligible effect on the measured axial pressure (Figs. 29 and 28).

Pick-up cone Type VI was like the conventional type used in an open-jet tunnel. It was hoped that the slight pressure rise near the downstream end of the test section could be reduced.

Results of tests on five variations of Type C-VI slotted walls (Assemblies 16 to 20) are shown in Figs. 30 to 34. The most uniform axial pressure was obtained with Assembly 20, with a 1-in. gap between the end of the guide bars and the diffuser entrance and with a 0.5-in. space between the pick-up cone and the downstream reservoir flange (Fig. 34). This axial pressure distribution compared favorably with that for Assembly 14 (Fig. 28) and also with that for a diverging closed-jet test section.

D. Type D Assembly

Type D slotted wall was made primarily to test its cavitation characteristics, and no axial pressure measurements were made.

E. Type E Assemblies

Type E slotted wall was similar to Type C except that it was longer and had two slots omitted for optical reasons (p. 18). It was made as long as was allowable for the $1.03\ D_o$ diffuser entrance diameter. Except for this length, Assemblies 20 (Type C-VI) and 22 (Type E-VI) were similar. The measured axial pressure for Type E-VI (Fig. 35) was similar to that for Type C-VI (Fig. 34), although the slight gradient near the upstream end indicates that the diffuser entrance could probably have been increased to about $1.04\ D_o$, thus permitting a longer test section--about an additional 1/12 diameter for a total length of about 2.5 test-section diameters.

Reducing the reservoir diameter to $1.75\ D_o$ for Type E-VI produced a rather marked change in the axial pressures (compare Figs. 35 and 36) compared to the negligible change for Type C-V (Figs. 28 and 29). The smaller reservoir diameter seemed to be all right with the Type V pick-up cone, but not with the Type VI pick-up cone, as far as the axial pressures were concerned.

IV. VELOCITY PROFILES

Velocity profiles were measured at two locations in the test section (at x/D_o = 0.5 and 1.0), at the downstream end of the main diffuser, and downstream of the elbow following the main diffuser. Those in the test section were measured to determine the flow quality there. Those at the end of the diffuser were measured in order to compute the energy losses through the combined test section and diffuser, and to determine the magnitude of the core velocity in connection with the possibility of vane cavitation in the elbow immediately downstream. One set of velocity measurements was made downstream of the first elbow following the main diffuser in order to determine extent of the influence of the slotted-wall test section on the flow and losses in the tunnel loop.

A. Test Sections

Horizontal velocity traverses were made at x/D_o = 0.5 and at 1.0 for Assemblies 3 (Type B-I) and 21 (Type D). The results are shown in Figs. 37 and 38. In Assembly 3 the contraction dynamometer shaft housing was installed, and extended about 1 diameter into the test section. Thus, the profile in Fig. 37(a) indicates the boundary layer of the shaft housing as well as that of the test-section guide bars, and the central portion of the profile of Fig. 37(b) shows the wake of this shaft housing.

Similar measurements in a cylindrical closed-jet test section compare favorably with those for the slotted wall [Figs. 37(a) and 38(b)]. The velocities were uniform within 1 per cent of the maximum over more than 90 per cent of the diameter at x/D_o = 0.5, and over more than 80 per cent of the diameter at x/D_o = 1.5, neglecting the effect of the dynamometer shaft housing.

B. Downstream End of Main Diffuser

Velocity profiles at the end of the main diffuser were measured on both a horizontal and a vertical axis for 12 of the test-section assemblies. The results are tabulated in Table II which lists the ratio of the maximum to the mean measured velocity and the kinetic-energy correction factor α. This factor is applied to the kinetic energy based on the mean velocity to obtain the actual kinetic energy.

TABLE II

VELOCITY PROFILE DATA MEASURED AT DOWNSTREAM END OF MAIN DIFFUSER

Assembly	Section	Reservoir Diameter, D_o	Test Section Length, D_o	V_o, fps	$\frac{V_{max}}{V_{av}}$	α
1	A	2.5	2.18	39.9	1.76	1.61
2	A-I	2.5	2.18	45.3	1.71	1.62
3	B	2.5	2.18	45.3	1.79	1.63
4	B-I	2.5	2.18	45.3	1.81	1.66
5	C-IV	2.5	2.18	45.3	1.68	1.51
6	C-III	2.5	2.18	45.3	1.70	1.62
7	C-III	2.5	2.18	45.3	1.71	1.61
8	C-III	2.5	2.18	45.3	1.74	1.63
9	C-III	2.5	2.38	45.3	1.86	1.74
15	C-V	1.75	2.18	45.3	1.71	1.62
16	C-VI	2.5	2.18	45.3	1.76	1.68
20	C-VI	2.5	2.18	45.3	1.75	1.69

The ratio of the maximum to the mean velocity ranged from 1.68 for Assembly 5 (Type C-IV with no guide-bar gap) to 1.86 for Assembly 9 (Type C-III with a 2.25-in. guide-bar gap). The profiles for these assemblies are shown in Fig. 39 together with similar profiles for the open- and closed-jet test sections [6]. The range of maximum core velocities for the slotted walls was below the maximum for the open jet and slightly below that for the closed jet. From the tests of Assemblies 6 to 9, increasing the guide-bar gap increased the core velocity. Since the velocity profiles for the slotted walls were quite similar to those measured for the open- and closed-jet tunnels which were shown to be free of cavitation [6], there should be no likelihood of guide-vane cavitation in the first elbow for the assemblies tested.

The range of α, the kinetic-energy correction factor, was from 1.51 to 1.74, with most values between 1.6 and 1.7. Comparable values for the closed jet averaged 1.52; and for the open jet, 1.65 [6].

C. Downstream of Elbow I Following the Main Diffuser

One set of measurements was made to determine the velocity profile between the main diffuser and the pump. The measured value of α, the kinetic-energy correction factor, was 1.38 as compared with an estimated value of 1.14 with the open- or closed-jet tunnels [6]. This difference appears to be large considering the similarity of velocity profiles at the downstream end of the main diffuser. It may be due to a shorter second diffuser between the main-diffuser elbow and the pump elbow, and thus should not be considered an effect of a slotted-wall test section.

V. ENERGY LOSSES

The energy losses through the test sections and the main diffuser were computed from measurements of the change in pressure and in velocity profiles and from computed friction losses. This procedure combined the losses through the test sections and the diffuser, and does not indicate the performance of the slotted-wall test sections alone. It was believed that an overall measurement was more accurate and descriptive. Nevertheless, the performance of the test sections and diffuser does not reflect the entire effect of the slotted-wall test sections, since the losses in other tunnel components may have changed as well. In addition to these measurements, the pressure rise through the pump was measured for various test-section assemblies in order to make comparisons between various assemblies and with similar measurements with the open- and closed-jet tunnels.

A. Energy Loss through Test Sections and Main Diffuser

Loss coefficients have been computed for the 36-in. water tunnel proposed for construction at the David Taylor Model Basin at Carderock, Maryland.

The form-loss coefficient, in terms of the test-section velocity head is

$$K_o = \alpha_o - \alpha_5 \left(\frac{A_o}{A_5}\right)^2 - \frac{h_5 - h_o}{V_o^2/2g} - \frac{h_f}{V_o^2/2g}$$

where α is the kinetic-energy correction factor, A the area, h the piezometric head, and V the velocity. Subscripts o and 5 refer to the beginning

of the test section and the end of the diffuser, respectively; h_f is the friction head loss from points o to 5. The first three terms were measured in the model tunnel, and the fourth was computed for the model for the various test-section assemblies. The resulting form-loss coefficient for the model was increased by 0.002 for the prototype to correct for slight differences in the model and prototype diffuser angles. The friction-loss coefficient for the prototype was computed on the same basis as for the model and the two loss coefficients were added to obtain the total loss coefficient.

The measured pressure rise through the various slotted-wall test sections and the main diffuser is shown in Fig. 40. A summary of the energy-loss coefficients is shown in Table III for a test-section velocity of 48 fps. Values for the loss coefficient for the test-section-and diffuser combinations range from about 0.17 to 0.22 as compared with 0.16 for the open-jet and 0.09 for the closed-jet tunnels [6]. Those assemblies with the most uniform axial pressures (Assemblies 14, 15, 20, and 22) had loss coefficients between 0.18 and 0.20, the lower values for the 2.18 D_o test-section lengths, and the higher value for the 2.38 D_o test-section lengths. Computations indicate a loss coefficient for the slotted-wall test section alone of about 0.06 per diameter, and this figure may be used to make crude estimates on the effect of increasing test-section length. A first-order approximation of the loss coefficient for the open-jet test section also indicates 0.06 per diameter of length [6]. Thus, the two types are comparable as far as energy losses are concerned.

Assemblies 15 and 23 were with a reservoir diameter of 1.75 D_o, and may be compared with Assemblies 14 and 22, respectively, which were identical except for a 2.5 D_o reservoir diameter. The energy-loss coefficient for the smaller reservoir diameters were essentially the same as for the larger reservoir diameters, 0.186 and 0.18 for Assemblies 15 and 14, and 0.20 and 0.20 for Assemblies 23 and 22.

The total loss coefficient for the 36-in. open-jet water tunnel was estimated to be about 0.30 [6]. The slotted-wall test section of about 2.2 or 2.4 diameters' length will increase this by about 0.03, or 10 per cent (the estimated loss coefficients for the slotted-wall plus diffuser and the open jet plus diffuser are about 0.185 and 0.156, respectively). Thus, the power required for a given velocity will be about 10 per cent greater than

TABLE III

SUMMARY OF ENERGY LOSSES FOR SLOTTED-WALL TEST SECTIONS AND DIFFUSERS AT 48 FPS

Assembly	Model Test-Section and Diffuser Pressure Coefficient*	Prototype Form-Loss Coefficient, Computed*	Prototype Friction-Loss Coefficient, Estimated*	Prototype Test Section and Diffuser Overall Loss Coefficient, Estimated*	Pressure Rise through Model Pump $\frac{\Delta h}{V_6^2/2g}$
1	0.670	0.165	0.036	0.201	0.31
2	0.663	0.171	0.036	0.207	0.30
3	0.650	0.184	0.035	0.219	0.35
4	0.650	0.182	0.035	0.217	0.34
5	0.672	0.170	0.036	0.206	0.32
6	0.670	0.164	0.036	0.200	0.30
7	0.699	0.137	0.035	0.172	0.30
8	0.691	0.144	0.034	0.178	0.31
9	0.661	0.167	0.034	0.201	0.33
10	0.661	---	---	0.21	0.33
14	0.688	---	---	0.18**	0.30
15	0.684	0.152	0.034	0.186**	0.31
16	0.689	0.143	0.034	0.177	0.31
17	0.656	---	---	0.21**	0.34
18	0.650	---	---	0.22**	0.34
19	0.683	---	---	0.185**	0.31
20	0.684	0.147	0.034	0.181	0.31
22	0.668	---	---	0.20**	0.30
23	0.668	---	---	0.20**	0.30

*In terms of test-section velocity head

**Estimated from pressure coefficient

for the open-jet tunnel; or, with the same power available, the maximum velocity is expected to be reduced about 3 per cent.

B. Pressure Rise through Pump

The measured pressure rise through the model pump for the various test-section assemblies is shown in Fig. 41 and is tabulated for a test-section velocity of 48 fps in Table III. The velocity profiles just upstream and downstream from the pump rotor were not measured; thus, these pressure rises through the pump do not indicate the total energy added by the pump. However, they may be used for comparisons.

In general, the assemblies with the lowest estimated energy losses have the lowest pressure rise through the pump. Some variations were probably due to slight errors in measurement and in assumptions made in computing the losses, or to the possibility that losses in other tunnel components varied out of proportion to the losses through the test section and diffuser. Also, the kinetic-energy levels on both sides of the pump may not have been the same for the different test-section assemblies.

The measured pressure-rise coefficient for the model open-jet tunnel with one dynamometer shaft housing (average of Figs. 28 and 29 in [6]) was 0.30. This compares with values between 0.30 and 0.35 for the slotted-wall values in Table III. The 10 per cent increase estimated from measurements in the test-section regions is within these values.

VI. RESERVOIR FLOW

The flow pattern at the downstream end of the reservoir was studied in order to determine the optimum design for a pick-up cone. This flow was quite complex, and visual studies were made with bubbles injected into the reservoir. In addition, high-speed movies were taken of dye injected into the flow stream at the contraction wall 10 in. upstream of the test section and through a tube inserted into the reservoir near the downstream end.

The pick-up cones were originally designed in the form of a nozzle or contraction (Types I and II, Fig. 9) so that the fluid re-entering the main stream from the reservoir would be guided all the way from the outer part of the reservoir into the boundaries of the test stream. Visual observations, and more especially the high-speed movies, showed that the fluid flowed in an

outward radial direction over the greater part of the downstream end of the reservoir. The flow lines are shown schematically in Fig. 42. Frames from some high-speed movies taken of the area indicated in Fig. 43 are reproduced in Figs. 44 and 45. These show successive positions of dye clouds at about 1/80-sec intervals in Fig. 44 and 1/60-sec intervals in Fig. 45.

Movies of this type were used to determine the optimum lip diameter for pick-up cone Type VI, a type similar to a conventional pick-up cone for an open-jet test section. For the length of test section studied a lip diameter of about $1.25\ D_o$ [shown as 7.516 inches in Fig. 11(f)] appeared to be optimum. This would increase as the test-section length increased, and if the test section were long enough, a nozzle type of pick-up cone (Types I and II, Fig. 9) might be necessary.

Measurements indicated that a space between the open-jet type of pick-up cone and the downstream reservoir flange resulted in a more uniform axial pressure (Figs. 16 to 20). Studies made with air bubbles, yarns cemented to the surfaces, and with dye, indicated that there was no predominating flow direction through this space, either radially inward or outward.

VII. CAVITATION CHARACTERISTICS

The cavitation characteristics of 14 of the 23 assemblies were studied. In some instances, where initial measurements of axial pressures showed undesirable gradients, no further tests were made of that particular assembly. Some assemblies were very similar to other assemblies for which cavitation tests were run.

Incipient cavitation was determined visually and audibly. In some instances a Marsh Soundscope, manufactured by the Jas. P. Marsh Corporation of Skokie, Illinois, was used to amplify the sound. The cavitation index was based on vapor pressure and was referred to the upstream axis of the test section:

$$\sigma_o = \frac{h_o - h_v}{V_o^2/2g}$$

where h_o is the absolute pressure head at the upstream axis of the test section, h_v is the absolute vapor pressure head, and V_o is the test-section velocity.

Incipient cavitation for Types A and B slotted walls (Assemblies 1 to 4) occurred at the inside portion of the downstream end of the slots, as shown in Fig. 46, as a result of localized separation. The minimum cavitation index for these test sections (the value of σ_o when cavitation was incipient some place in the test-section region of the tunnel) ranged from 0.8 to 1.3, usually above 0.9.

Type D (Assembly 21) was essentially the same as Type A except that the downstream end of the slots had a 1.75-in.-radius rounded entrance to the diffuser (Fig. 9). Incipient cavitation occurred in separation zones localized near the outer edge of the rounded entrances at the ends of the slots at an index of about 0.7. Fig. 47 shows this assembly at cavitation indices of 0.7 down to 0.4. Cavitation at σ_o = 0.7 and 0.6 was too intermittent to photograph with the 1/5000-sec exposure used, although the form of the incipient cavitation is shown in Fig. 47(d) as the two semicircular separation zones at the right center of the picture. Cavitation occurred inside the slotted wall in the upstream portion at an index of 0.55 [Fig. 47(c)]; at this value, and more especially at 0.5 and 0.4, the reservoir became quite cloudy. All the white spots and flashes in Figs. 47(c), (d) and (e) which do not appear in (a) and (b) are the result of cavitation.

Incipient cavitation for the Type C-III and C-IV slotted walls (Assemblies 5, 7, 8 and 9) appeared as vortex cavities in the wakes of the Plexiglas guide bars at indices of 0.6 to 0.9. For the Type C-VI (Assemblies 16 to 20) incipient cavitation was the same, but occurred at a higher cavitation index, from 0.75 to 1.0. The vortex cavities appeared to be located adjacent to or just downstream of the guide-bar slots. Photographs of cavitation in one Type C-III slotted wall (Assembly 9) are shown in Fig. 48. Again, the cavities were too intermittent to photograph with a 1/5000-sec exposure. As before, the severity of cavitation increased as the cavitation index was lowered. Cavitation appeared upstream within the test section at an index of about 0.5, and at 0.4 the reservoir became quite cloudy.

For the Type C slotted wall, most favorable from axial pressure and energy points of view, incipient cavitation occurred at an index of 0.6 to 0.9. If the flow in the pick-up region were improved to eliminate incipient cavitation there, tests indicated that it would occur within the test section further upstream at an index of about 0.5. Below that, the reservoir became very cloudy. This value of 0.5 is of the same order as the minimum cavitation

index for an open-jet tunnel, but is considerably above the value of 0.03 for the model diverging closed-jet tunnel at 50 fps [9].

One series of tests at 45 fps was run with a 2-in. hemispherical head form mounted in the Type E-VI slotted wall (Assembly 22) as shown in Fig. 14. Cavitation noise was audible at a cavitation index of 0.9 but was not detected visually until it was lowered to 0.80. At that point intermittent cavitation streaks were observed just outside the slotted-wall cylinder adjacent to the slots at about $x/D_o = 0.6$. Incipient cavitation on the hemispherical head form occurred at an index of 0.67, and at that point the reservoir was cloudy.

VIII. OPTICAL DISTORTION

When an object in the test section of a slotted-wall tunnel is viewed from outside the reservoir, light rays pass out through the water in the test stream, the transparent guide bars, the reservoir water, a transparent portion of the reservoir barrel, and out into the air to the observer. These rays change direction when passing through an interface due to the refractive properties of the various mediums, and this may lead to distortions depending on the geometry of the system. The model test section and various prototype assemblies were analyzed analytically and graphically, and some model calculations were verified from photographs of a rectangular grid placed in the test section. Plexiglas with a refractive index of 1.49 (air to Plexiglas) was used as a guide bar and reservoir shell material. The index of refraction for air to water was taken as 1.33.

Magnification was defined as the ratio of an apparent length to the actual length, the axial magnification designated as M_a and the radial magnification as M_r. The ratio of radial to axial magnification at a point is called the distortion.

A. The Model Test-Section Assemblies

The axial magnification at a distance $\underline{a}$ along the axis from a zero point, which is the intersection of the test-section axis and the camera axis (Fig. 49), is given by the expression

$$\frac{1}{M_a} = \sum \frac{t_m}{n_{a-m}\, r_c\, C_m} \qquad (1)$$

a summation of terms for each material between the object and camera. In this equation

t_m = radial thickness of the material,

n_{a-m} = refractive index of the material with respect to air,

r_c = distance from camera to the test-section axis, and

$$C_m = \left[1 + \left(\frac{\underline{a}}{n_{a-m}\, r_c}\right)^2 \left(n_{a-m}^2 - 1\right)\right]^{3/2} \qquad (2)$$

where $\underline{a}$ = axial distance from the zero point. C_m is unity at the zero point.

The axial magnification depends on the test-section geometry, the distance to the camera, and the axial distance from the zero point to the point of interest. For the model tunnel with a camera at $r_c = 3.67\ D_o$ (22 in.), a reservoir diameter $2.5\ D_o$, a shell thickness of 1 in., and a guide-bar thickness of 0.5 in., values of M_a for various axial distances from the zero point are given in Table IV.

TABLE IV

AXIAL MAGNIFICATIONS IN MODEL SLOTTED-WALL TEST SECTION

Observer $3.67\ D_o$ from Axis

$\underline{a}/D_o$	M_a
0	1.114
0.5	1.118
1.0	1.130
2.0	1.178

The axial magnification was about 1.4 per cent greater at $\frac{\underline{a}}{D_o} = 1.0$ than at the zero point, and was about 5.6 per cent greater at $\frac{\underline{a}}{D_o} = 2.0$ than at the zero point.

The radial magnification near the zero point for the model, where the guide bars and reservoir barrel were concentric cylinders, is given by

$$M_r = n_{a-w} \qquad (3)$$

and is therefore independent of the diameter or thickness of the Plexiglas cylinders, the refractive index for the Plexiglas, and of the distance between

the camera and tunnel axis. The variation of M_r with the radius cannot be determined by the approximate analysis used to derive Eq. (3). However, measurements on photographs of a rectangular grid in the test section and a graphical-construction method of determining M_r did not indicate any variation of M_r with radius. The accuracy of these methods was estimated to be of the order of 1/2 per cent of M_r, which was 1.33 for the model.

The computed distortion, M_r/M_a, for the model configuration near the zero point was 1.193. The distortion measured from a photograph of a 2:5 rectangular grid (Fig. 50) taken at r_c = 22 in. (assumed in the calculations for Table III) was 1.198.

The guide-bar cylinder had no effect on the radial magnification but had a small effect on the axial magnification. This effect is indicated in Fig. 50 where the vertical grid lines are displaced inwardly about 0.005 a toward the zero point when showing through the slots. Type E slotted wall (Fig. 10) was designed to eliminate this line shift.

The photograph of Fig. 51 was taken at an angle of about 10° from the planes of the horizontal slots, and indicates the necessity of having parallel rather than radial slots.

B. The Prototype Slotted Wall

The effect of changing the transparent portion of the reservoir shell from a cylinder as in the model to flat or lens-shaped windows in the prototype tunnel was also examined. The lens-shaped window was flat on the outside and curved to the diameter of the reservoir on the inside.

The axial magnification is the same as for the model, and is given by Eqs. (1) and (2).

The radial magnification near the zero point is essentially unaffected by the guide bars if they are cylindrical, and thus the same equations [Eqs. (1) and (2)] may be used for both M_r and M_a for the flat windows. The guide-bar material must be included in computing M_a, but may be omitted in computing M_r.

The radial magnification near the zero point for the lens-shaped window is given by

$$\frac{1}{M_r} = \frac{1}{n_{a-w}} + \frac{r_c - r_r}{r_c}\left(\frac{n_{a-p} - 1}{n_{a-w}}\right) \tag{4}$$

where

n_{a-p} = index of refraction of Plexiglas with respect to air,

r_r = normal distance from tunnel axis to outer face of window, and

n_{a-w} and r_c are as previously defined.

The radial magnification decreases with the camera distance and increases as the reservoir diameter increases. It is also dependent on the refractive index of the window material. The variation of M_r with radius cannot be determined from Eq. (4) since certain simplifying assumptions were made in its derivation which makes it valid only near the zero point. Graphical constructions indicated a variation (if any) of less than 1 per cent over the central two-thirds of the test section.

Table V gives a summary of calculations and graphical determinations of magnification factors and distortions (M_r/M_a) near the zero point. The prototype geometry was considered to be geometrically similar with one exception: the reservoir windows were considered to be $1/12\ D_o$ (3 in.) thick, whereas the model reservoir cylinder was $1/6\ D_o$ (0.5 in.) thick.

It appears that if parallel rather than radial slots are used, if two slots are omitted on the viewing side of the test section, and if flat viewing windows are used in the reservoir barrel, the distortion should be negligible near the center of the camera field; and a slotted-wall test section should introduce few, if any, difficulties not encountered in photographing objects in an open-jet test section.

TABLE V

SUMMARY OF OPTICAL MAGNIFICATION AND DISTORTION FACTORS FOR VARIOUS SLOTTED-WALL TEST SECTIONS NEAR THE ZERO POINT

Camera Distance	Reservoir ID	Model			Prototype					
					Flat Reservoir Windows			Lens-shaped Windows		
		M_a	M_r	Distortion	M_a	M_r	Distortion	M_a	M_r	Distortion
2 D_o	2.5 D_o	1.23	1.33	1.08	1.21	1.20	0.99	1.21	1.14	0.95
2 D_o	1.75 D_o	1.16	1.33	1.15	1.14	1.14	1.00	1.14	1.05	1.09
3.67 D_o	2.5 D_o	1.11	1.33	1.21	1.10	1.10	1.00	1.10	1.01	1.08

IX. TESTS WITH A HEMISPHERICAL HEAD FORM

A smooth 2-in. hemispherical head form about 8 in. long (Fig. 14) was mounted in two Type E slotted-wall test sections (Assemblies 22 and 23), in the diverging closed-jet test section of the 6-in. water tunnel, and in the 10-in. free-jet water tunnel at the Laboratory. Measurements were made to determine the effect of the wide guide bar of the Type E slotted wall on the pressure distribution around the body, the ability of the slotted wall to produce an essentially free-field flow around the body, the effect of this body on the tunnel wall pressure, and the guide-bar boundary pressures for various head-form positions.

A. Effect of Wide Guide Bar

For optical reasons (p. 18) Type E slotted wall had two adjacent slots omitted so that one guide bar was about three times the width of the others. In order to determine whether this would produce an unsymmetrical pressure distribution around the test section, measurements were made of the pressures on the 2-in. head form as it was rotated about its axis in the test section. A plot of typical results for the piezometer tap at $s/d = 2.0$ [Fig. 14(b)] is shown in Fig. 52. Peripheral pressures varied about 1 per cent of the free-stream dynamic pressure, the minimum values being adjacent to the

wide guide bar. Readings were taken and plotted at angles corresponding to slot and guide-bar centerline positions, except for the two points on either side of the 90° position, and indicate that the normal slot spacings were adequate.

B. Pressure Distribution along Hemispherical Head Form

The pressures along the surface of the 2-in. hemispherical head form were measured by means of the ten piezometer taps indicated in Fig. 14(b). Measurements were made in Assembly 22 slotted wall with a $2.5\ D_o$ reservoir diameter, in Assembly 23 with a $1.75\ D_o$ reservoir diameter, in the diverging closed-jet test section, and in the 10-in. free-jet water tunnel and were compared with measurements on a long hemispherical head cylinder reported by Rouse and McNown [10]. Measurements in the slotted wall were made with the body at two axial positions. Results are shown in Fig. 53 excluding data taken near the wide guide bar. No wall-interference corrections were made for any of the measurements.

C. Influence of Body on Tunnel-Wall and Guide-Bar Pressures

Pressures on the hemispherical head form in the slotted-wall test section and on the guide bars were measured with respect to manifolded piezometer taps located on the contraction wall $0.5\ D_o$ upstream of the test section. In converting the pressure data to the axial free-stream pressure, corrections were made for the pressure field of the body at these reference piezometer taps. The change in pressure at these taps was measured as the nose of the body was moved axially along the test section. The curve of Fig. 54 shows the effect of the body position on this reference pressure. All measurements of other boundary pressures were corrected by means of this curve to obtain results based on the free-stream pressure.

Pressures along one guide bar opposite the wide guide bar in Assembly 22 were measured without the test body and with the test body nose at three axial positions. The results are shown in Fig. 55. The guide-bar pressures for the empty test section were constant and equal to the upstream axial pressure within 1/2 per cent of the free-stream dynamic pressure and agreed well with the axial pressures shown in Fig. 35. With the test body in place, guide-bar pressures just upstream of the nose showed the characteristic increase, and just downstream, the characteristic decrease expected from potential theory. Actual values in a free stream at 3 body radii from the axis would be very difficult to calculate for the body shape used.

D. General Discussion of Results

The free-jet measurements coincided with the curve given by Rouse and McNown [10] for the upstream portion of the body, and may be considered as essentially representing the true infinite-field pressure distribution for the body. Apparently the low pressures in the tapered tail-section were reflected upstream as far as tap 6, and the gradual drop in pressure over the after portion of the body was a result of its short length. The body was considered to be about as long as practicable for the relatively short 2.38 D_o slotted-wall test-section length.

Best agreement with the free-jet results was obtained in Assembly 23, with the smaller reservoir diameter of 1.75 D_o. The lesser pressure decrease over the after portion of the body than for the tests in Assembly 22 is commensurate with the rise in axial pressure shown in Fig. 36. The lower slotted-wall curve of Fig. 53 was obtained with the body nose at $x = 1.0\ D_o$, and the body extended downstream beyond the pick-up cone. Thus, a choking effect would be expected with a lowering of the pressures in the downstream region of the body. This is not indicated by the guide-bar pressures in Fig. 55, however, since pressures opposite tap 7 on the body (0.75 D_o downstream of the body nose) were about the same for the body nose at $x/D_o = 0.5$ and $x/D_o = 1.0$.

All curves for the slotted-wall tests agreed well with the free-jet curve for the upstream portion of the body (Fig. 53), and the gradual divergence from the free-jet curve downstream might indicate that the slotted-wall test section was too short even for the relatively short test body.

The results from the closed-jet measurements (Fig. 53) were plotted directly in order that the relative magnitude of interference corrections for the closed-jet and slotted-wall test sections could be better compared.

The curve showing the influence of the body position on the wall pressure in the downstream end of the contraction (Fig. 54) indicates that the body nose should be at least 1 test-section diameter beyond the end of the contraction. In the model, the velocity was indicated by the pressure drop across the upper half of the contraction, and was believed to be unaffected by the nose position in the test section. If the pressure drop across the entire contraction were used to indicate the test-section velocity, considerable error would be introduced when a large test body is too close to

the contraction. The added head loss with an accompanying decrease in velocity as the body was moved towards the contraction did not fully compensate for the change in wall pressure. The data of Fig. 54 were obtained at constant velocity, and the pump speed was varied to maintain it constant.

X. GENERAL COMMENTS AND CONCLUSIONS

Model tests on a slotted-wall test section which could be included as an alternate test section for the proposed 36-in. water tunnel at the David Taylor Model Basin indicated that a maximum length of about $2.5\ D_o$ could be used if the axial pressure were to be essentially constant. Pressure measurements on a hemispherical head form $1/3\ D_o$ in diameter and about $1.4\ D_o$ long indicated that the $2.38\ D_o$ test section was too short to produce an essentially free-stream pressure distribution over the entire body. Thus, this length of test section would be limited to bodies $1/3\ D_o$ in diameter less than 4 (perhaps 3 or even less) body diameters in length. If the longest body which could be tested in a closed-jet tunnel were to be tested in the same diameter slotted-wall tunnel, the body diameter could be doubled, and thus the length of the slotted wall would have to be at least doubled to accommodate the larger body. For the 36-in. DTMB tunnel, this would indicate a length of 4.5 to $5\ D_o$. In order to do this without moving the vertical legs of the tunnel, the diffuser angle would have to be increased to about 10°, and an alternate test-section-and-diffuser combination would be required. The power requirements would increase of the order of 50 to 75 per cent.

The major characteristic of the slotted walls tested which would limit their usefulness was that of cavitation. From an acoustic point of view, inception occurred at a cavitation index of about 0.6 to 0.9 for the best designs, although this did not occur in the test-area portion of the test section. At an index of about 0.5, however, cavitation occurred within the test-section proper, and below that value the reservoir became cloudy.

A brief summary of conclusions is as follows:

1. An axial pressure in the bare test section constant within 1/2 per cent of the free-stream dynamic pressure for a length of 2 test-section diameters (D_o) was obtained with a slotted wall. This was essentially as uniform as that for a diverging closed-jet test section.

2. Measured pressures along a guide bar and along the axis indicated essentially no radial pressure gradients in the guide-bar portion of the test section.

3. The energy losses in the 36-in. water tunnel with an air-bubble resorber for an alternate slotted-wall test section 2.4 D_o in length are estimated to be about 10 per cent greater than those for the shorter open-jet test section which was 1.6 D_o in length.

4. Measured velocities in the slotted-wall test section were uniform within 1 per cent of the maximum over more than 90 per cent of the diameter at $x/D_o = 0.5$ and over more than 80 per cent of the diameter at $x/D_o = 1.5$. This compares favorably with the closed-jet test section.

5. Incipient cavitation in the bare slotted-wall test section occurred in the wakes of the guide bars at a cavitation index of 0.6 to 0.9, and in the test section proper at about 0.5; below that value the reservoir became cloudy. Comparable values for an open-jet and diverging closed-jet test section are about 0.4 and 0.03, respectively. With a 1/3 D_o test body in place (Fig. 14) noise from incipient cavitation occurred at an index of about 0.9, but cavitation along the slots in the central part of the test section occurred at an index of 0.8 compared with 0.5 for the bare test section.

6. Optical discontinuities may be eliminated by omitting two adjacent slots on one side of the slotted-wall cylinder. In the model, this resulted in a peripheral pressure variation of 1 per cent of the free-stream dynamic pressure on a 1/3 D_o test body.

7. Flat viewing windows are necessary in the reservoir to eliminate distortion near the center of the viewing field. The distortion will increase upstream and downstream from this point.

8. The geometry of the diffuser transition, which governs the cavitation limits for a closed-jet test section, was not critical for the slotted-wall assemblies tested.

9. Tests with a reservoir diameter 1.75 and 2.5 D_o indicated that, for a test section 2.4 D_o long, a reservoir 1.75 or 2 D_o should be large enough.

10. Pressures measured along a hemispherical head form 1/3 D_o in diameter and 1.4 D_o (about 4 body diameters) long in a slotted-wall test section agreed with those measured in a free-jet tunnel over the upstream portion of the body, but were below over the after portion, indicating that the body was too long for the test section.

BIBLIOGRAPHY

[1] Christopherson, C. D. Description of a Ten-Inch Free-Jet Water Tunnel. University of Minnesota, St. Anthony Falls Hydraulic Laboratory Project Report No. 35, January, 1953.

[2] Vandrey, F. and Wieghardt, K. Wind Tunnel with Slotted Walls - Preliminary Tests. Admiralty Research Laboratory Report ARL/R1/G/HY/4/1, January, 1950.

[3] Vandrey, F. and Wieghardt, K. Experiments on a Slotted-Wall Section in a Wind Tunnel. Admiralty Research Laboratory Report ARL/R4/G/HY/4/1, March, 1952.

[4] Vandrey, F. Further Experiments with a Slotted-Wall Test Section. Admiralty Research Laboratory Report ARL/R5/G/HY/4/1, March, 1953.

[5] Project Proposal for Tests on a Slotted-Wall Test Section for a Water Tunnel. Submitted to the David Taylor Model Basin, Bureau of Ships, Department of the Navy, November, 1952, by the St. Anthony Falls Hydraulic Laboratory, University of Minnesota [Contract Nonr-710(06)].

[6] Olson, R. M. Model Studies of a Water Tunnel with an Air-Bubble Resorber. University of Minnesota, St. Anthony Falls Hydraulic Laboratory Project Report No. 29, February, 1952.

[7] Olson, R. M. Model Studies of a Water Tunnel with an Air-Bubble Resorber: A Diverging Closed-Jet Test Section for a Water Tunnel. University of Minnesota, St. Anthony Falls Hydraulic Laboratory Project Report No. 32, June, 1952.

[8] Wright, R. H. and Ward, V. G. NACA Transonic Wind-Tunnel Test Sections. National Advisory Committee for Aeronautics Research Memo No. L8J06, October, 1948.

[9] Bates, G. P. Preliminary Investigation of 3-Inch Slotted Transonic Wind-Tunnel Test Sections. National Advisory Committee for Aeronautics Research Memo No. L9D18, September, 1949.

[10] Rouse, Hunter and McNown, John S. Cavitation and Pressure Distribution, Head Forms at Zero Angle of Yaw. State University of Iowa. (Sponsored by Office of Naval Research, Contract N8onr-500) 1948. 70 pages.

APPENDIX
(Figures 1 to 55)

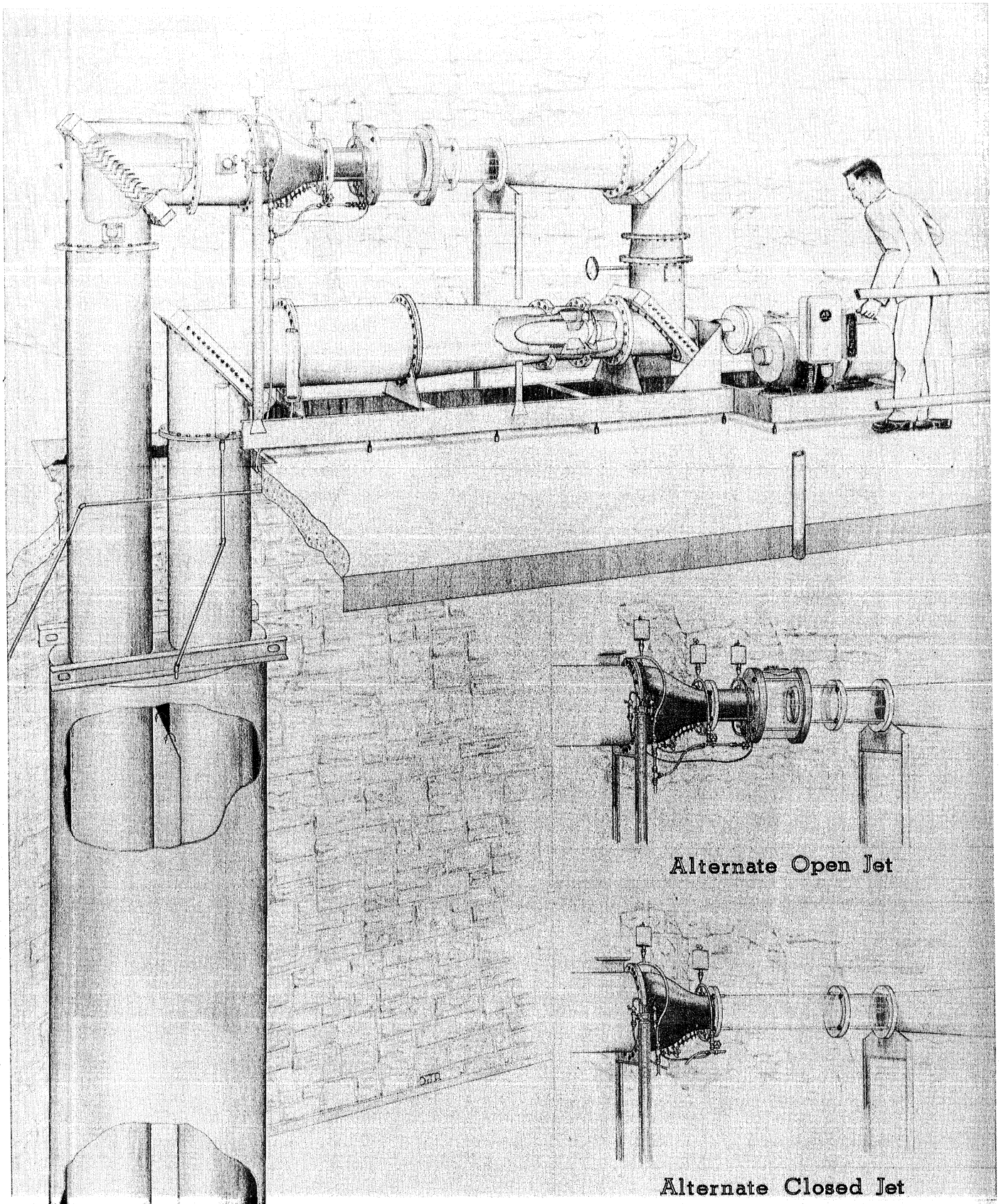

Alternate Open Jet

Alternate Closed Jet

ST. ANTHONY FALLS
MODEL WATER TUNNEL

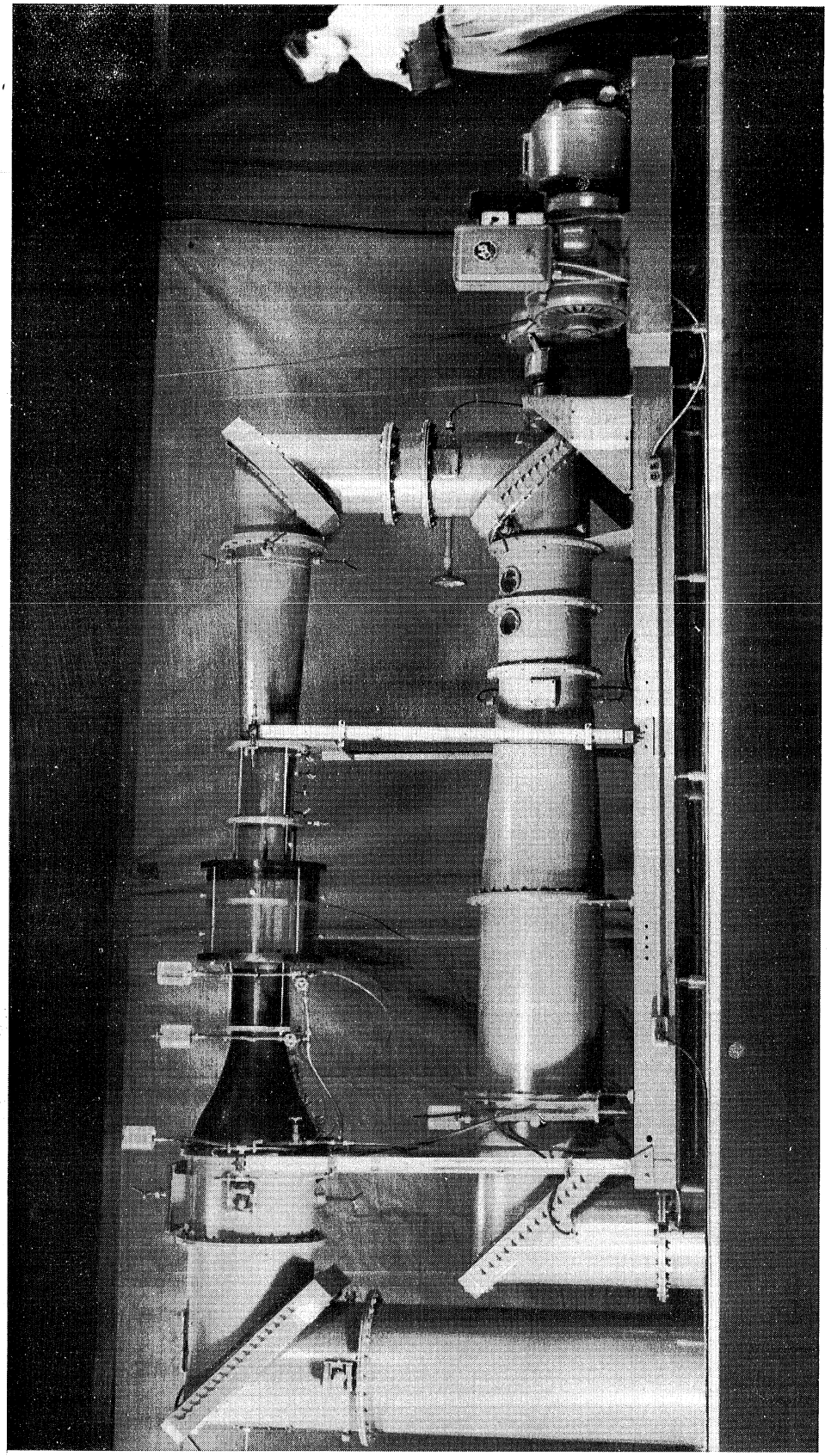

Fig. 1 - Six-Inch Model Water Tunnel

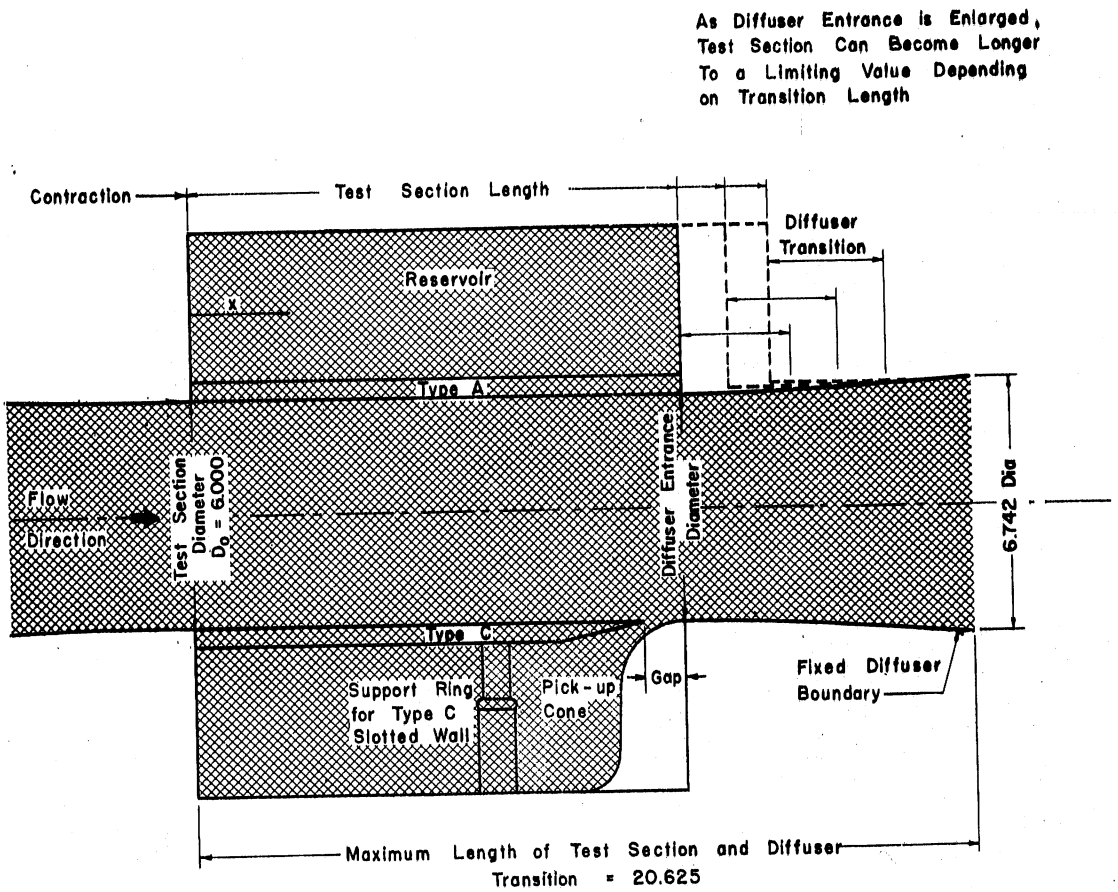

Fig. 2 - Test-Section Geometry

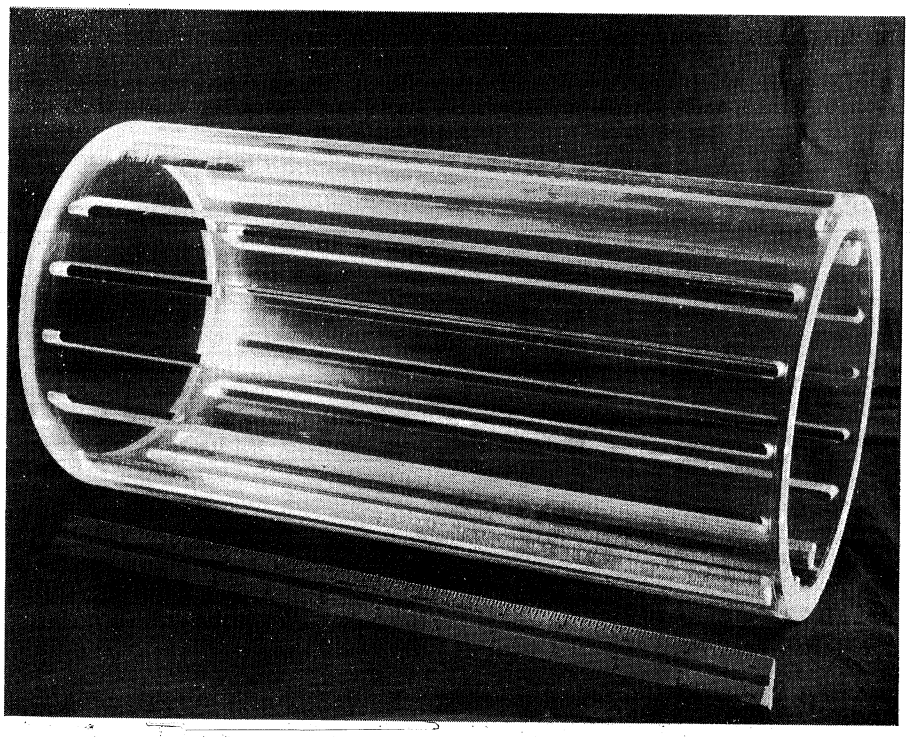

Fig. 3 - Type A Slotted-Wall Cylinder

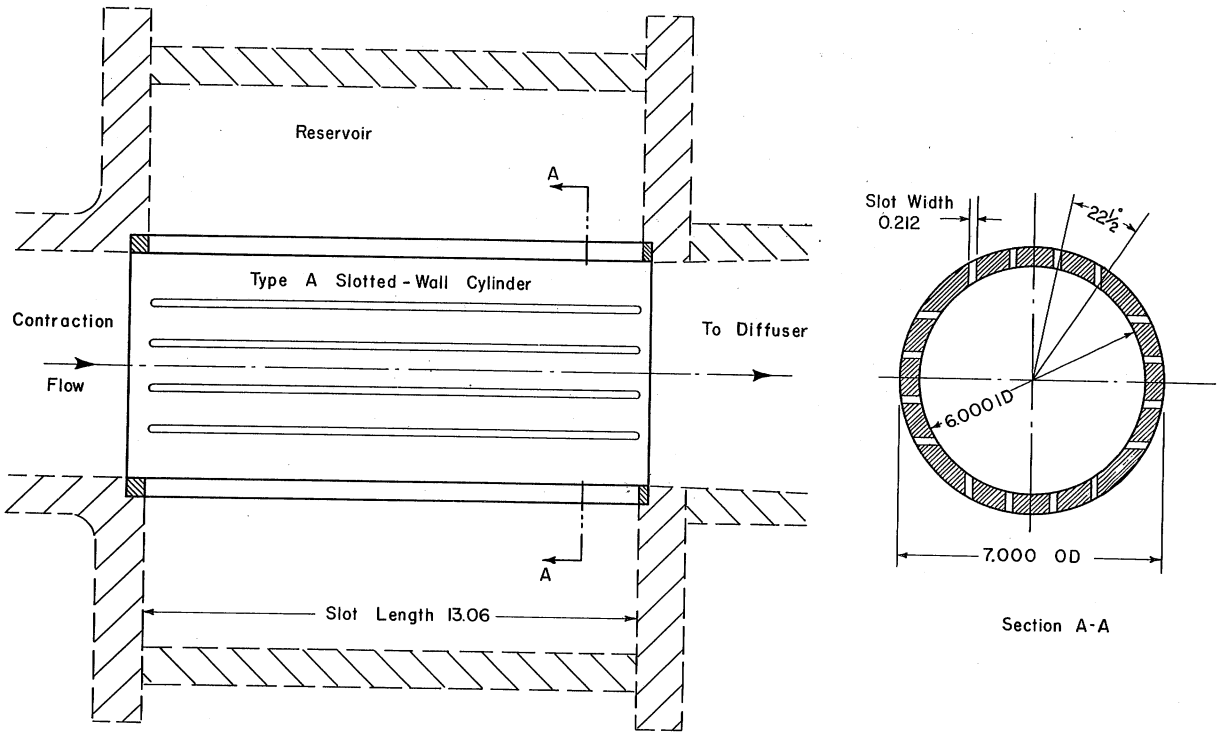

Fig. 4 - Type A Slotted Wall
Dimensions Are in Inches

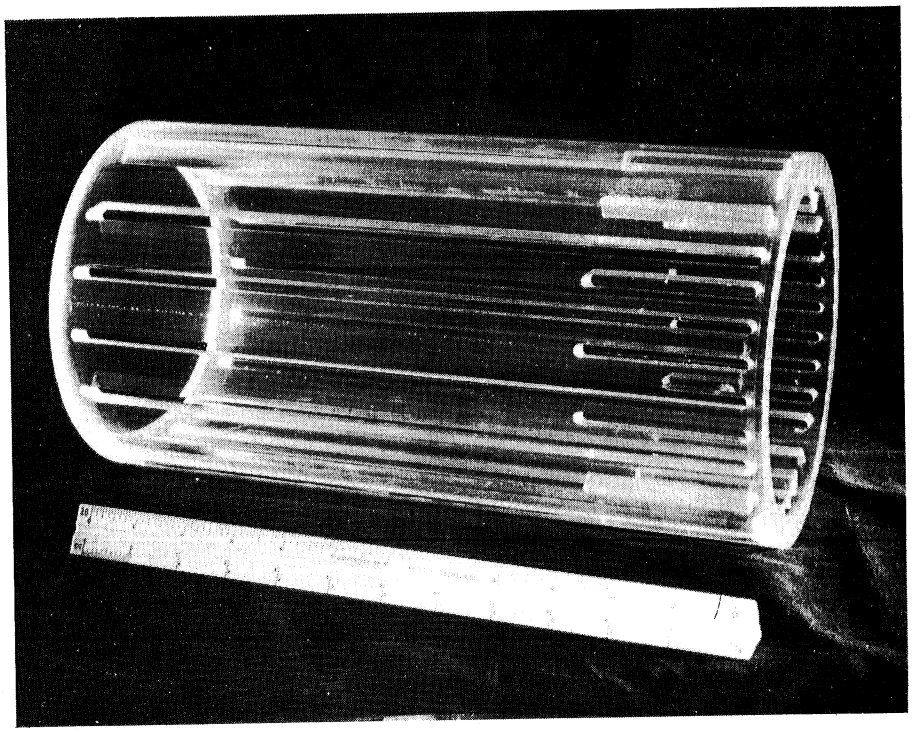

Fig. 5 - Type B Slotted-Wall Cylinder

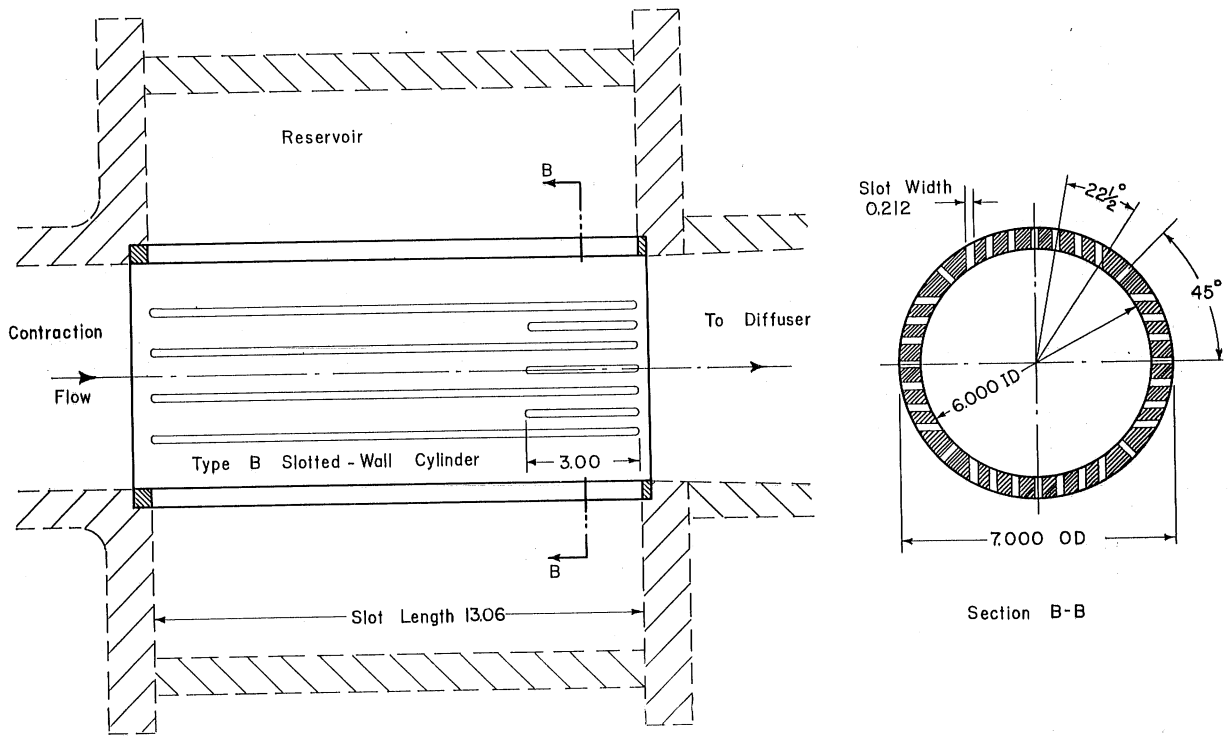

Fig. 6 - Type B Slotted Wall
Dimensions Are in Inches

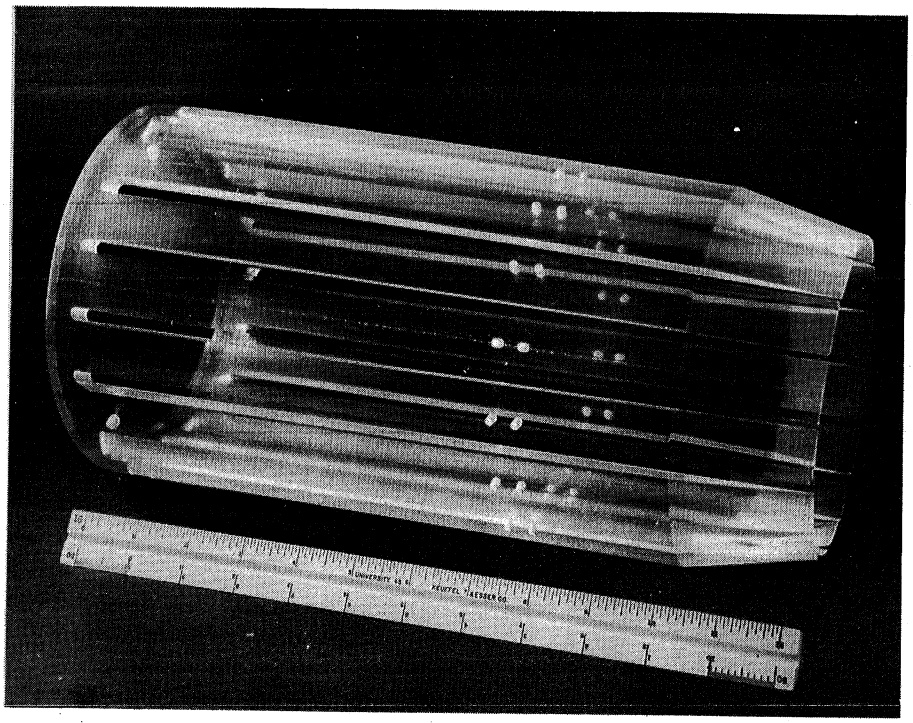

Fig. 7 - Type C Slotted-Wall Cylinder

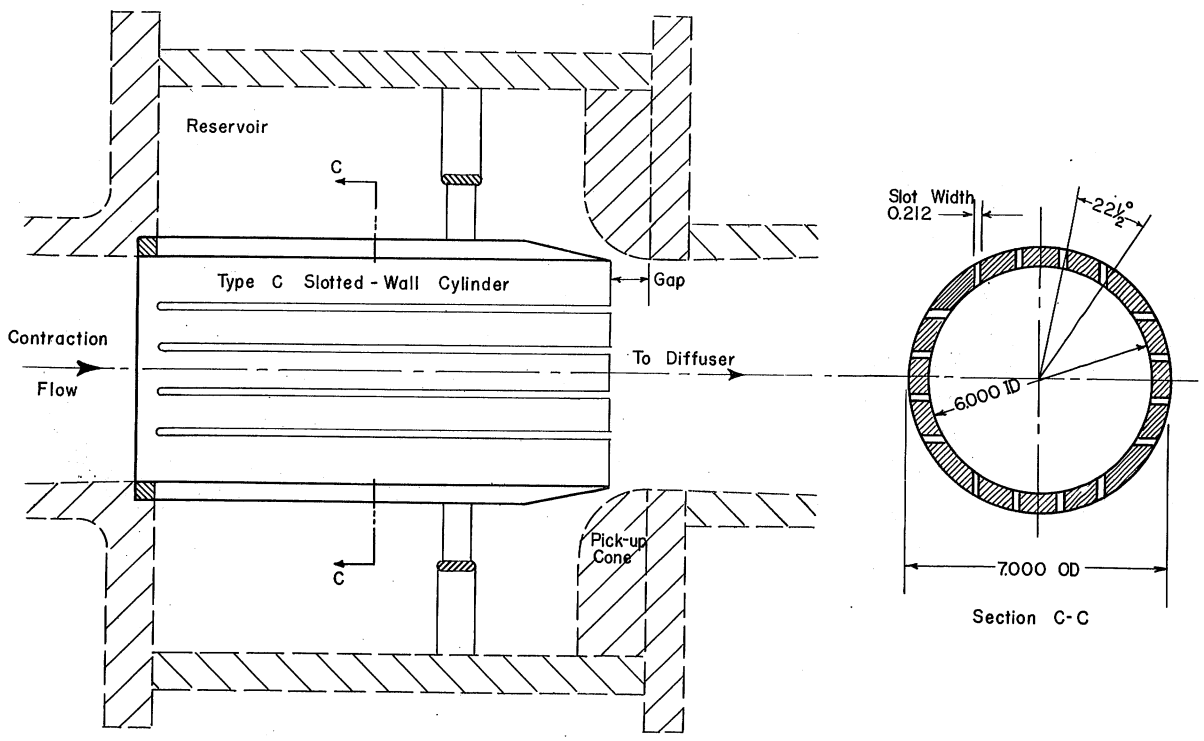

Fig. 8 - Type C Slotted Wall
Dimensions Are in Inches

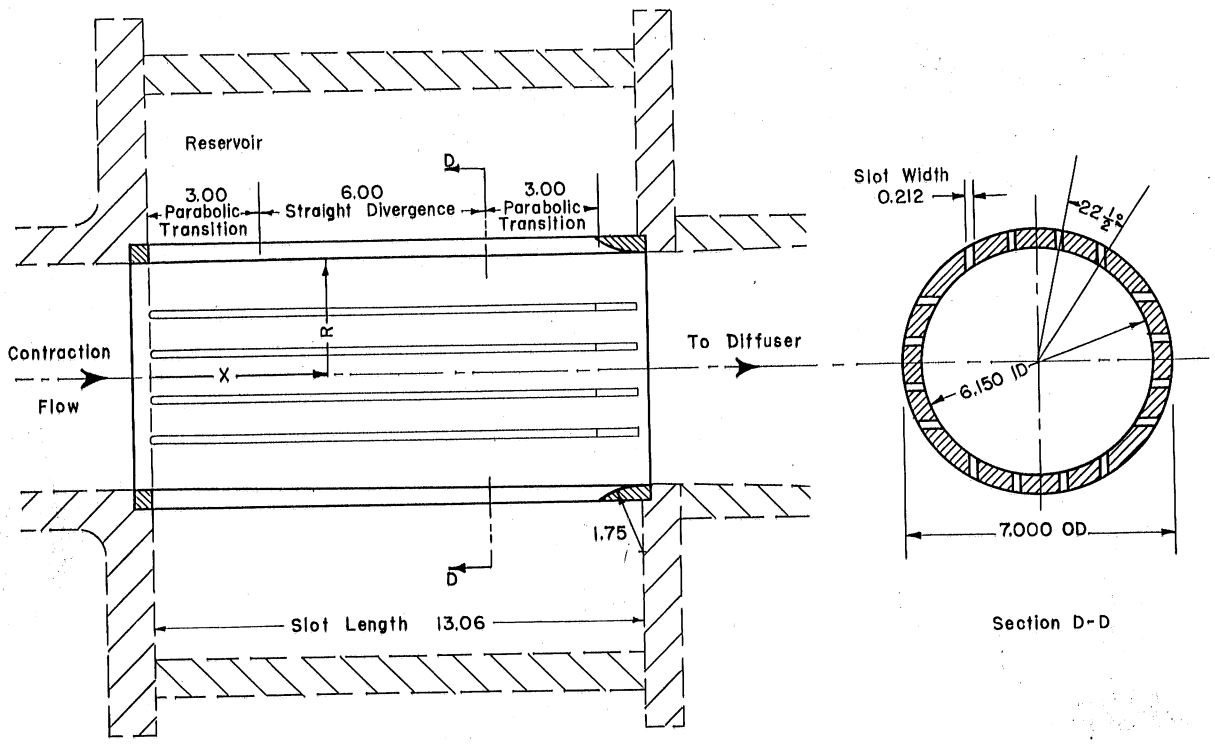

Fig. 9 - Type D Slotted Wall
Dimensions Are in Inches

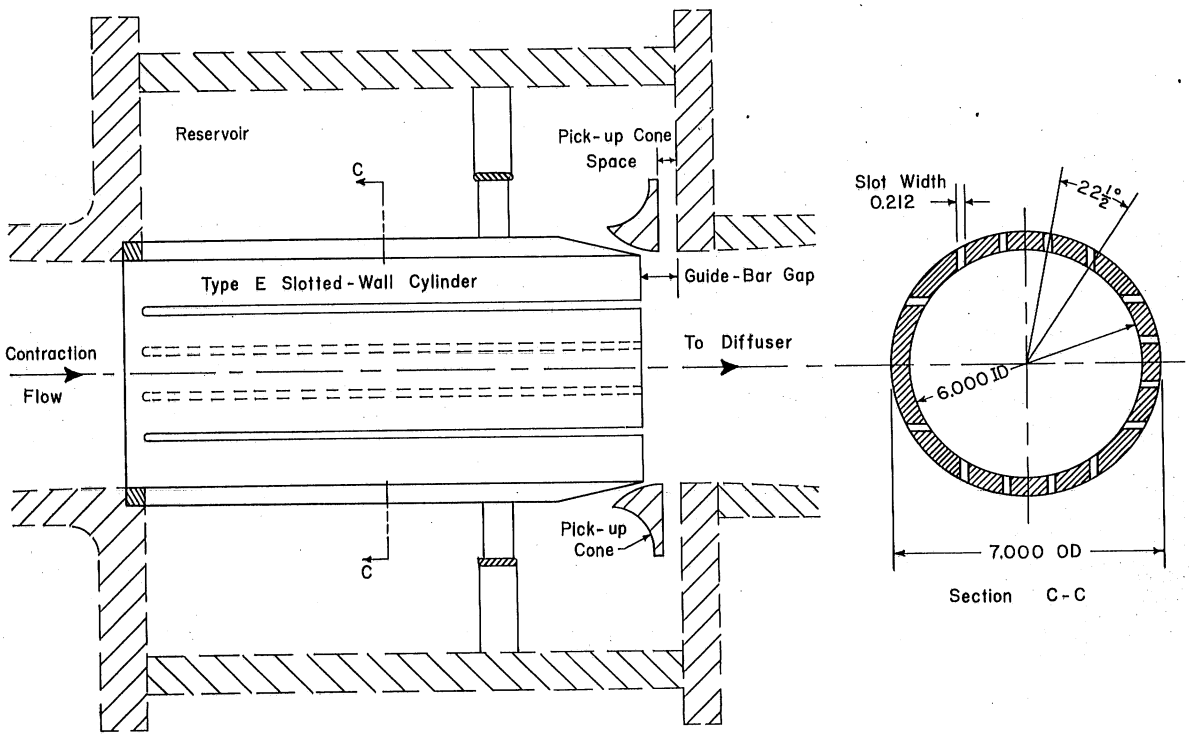

Fig. 10 - Type E Slotted Wall
Dimensions Are in Inches

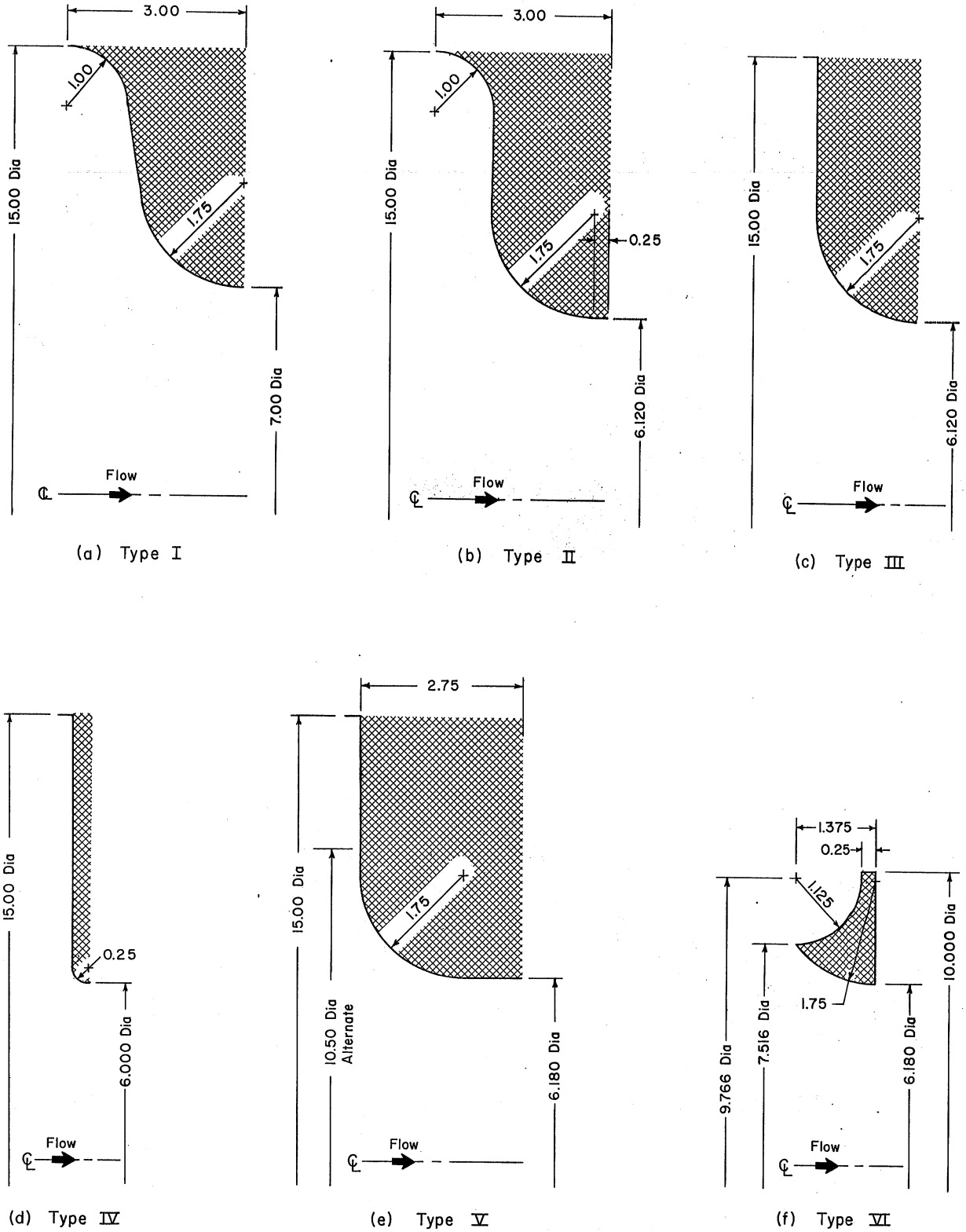

Fig. 11 - Reservoir Pick-up Cones
Dimensions Are in Inches

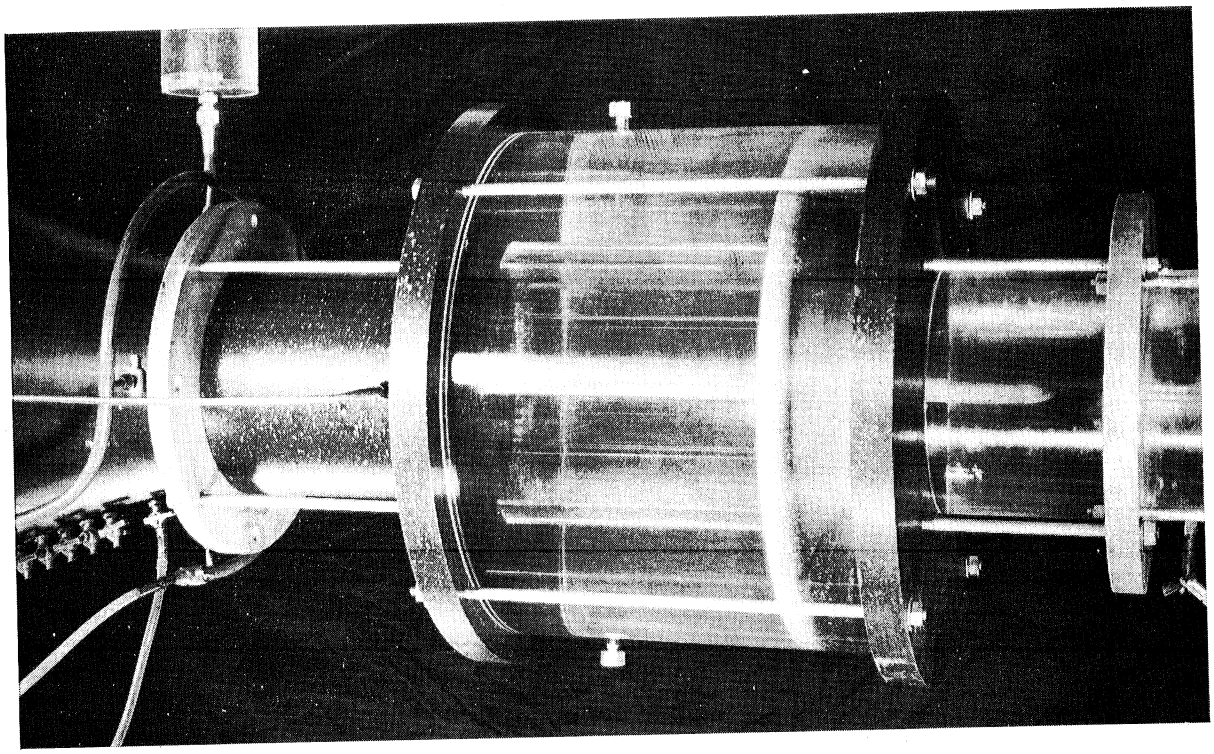

Fig. 12 - Type A-1 Slotted-Wall Test Section (Assembly 2)

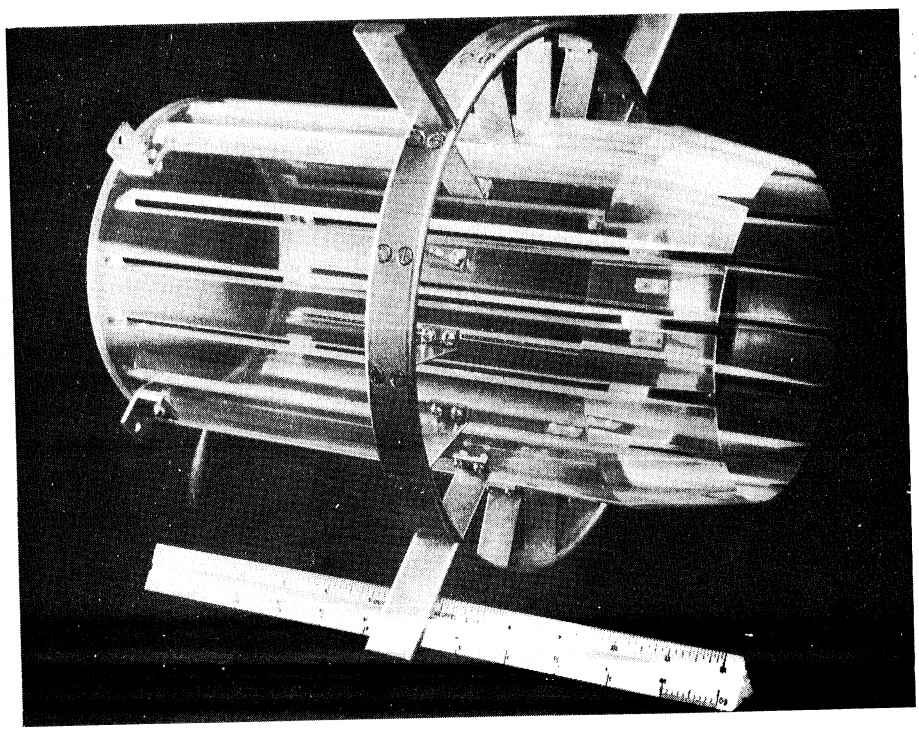

Fig. 13 - Type C Slotted Wall

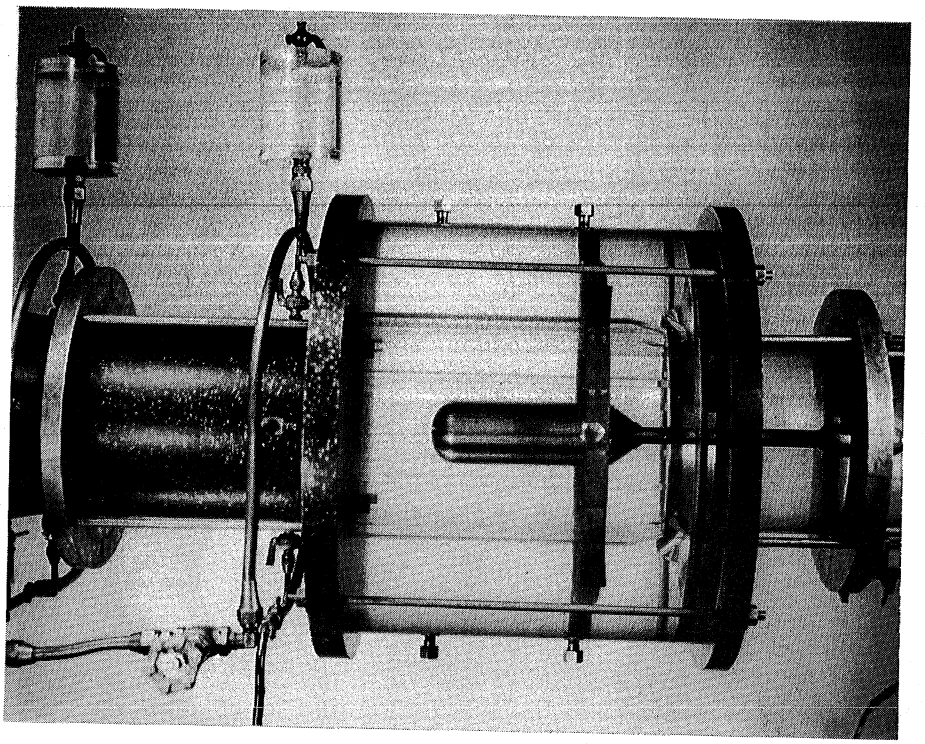

a) Type E-VI Slotted-Wall Test Section (Assembly 22)

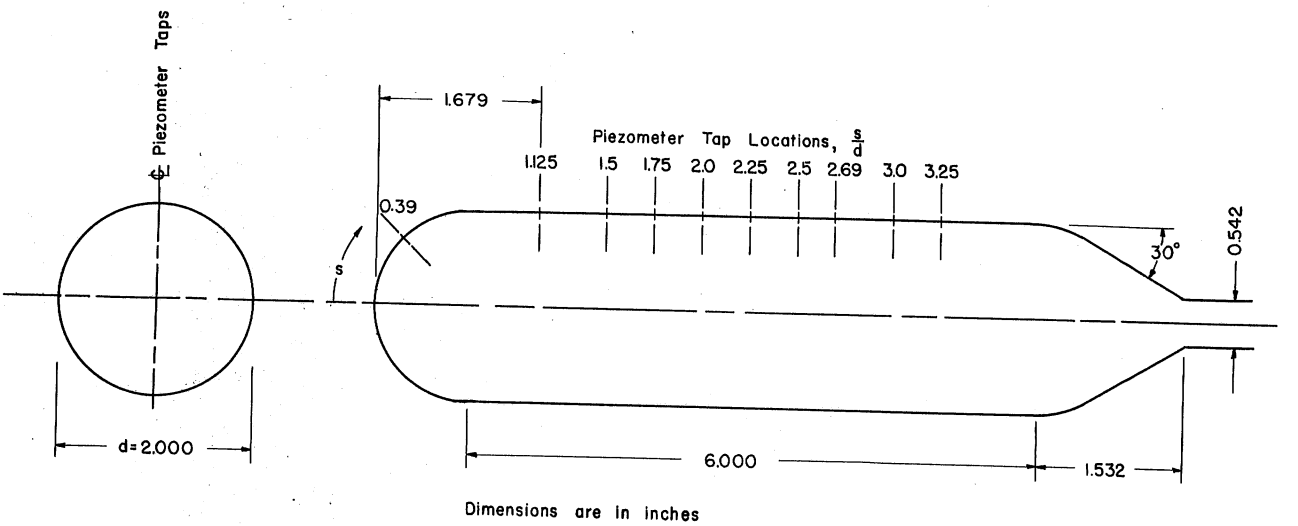

b) 2-Inch Hemispherical Head Form

Fig. 14 - Type E-VI Slotted-Wall Test Section (Assembly 22) with 2-In. Hemispherical Head Form

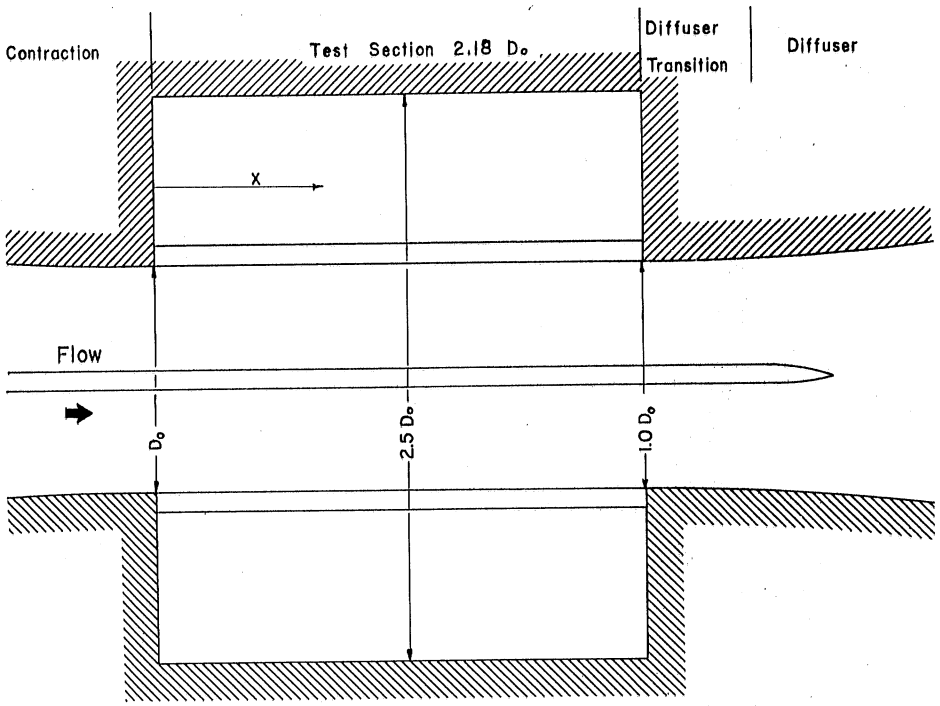

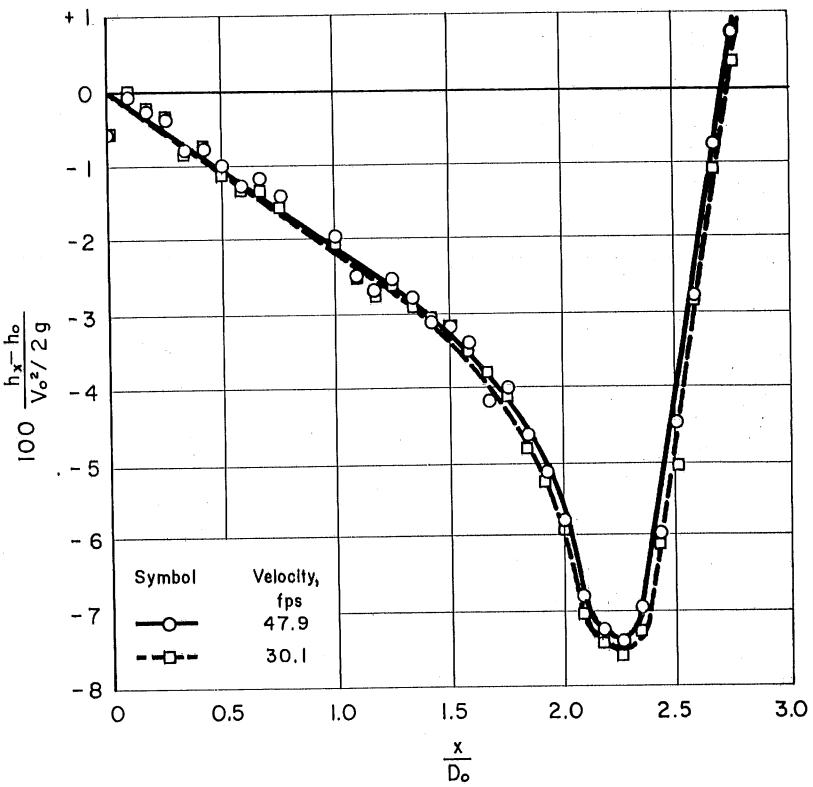

Fig. 15 - Measured Axial Pressures in Type A Slotted-Wall Test Section (Assembly 1)

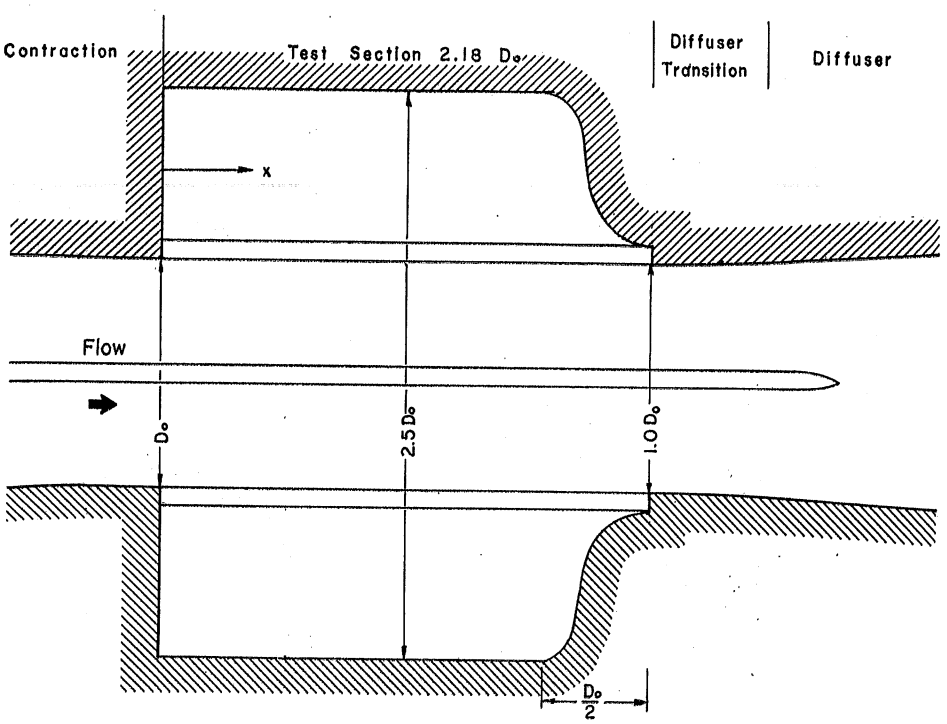

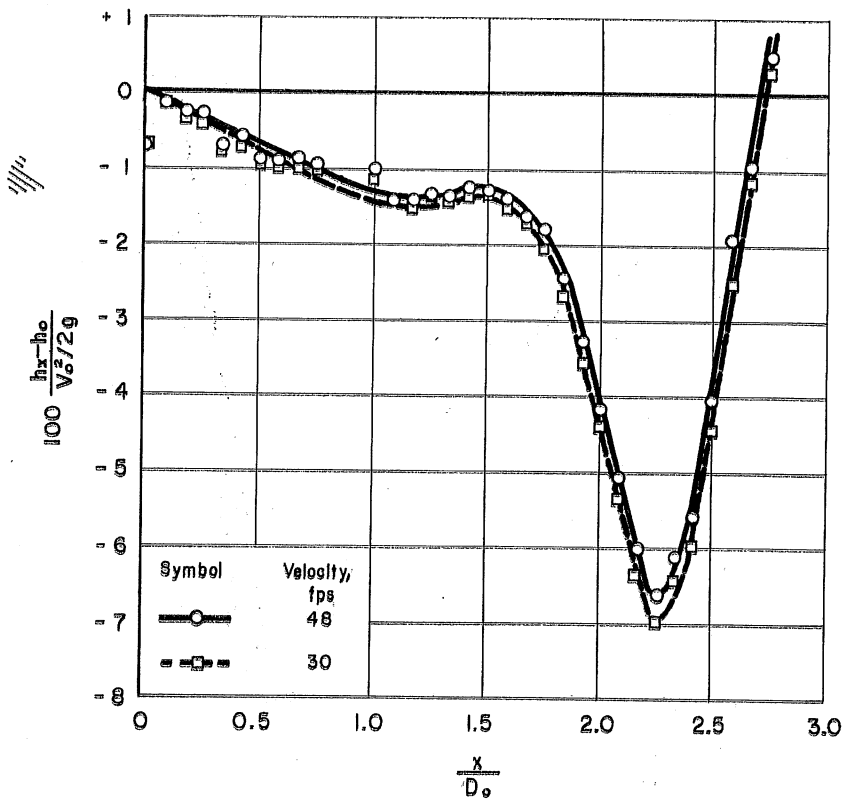

Fig. 16 - Measured Axial Pressures in Type A-1 Slotted-Wall Test Section (Assembly 2)

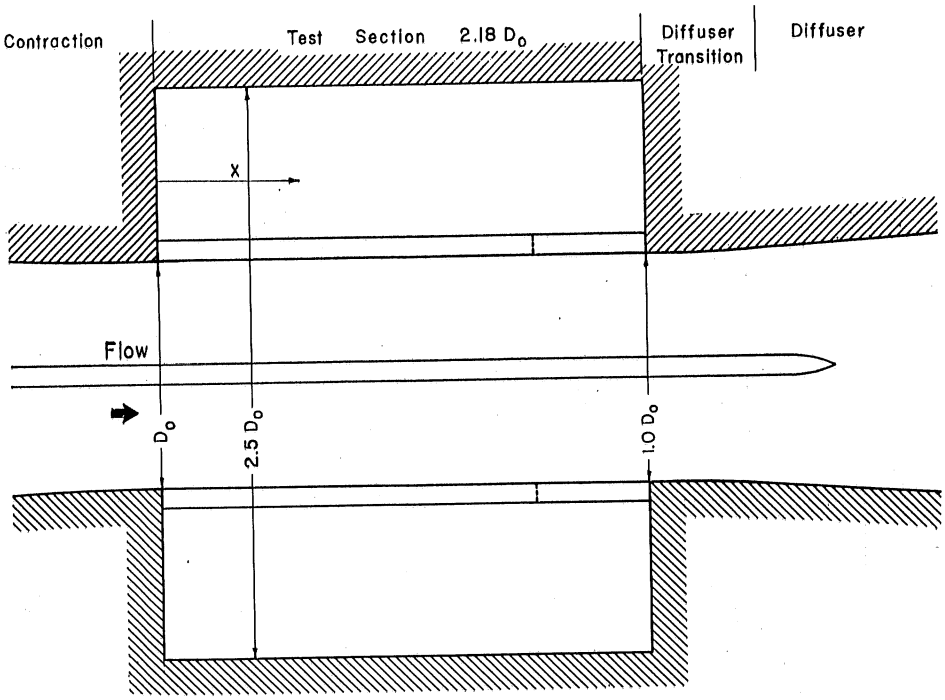

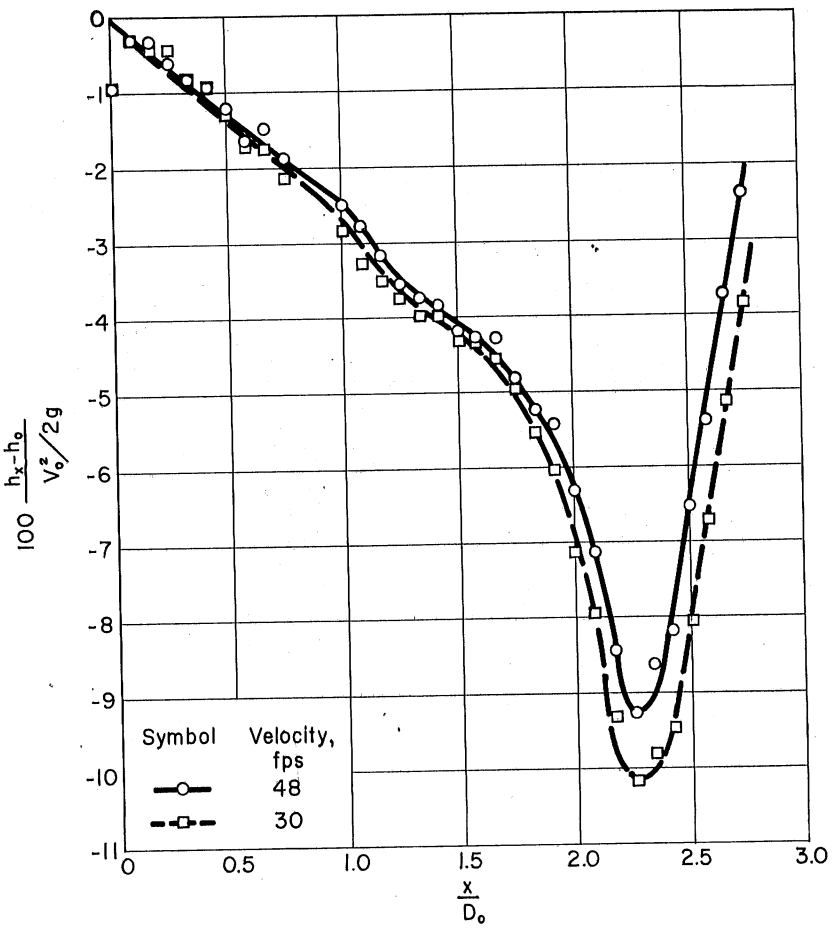

Fig. 17 – Measured Axial Pressures in Type B Slotted-Wall Test Section (Assembly 3)

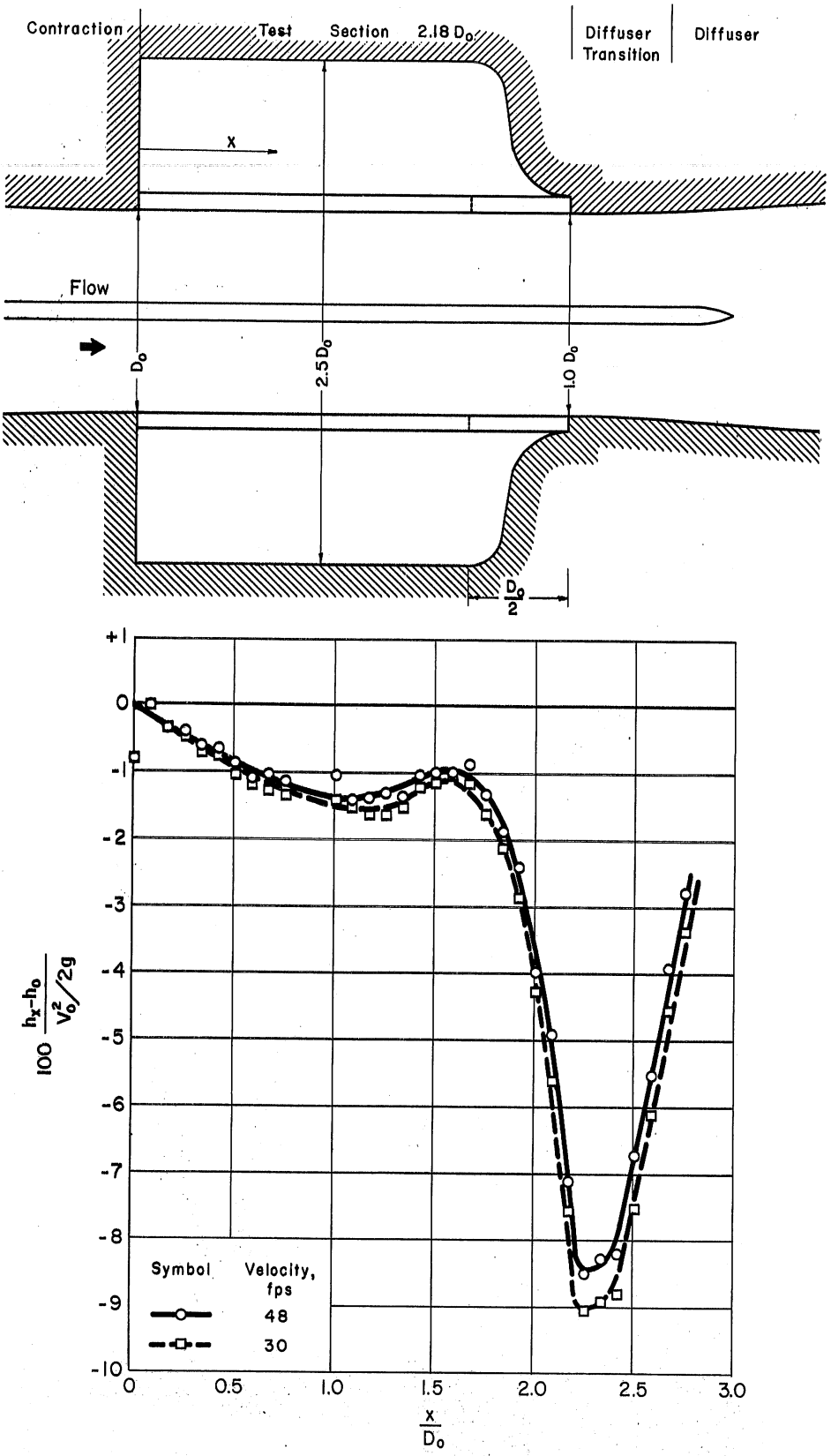

Fig. 18 - Measured Axial Pressures in Type B-1 Slotted-Wall Test Section (Assembly 4)

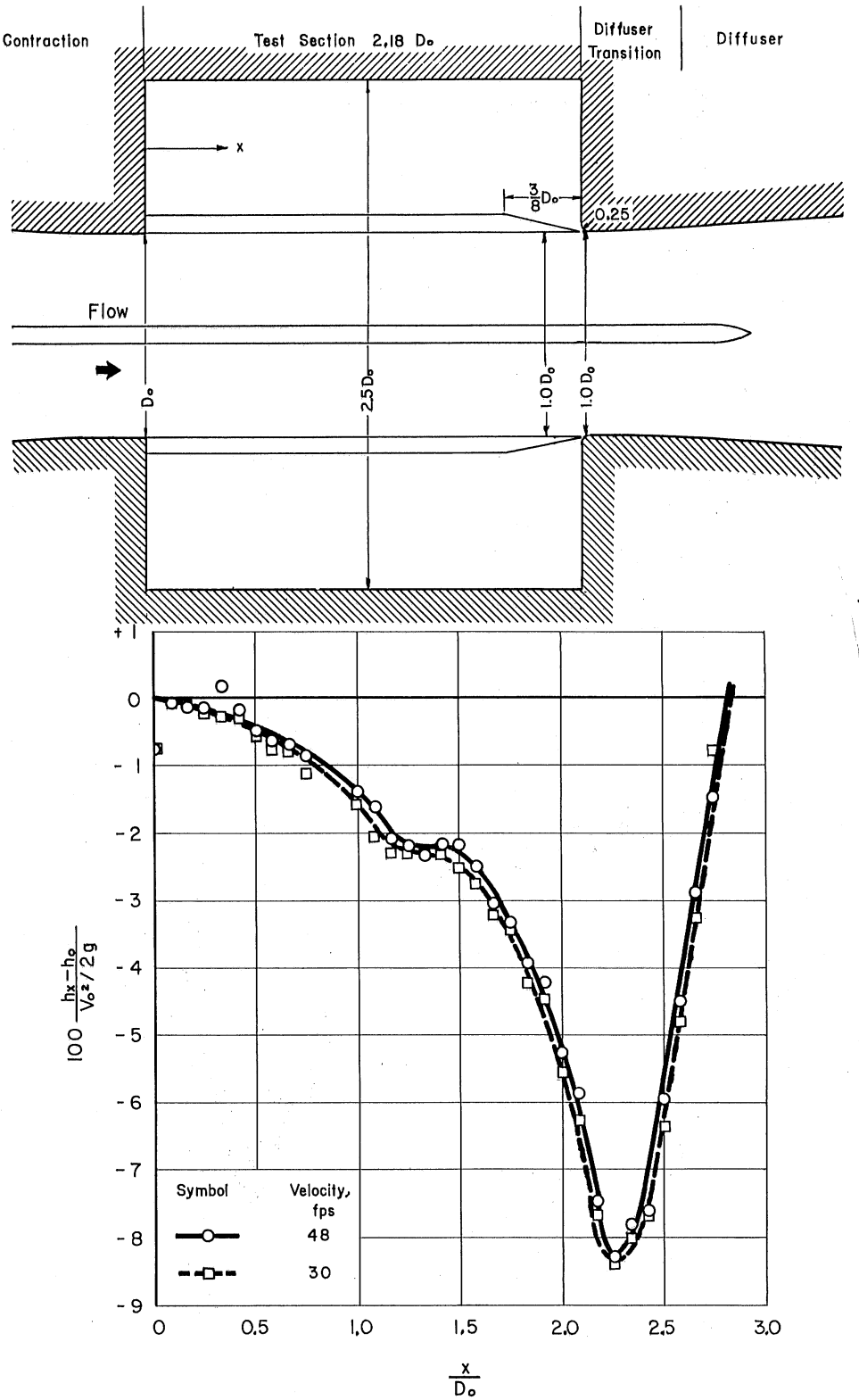

Fig. 19 - Measured Axial Pressures in Type C-IV Slotted-Wall Test Section (Assembly 5)

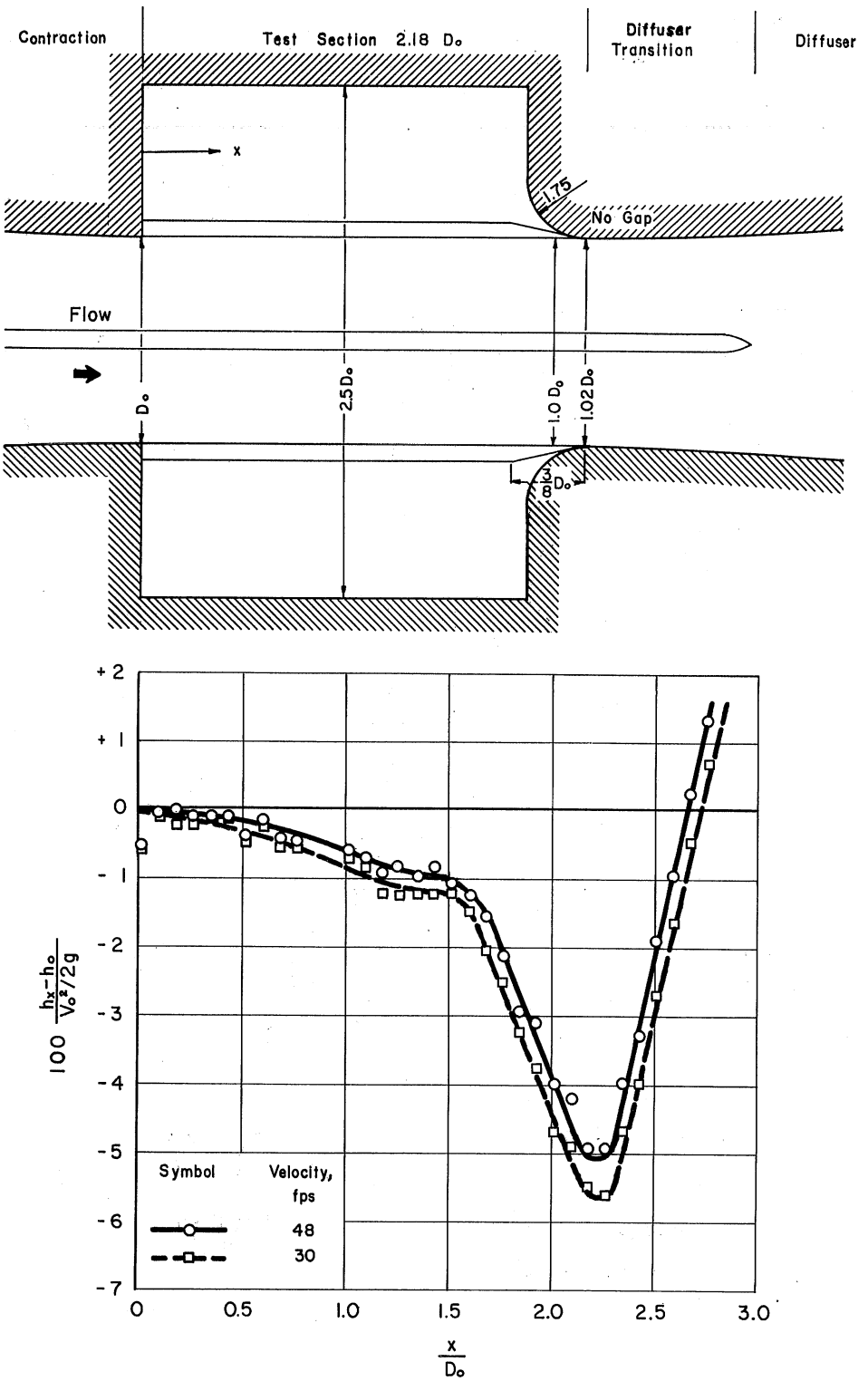

Fig. 20 - Measured Axial Pressures in Type C-III Slotted-Wall Test Section with No Gap (Assembly 6)

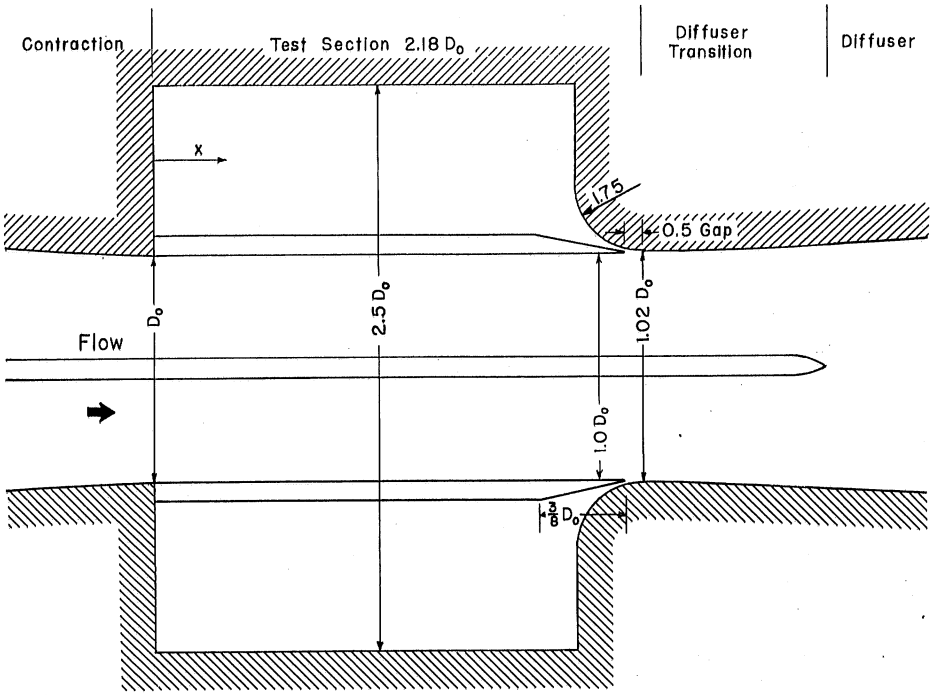

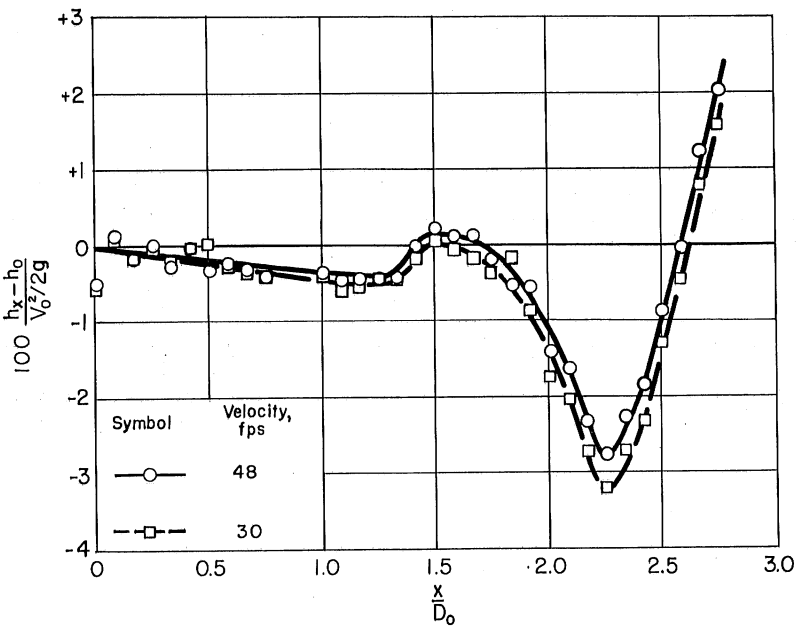

Fig. 21 - Measured Axial Pressures in Type C-III Slotted-Wall Test Section with 0.5-In. Gap (Assembly 7)

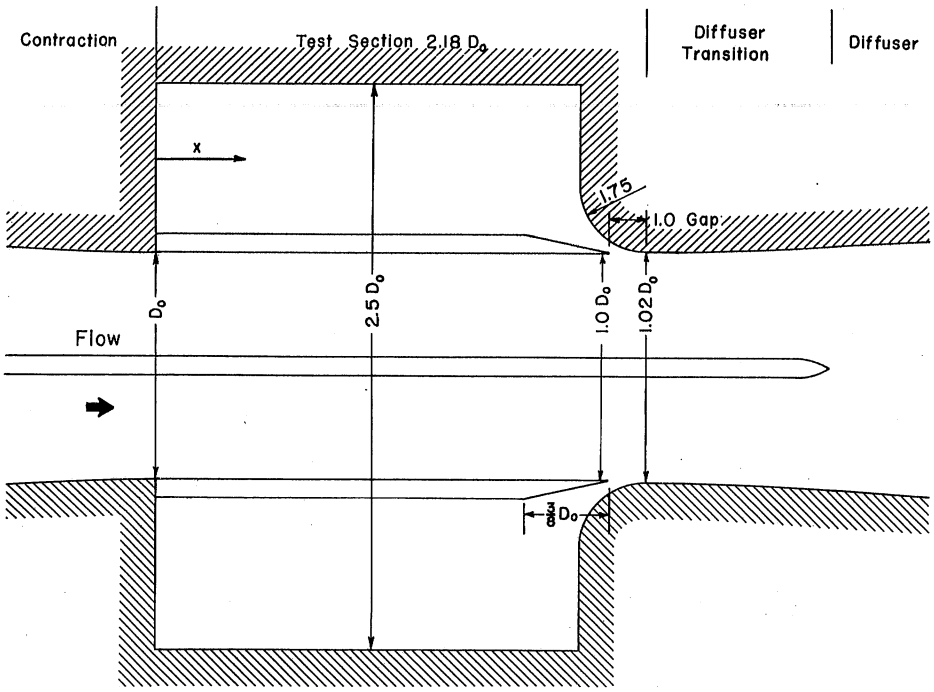

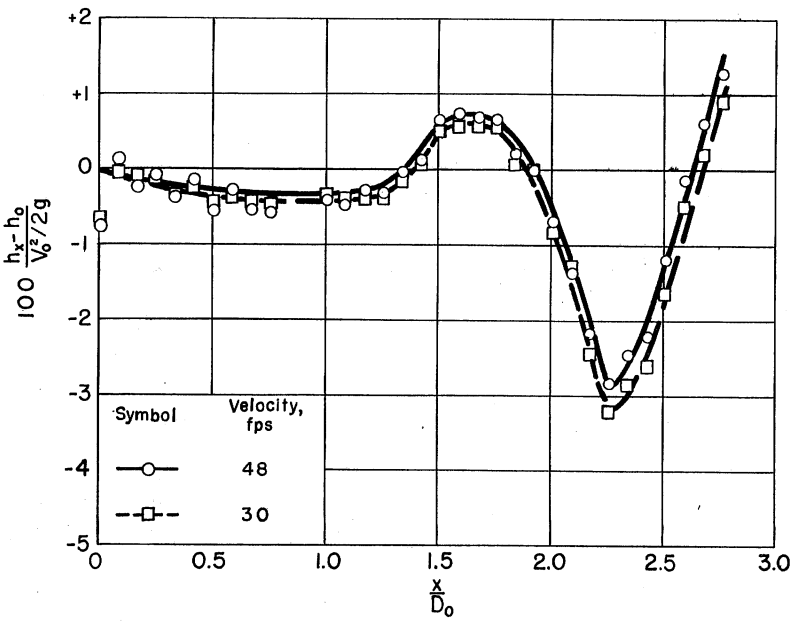

Fig. 22 - Measured Axial Pressures in Type C-III Slotted-Wall Test Section with 1.0-In. Gap (Assembly 8)

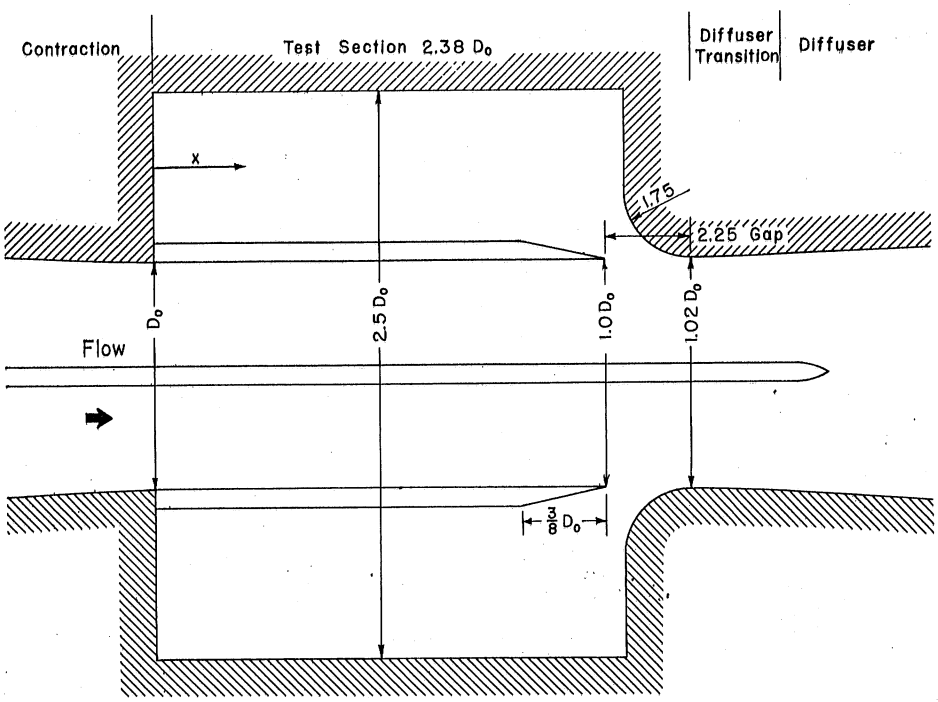

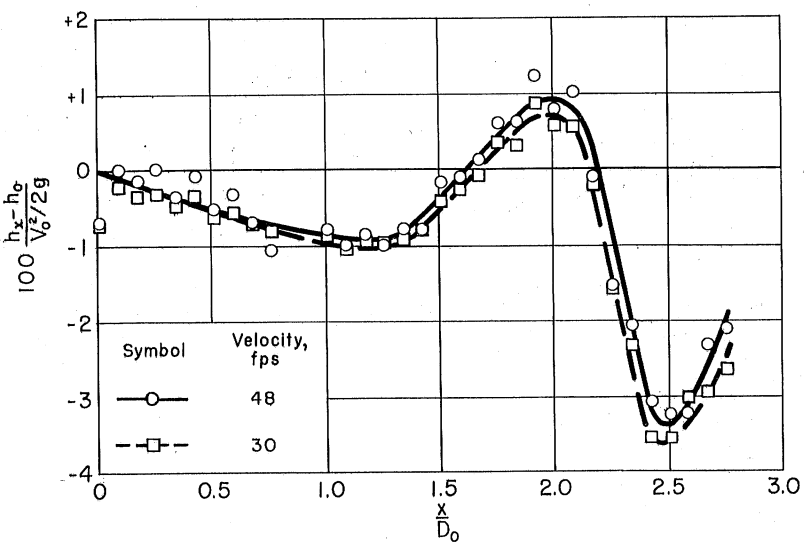

Fig. 23 - Measured Axial Pressures in Type C-III Slotted-Wall Test Section with 2.25-In. Gap (Assembly 9)

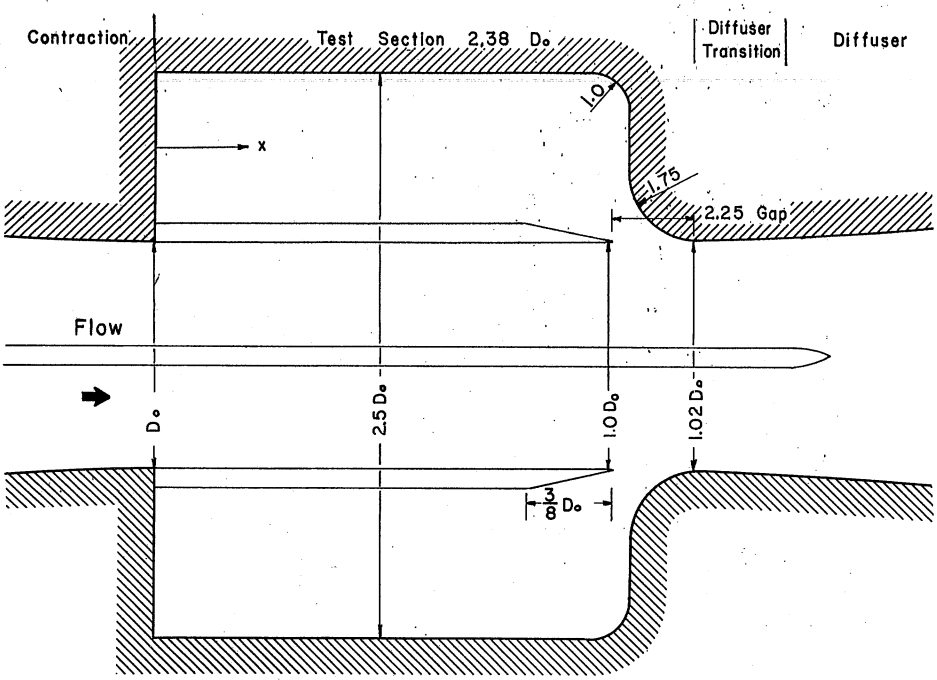

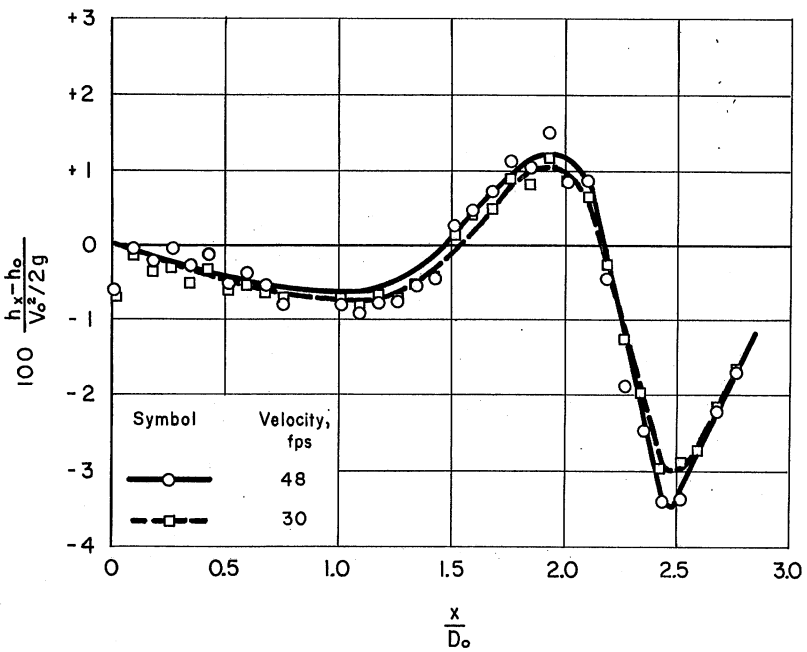

Fig. 24 - Measured Axial Pressures in Type C-II Slotted-Wall Test Section with 2.25-In. Gap (Assembly 10)

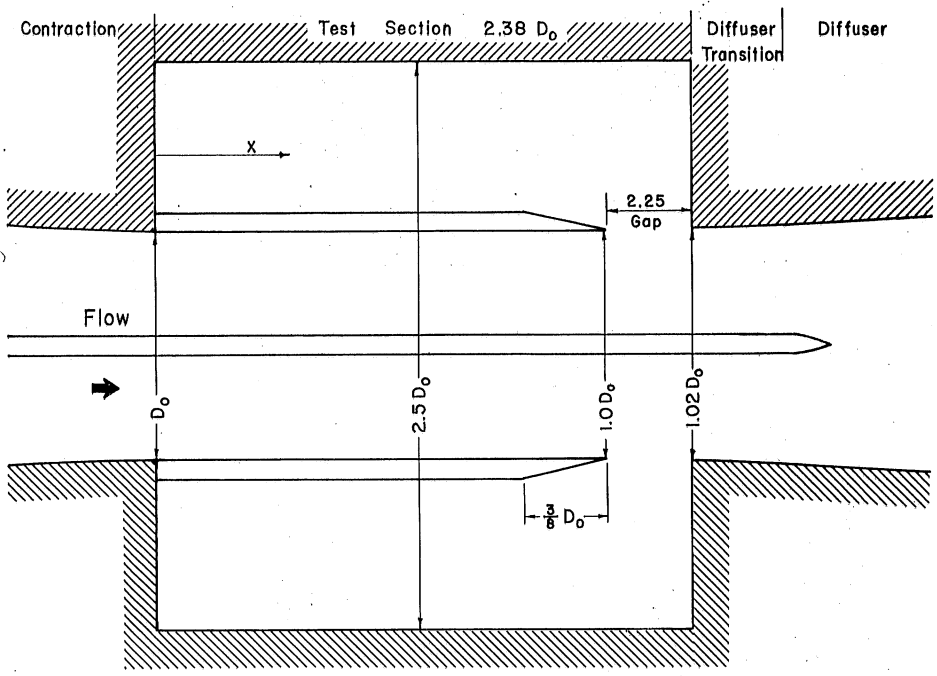

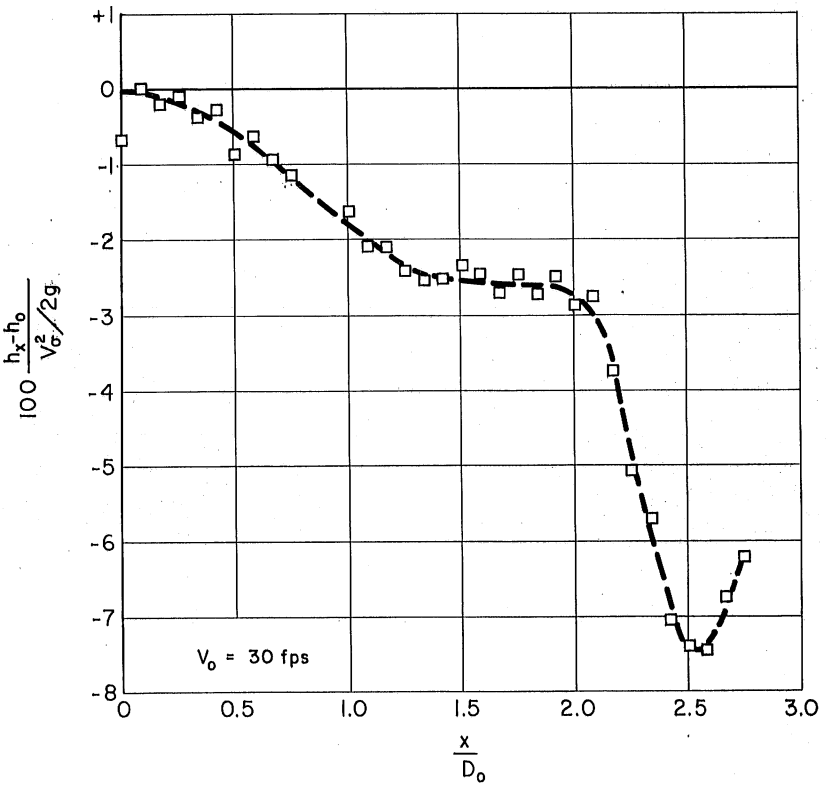

Fig. 25 - Measured Axial Pressures in Type C Slotted-Wall Test Section with 2.25-In. Gap (Assembly 11)

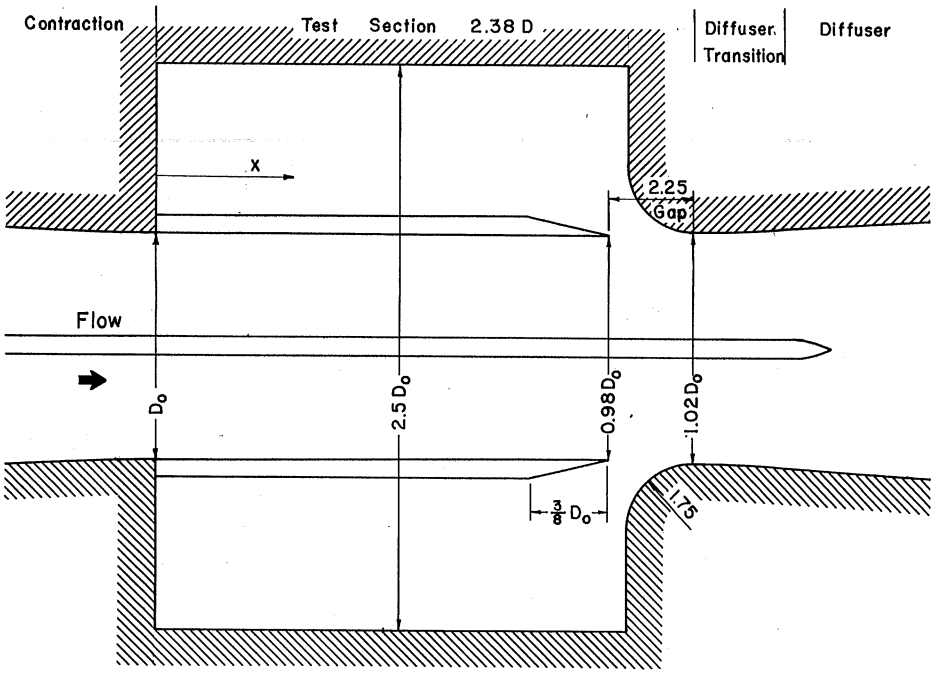

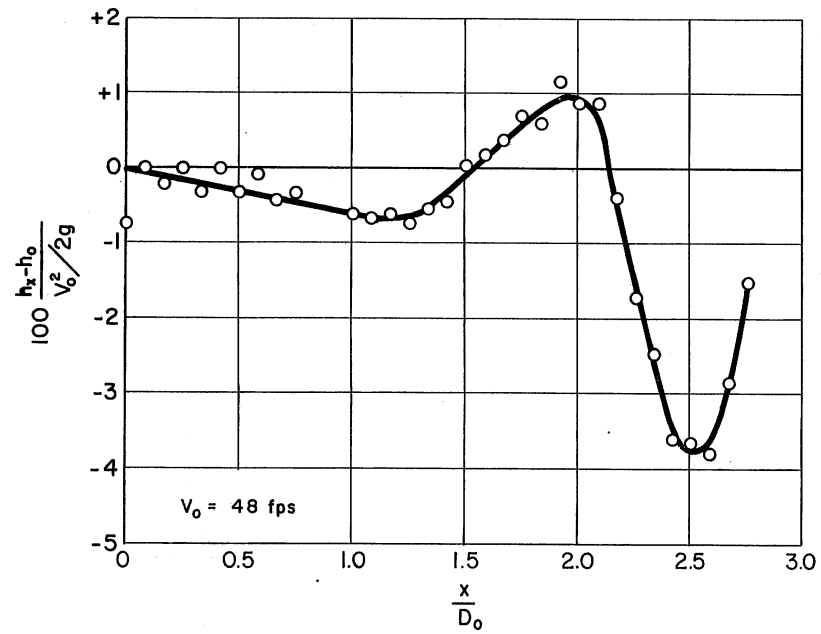

Fig. 26 - Measured Axial Pressures in Type C-III Slotted-Wall Test Section with 2.25-In. Gap (Assembly 12)

Guide Bars Converged to $0.98\ D_o$ at Downstream End

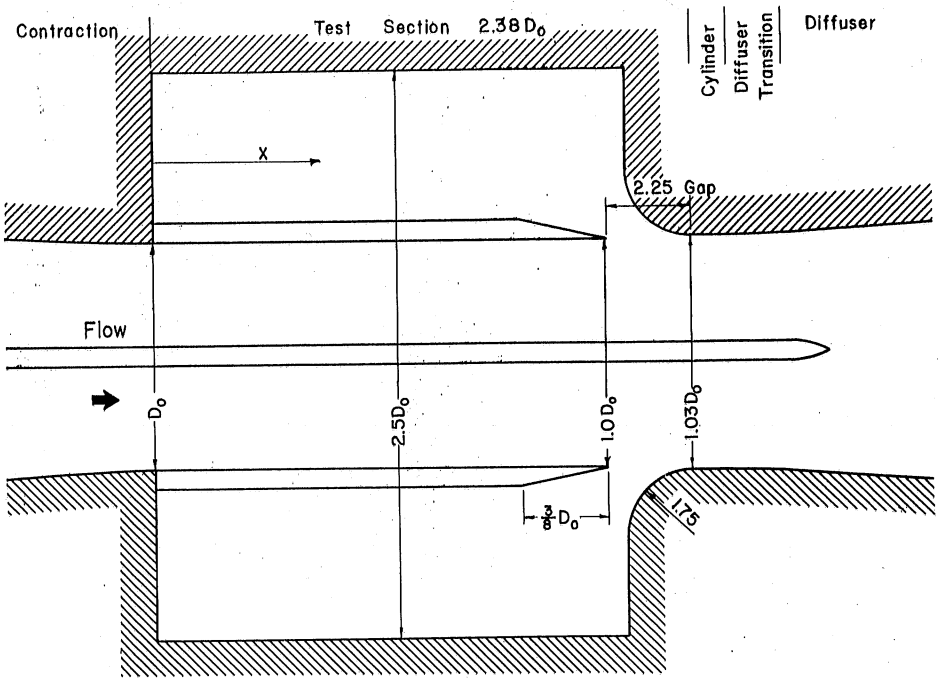

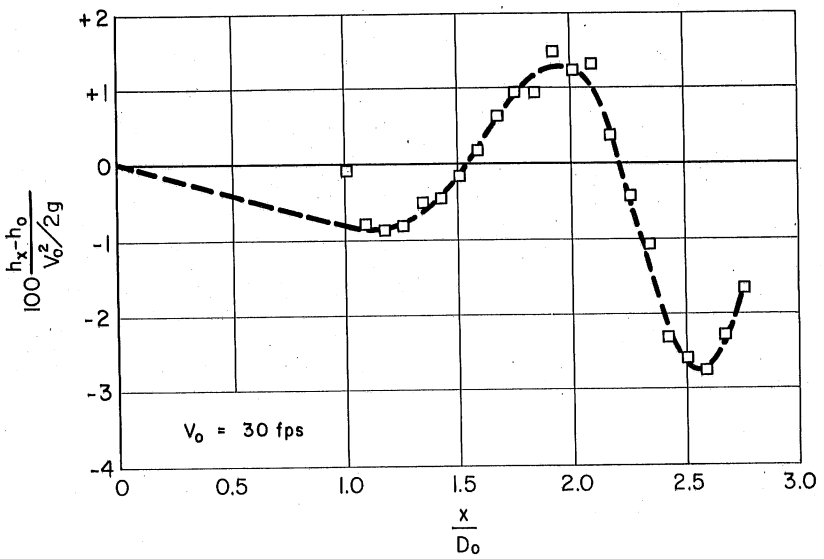

Fig. 27 - Measured Axial Pressures in Type C-V Slotted-Wall Test Section with 2.25-In. Gap (Assembly 13)

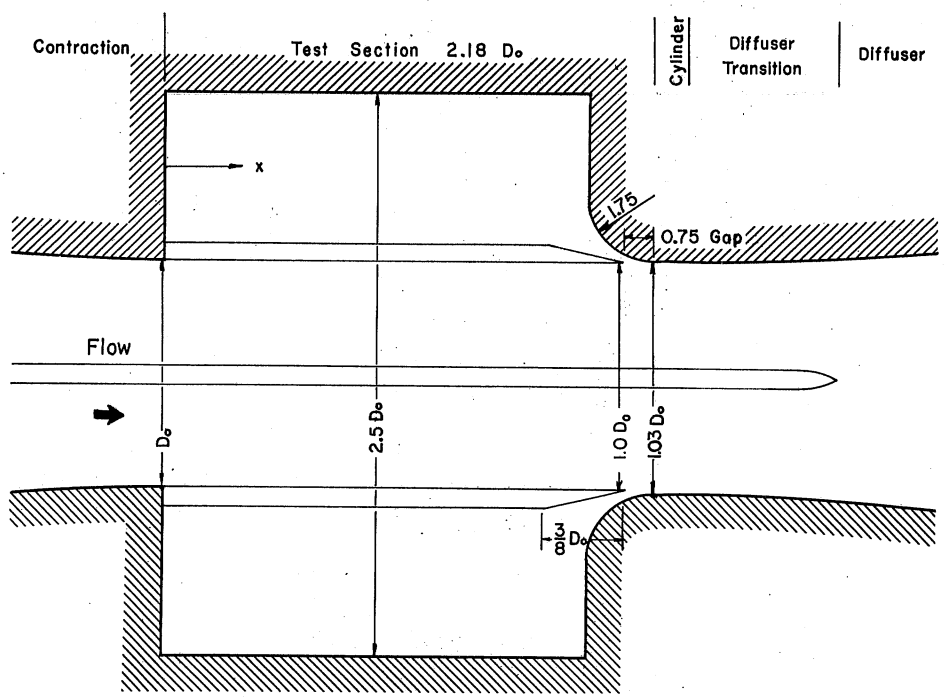

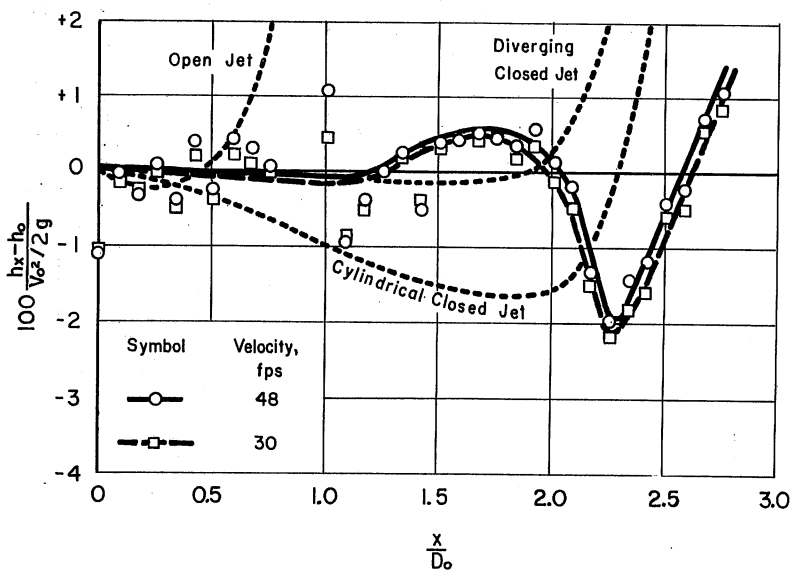

Fig. 28 – Measured Axial Pressures in Type C-V Slotted-Wall Test Section with 0.75-In. Gap (Assembly 14)

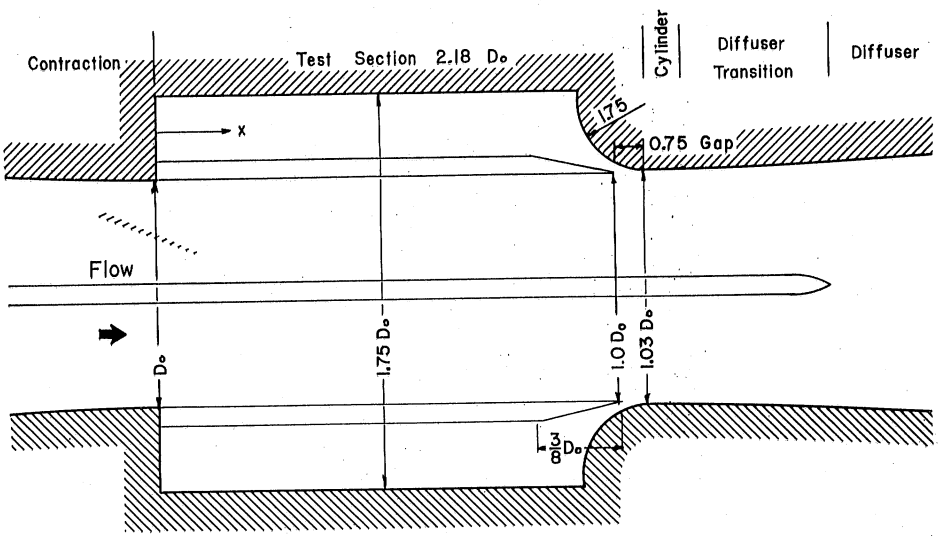

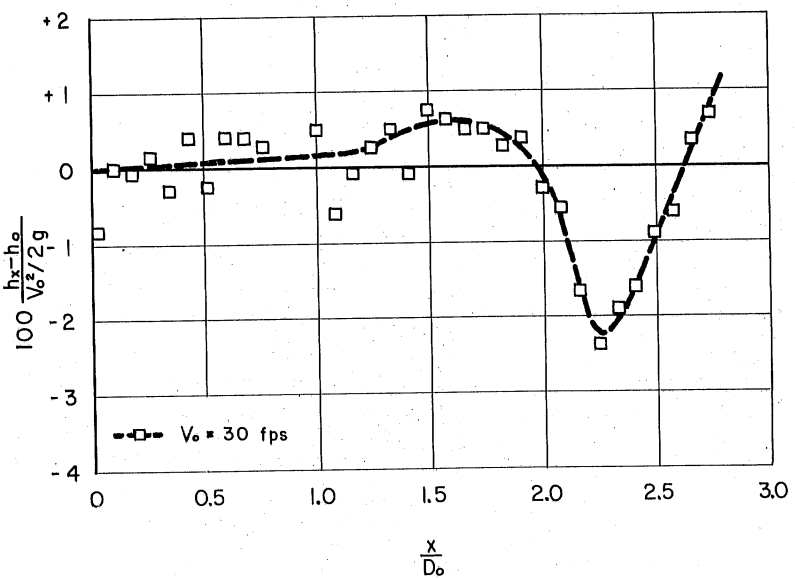

Fig. 29 – Measured Axial Pressures in Type C-V Slotted-Wall Test Section with 0.75-In. Gap (Assembly 15)

Reservoir 1.75 D_o

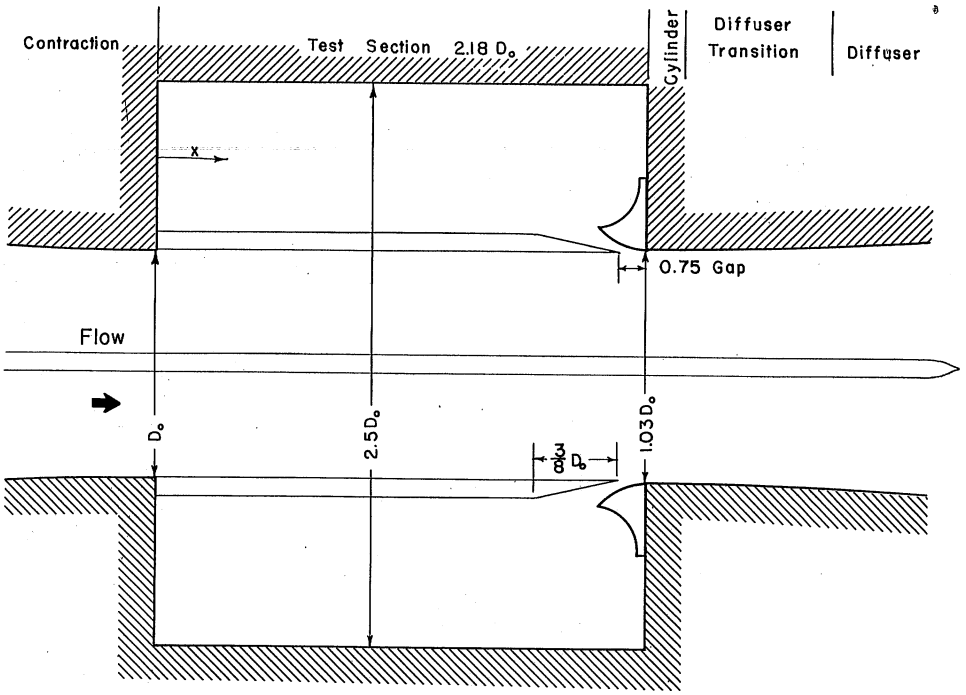

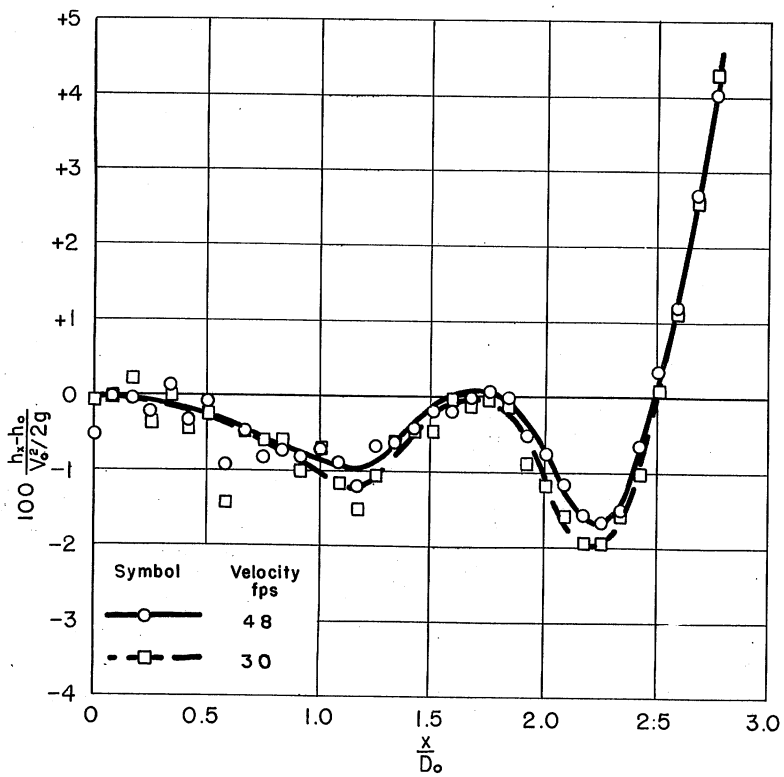

Fig. 30 - Measured Axial Pressures in Type C-VI Slotted-Wall Test Section with 0.75-In. Gap (Assembly 16)

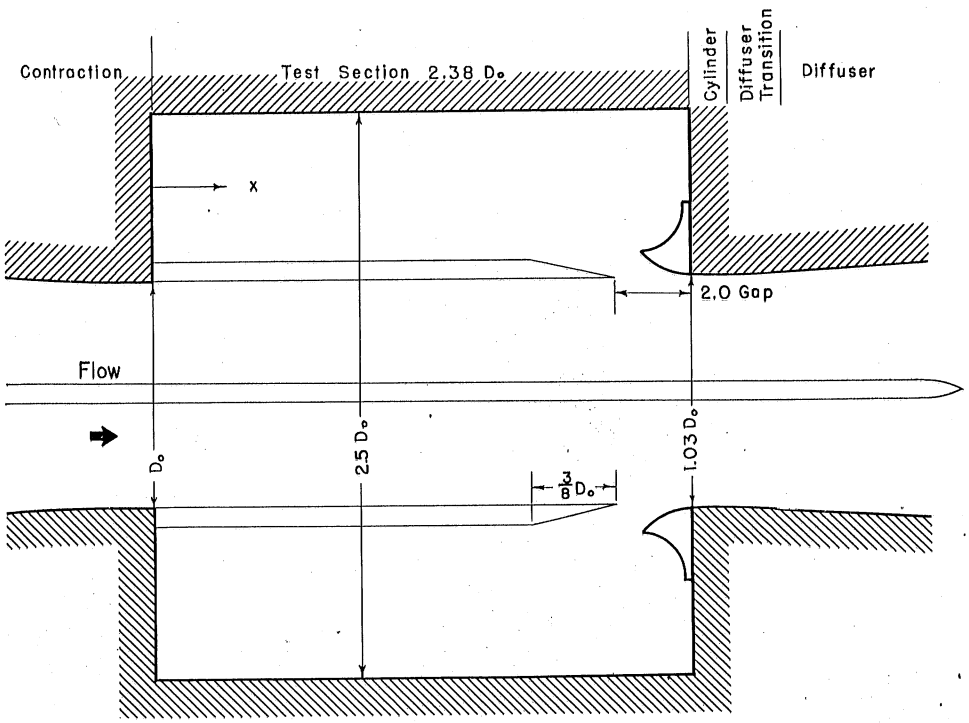

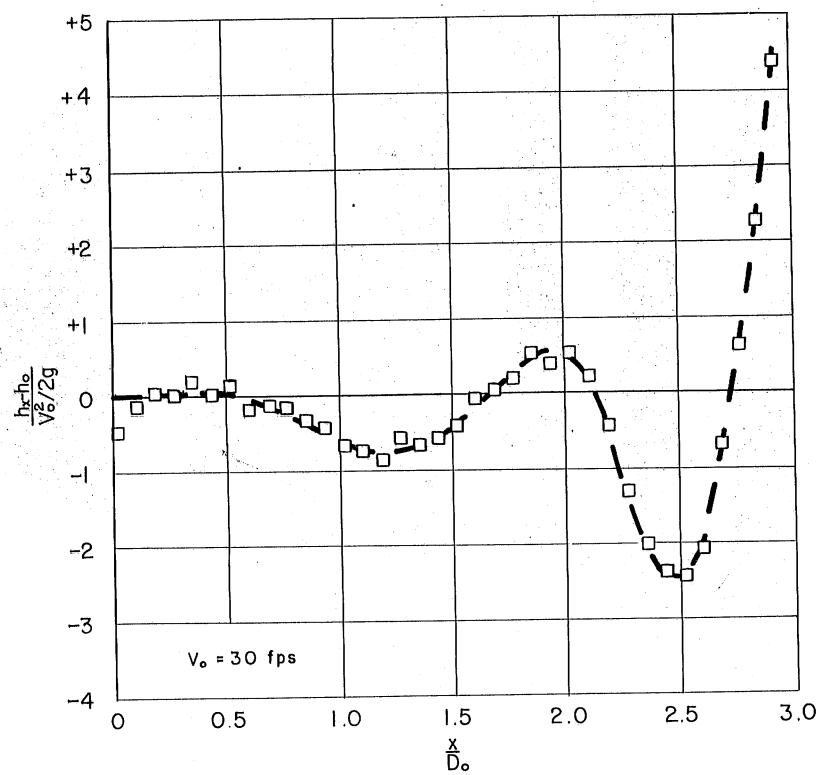

Fig. 31 - Measured Axial Pressures in Type C-VI Slotted-Wall Test Section with 2.0-In. Gap (Assembly 17)

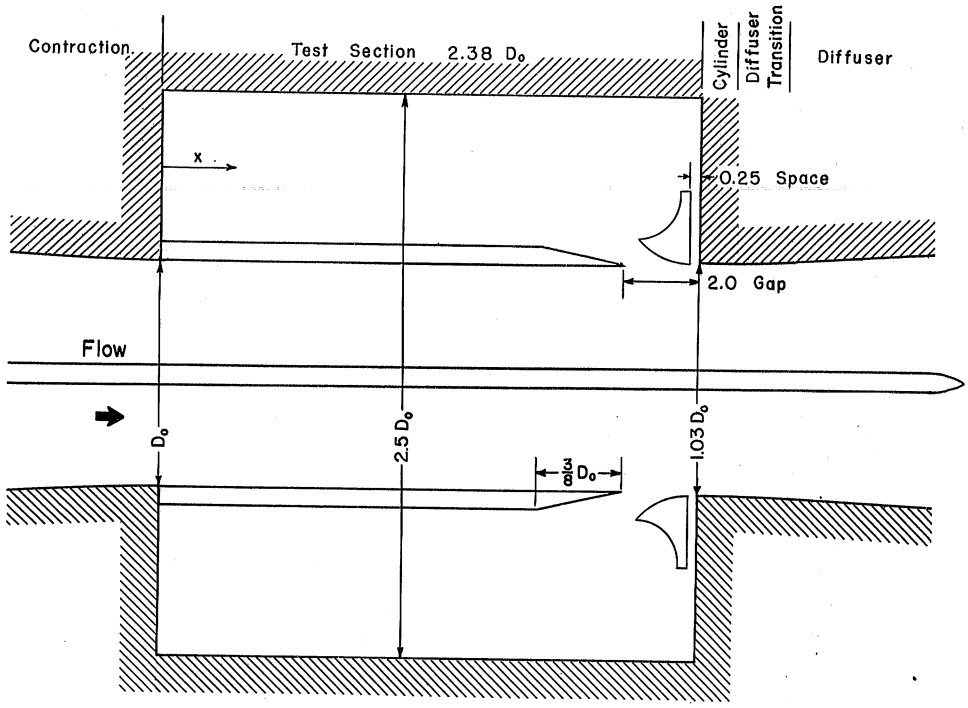

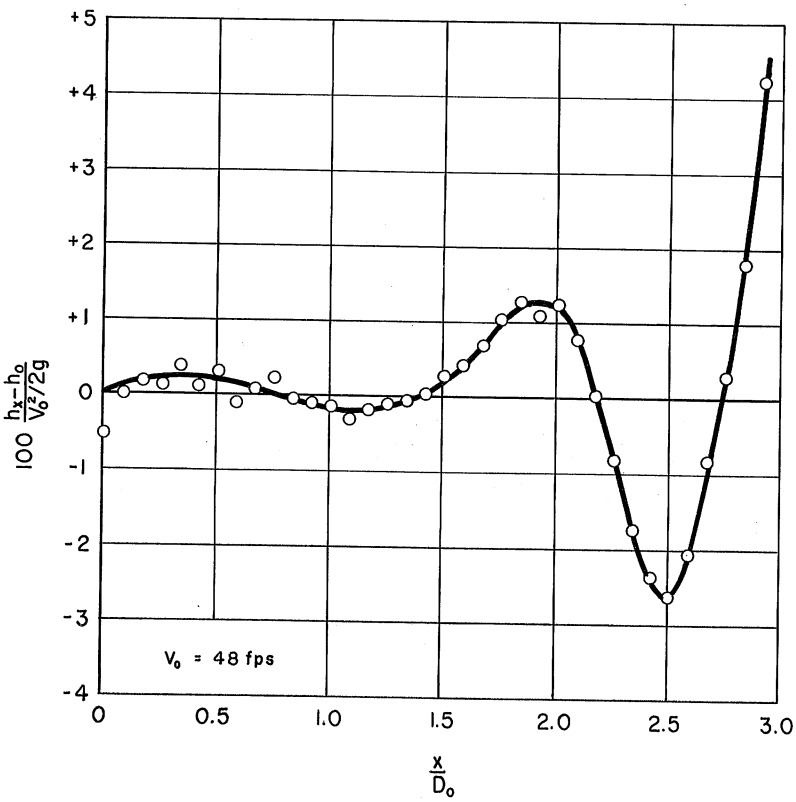

Fig. 32 - Measured Axial Pressures in Type C-VI Slotted-Wall Test Section with 2.0-In. Gap (Assembly 18)

Pick-up Cone Space 0.25 inch

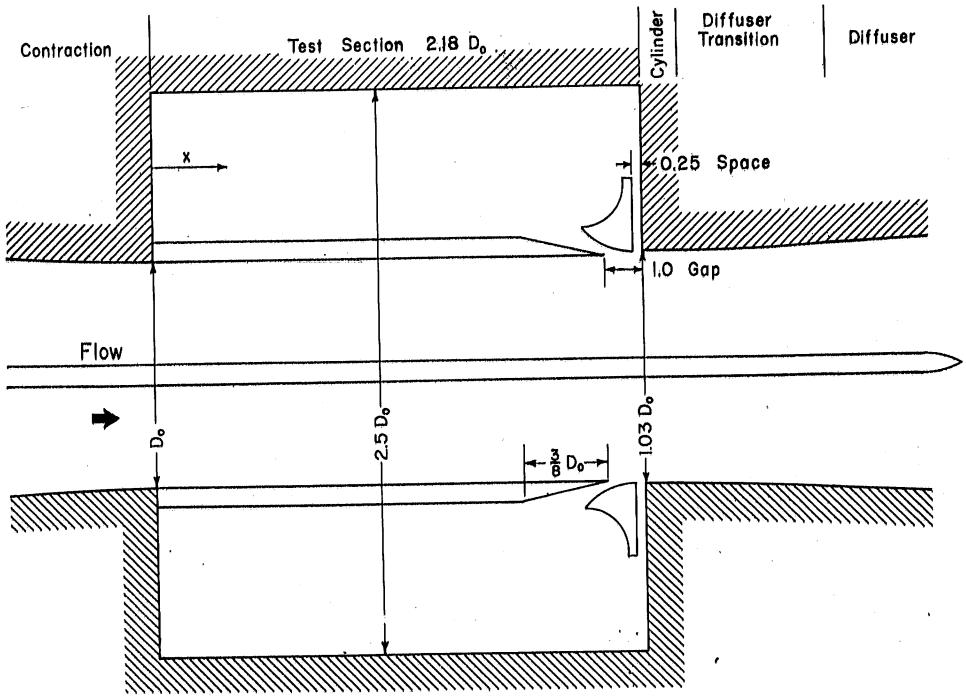

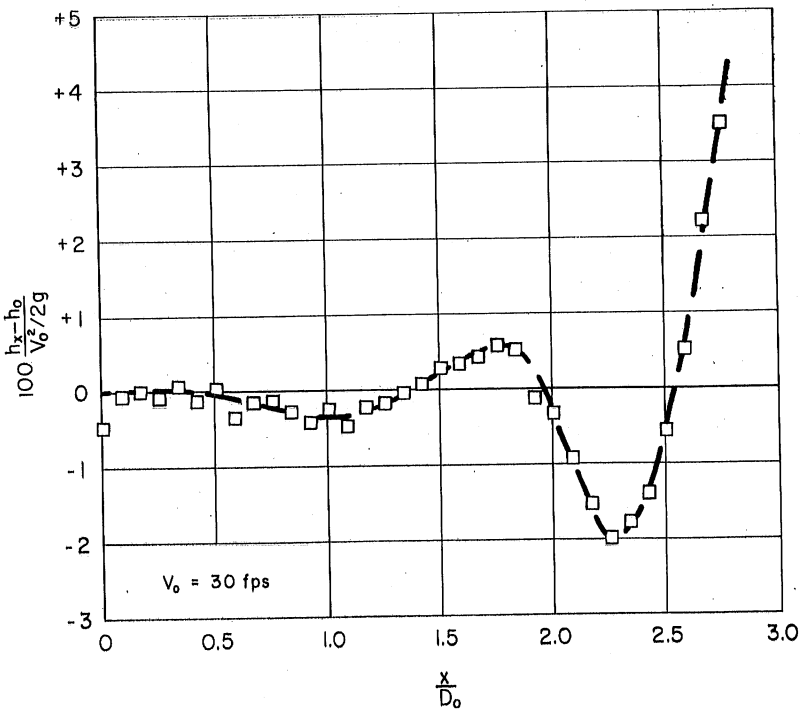

Fig. 33 - Measured Axial Pressures in Type C-VI Slotted-Wall Test Section with 1.0-in. Gap (Assembly 19)

Pick-up Cone Space 0.25 inch

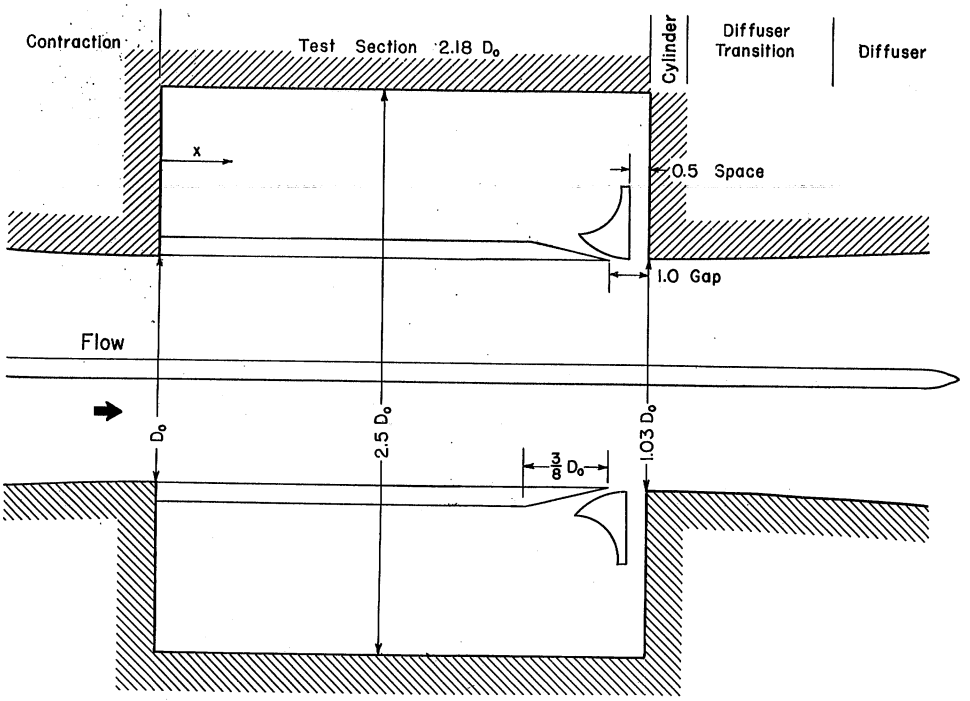

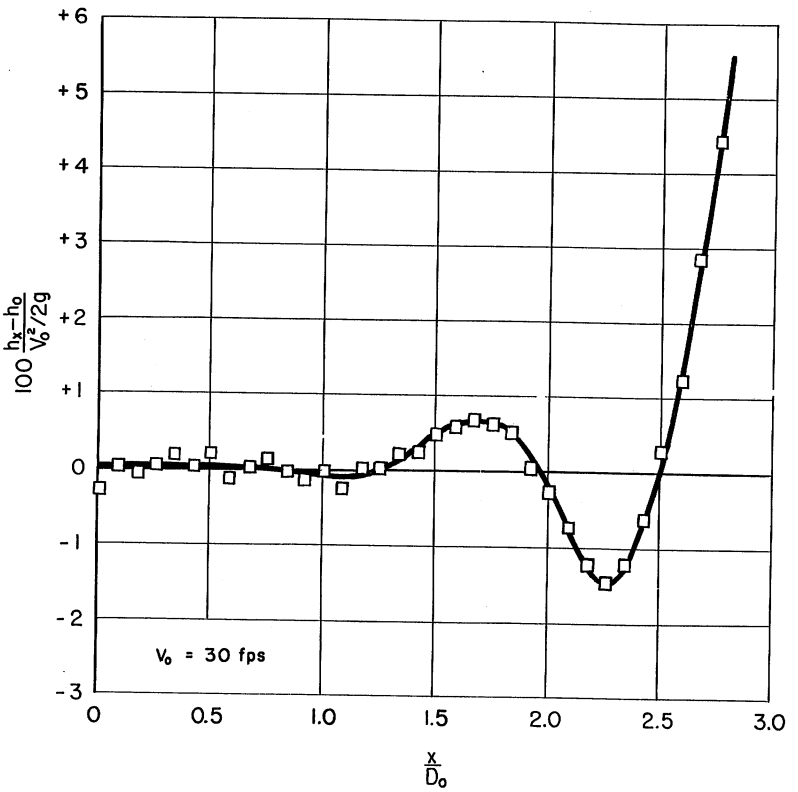

Fig. 34 - Measured Axial Pressures in Type C-VI Slotted-Wall Test Section with 1.0-In. Gap (Assembly 20)

Pick-up Cone Space 0.5 inch

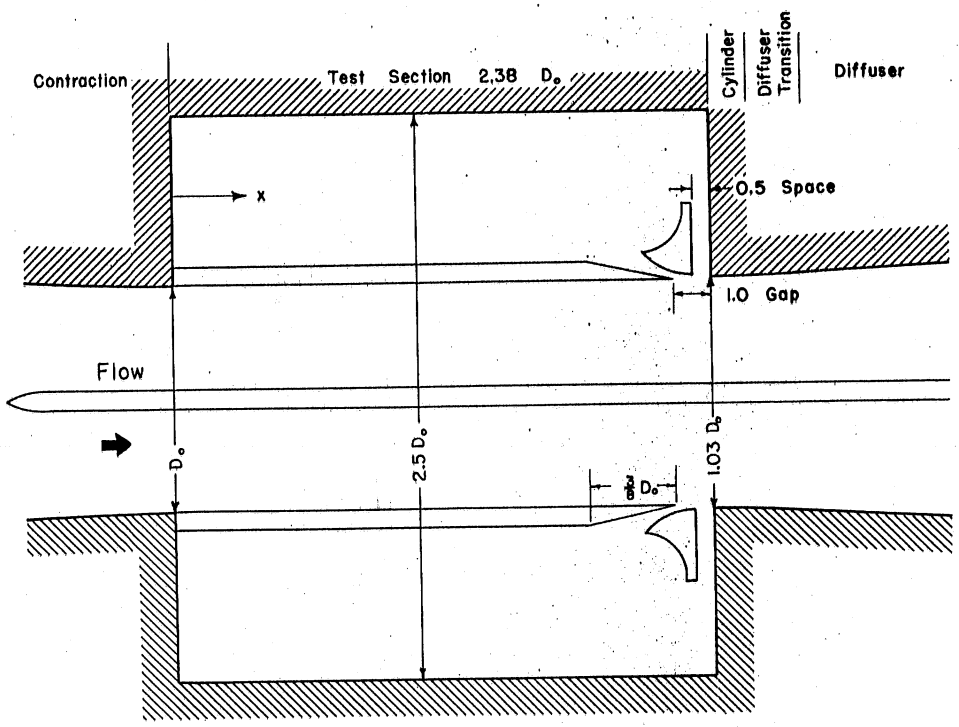

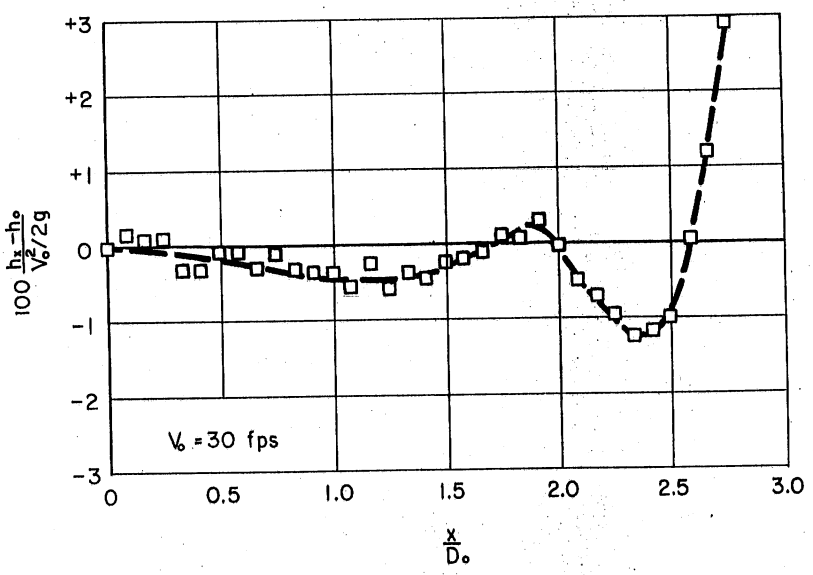

Fig. 35 - Measured Axial Pressures in Type E-VI Slotted-Wall Test Section with 1.0-In. Gap (Assembly 22)

Pick-up Cone Space 0.5 inch

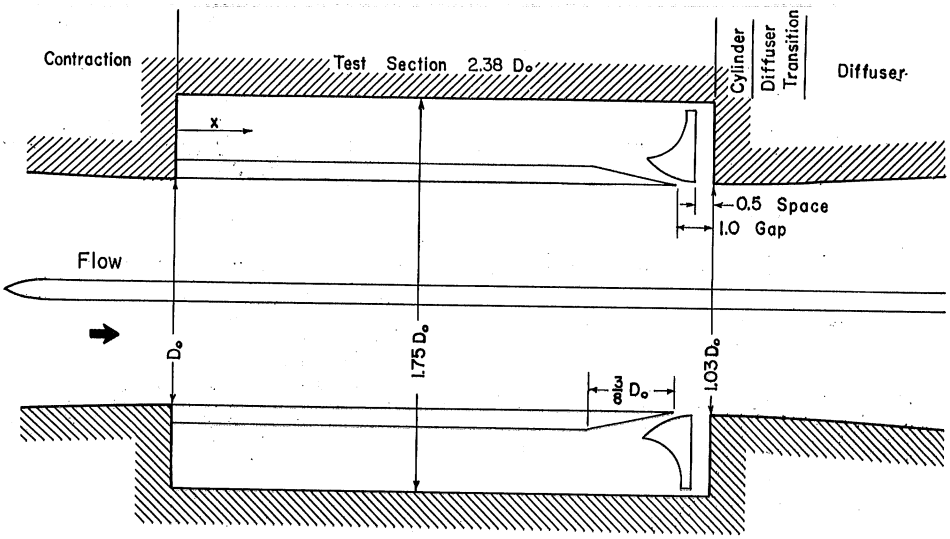

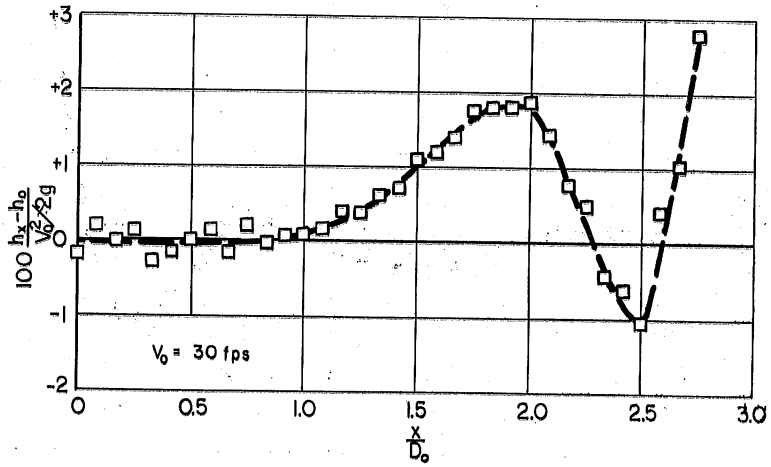

Fig. 36 - Measured Axial Pressures in Type E-VI Slotted-Wall Test Section with 1.0-In. Gap (Assembly 23)

Pick-up Cone Space 0.5 inch
Reservoir 1.75 D_o

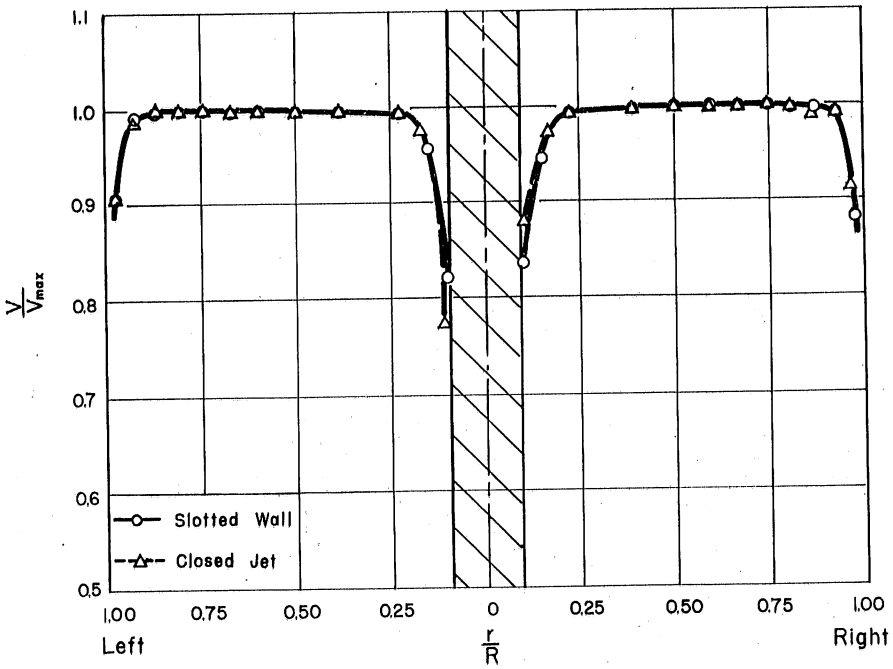

a) At $\frac{x}{D_o} = 0.5$

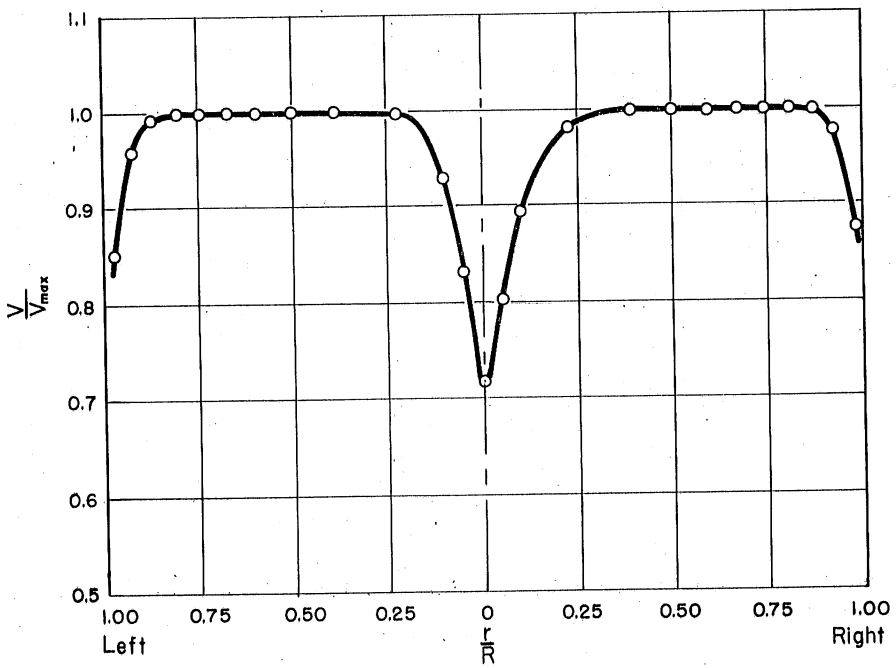

b) At $\frac{x}{D_o} = 1.5$

Fig. 37 - Measured Horizontal Velocity Profiles in Type B-1 Slotted-Wall Test Section (Assembly 4) with Contraction Dynamometer Shaft Housing

$V_o = 45.4$ fps

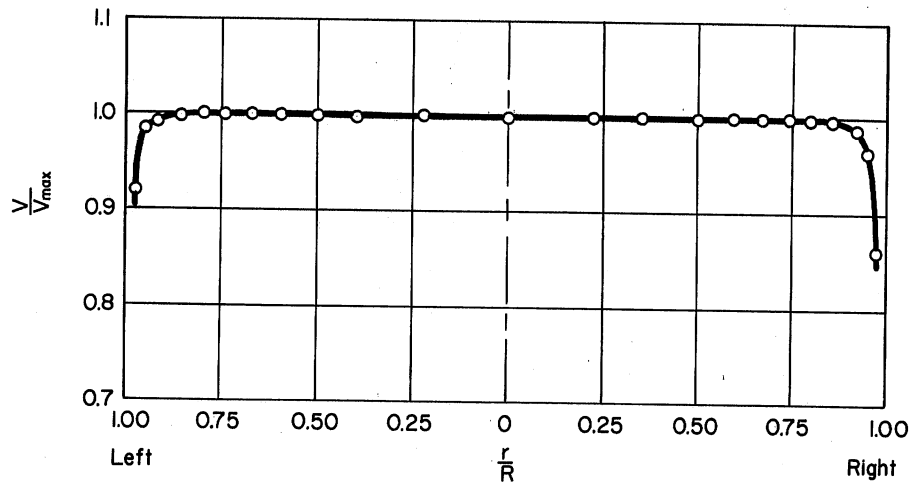

a) At $\frac{x}{D_o}$ = 0.5

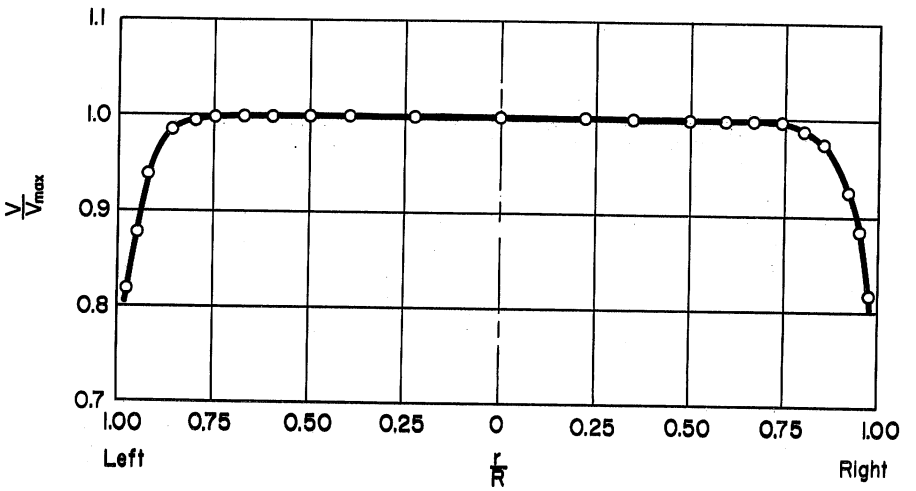

b) At $\frac{x}{D_o}$ = 1.5

Fig. 38 - Measured Horizontal Velocity Profiles in Type D Slotted-Wall Test Section (Assembly 21)

V_o = 45.3 fps

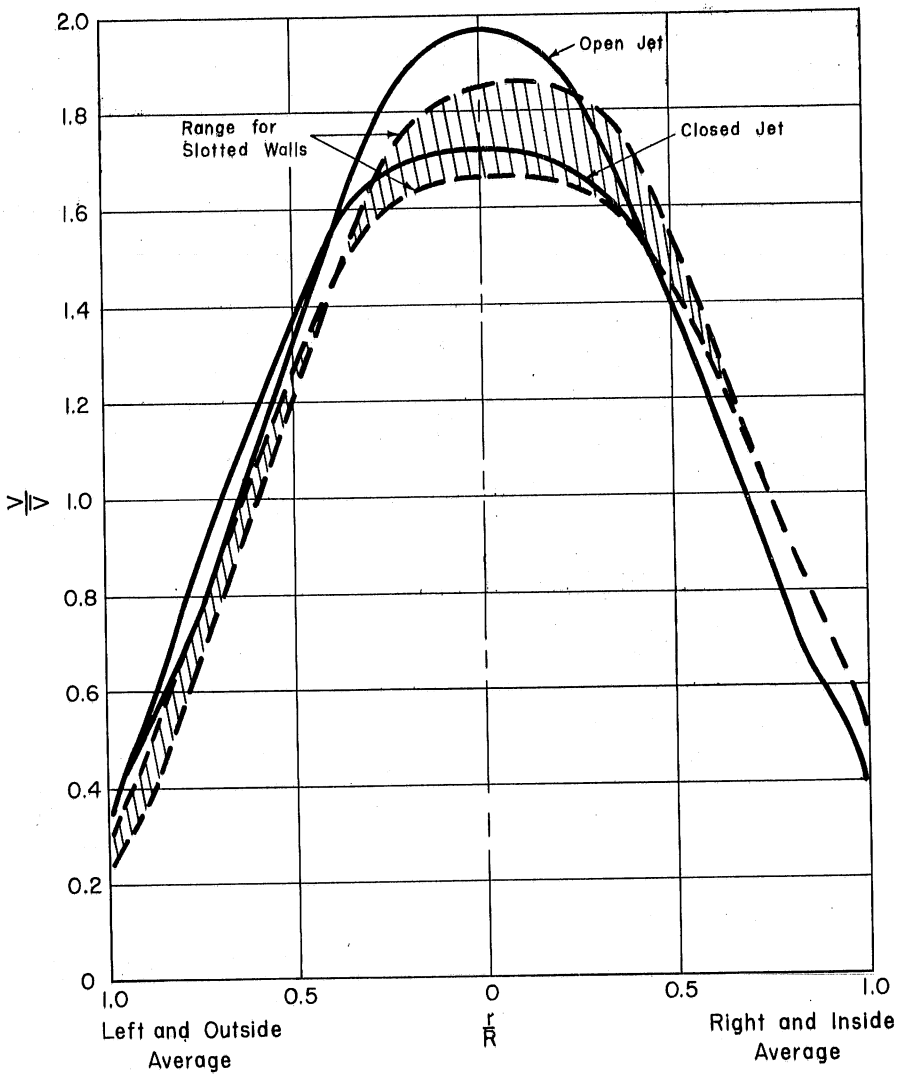

Fig. 39 - Measured Velocity Profiles at Downstream End of Diffuser for Various Test Sections

V_o = 45 fps

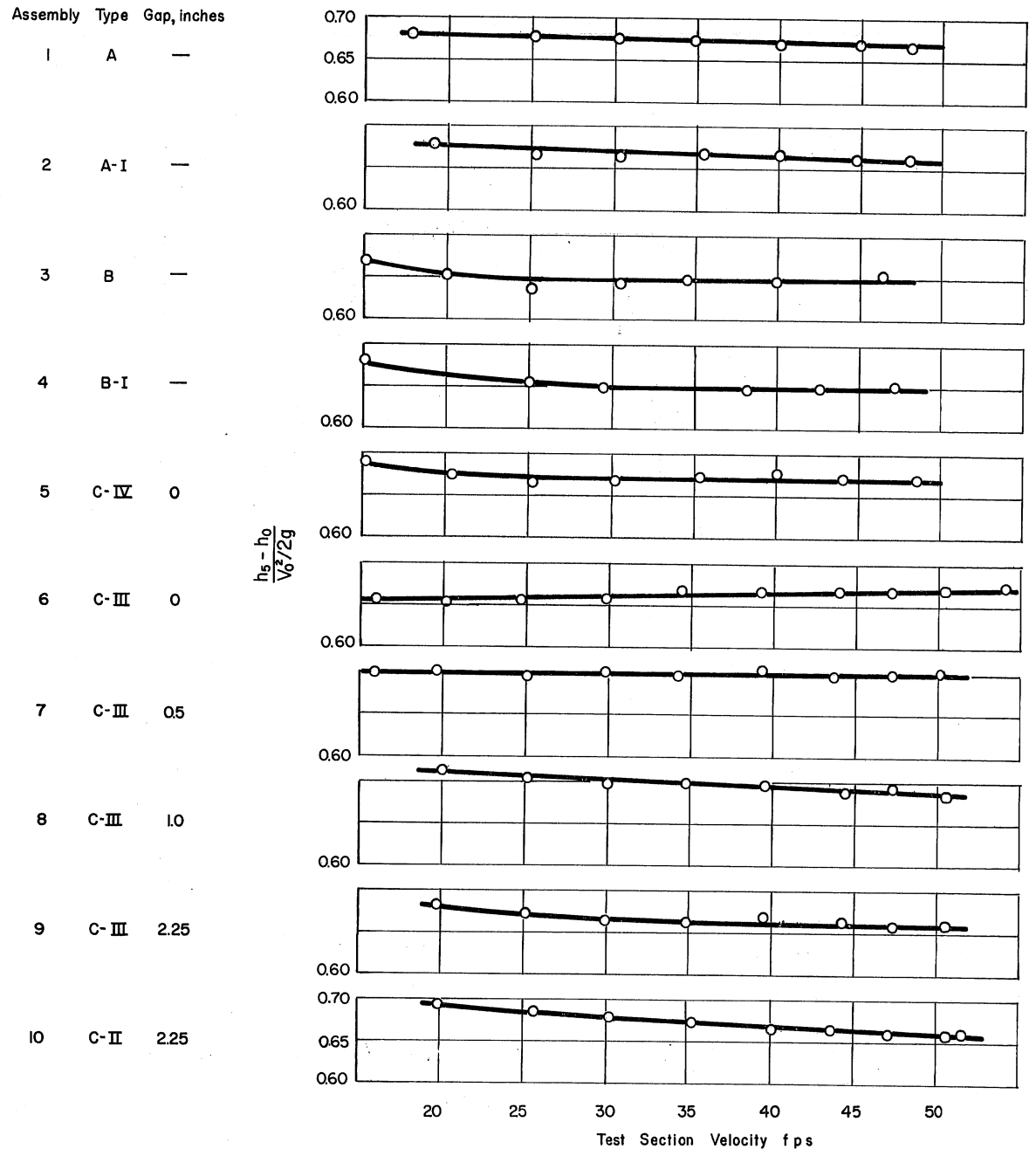

Fig. 40 – Measured Pressure Rise through Model Slotted-Wall Test Sections and Diffuser

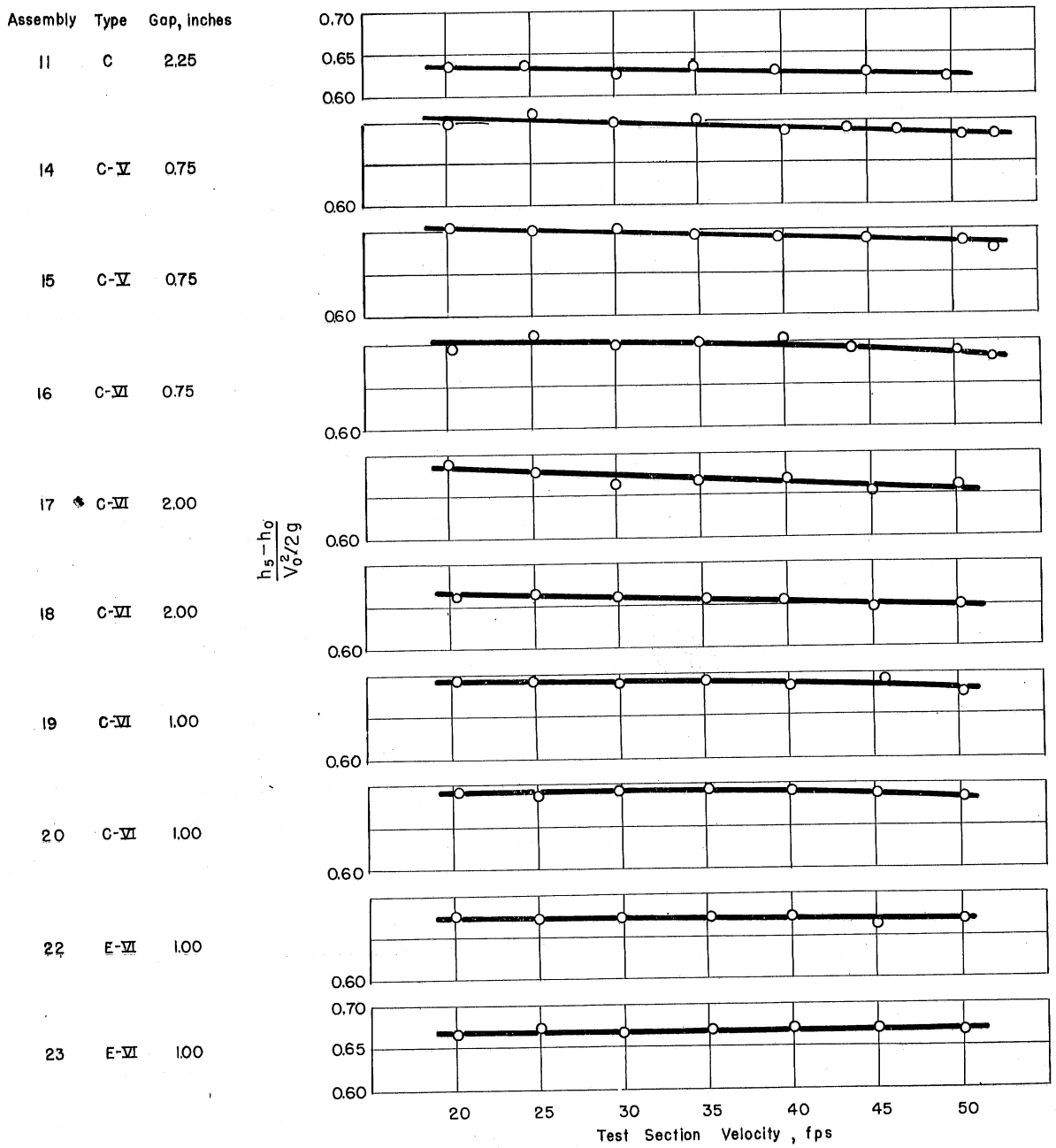

Fig. 40 (Concluded) - Measured Pressure Rise through Model Slotted-Wall Test Sections and Diffuser

Assembly	Type	Gap, inches
1	A	—
2	A-I	—
3	B	—
4	B-I	—
5	C-IV	0
6	C-III	0
7	C-III	0.5
8	C-III	1.0
9	C-III	2.25
10	C-II	2.25

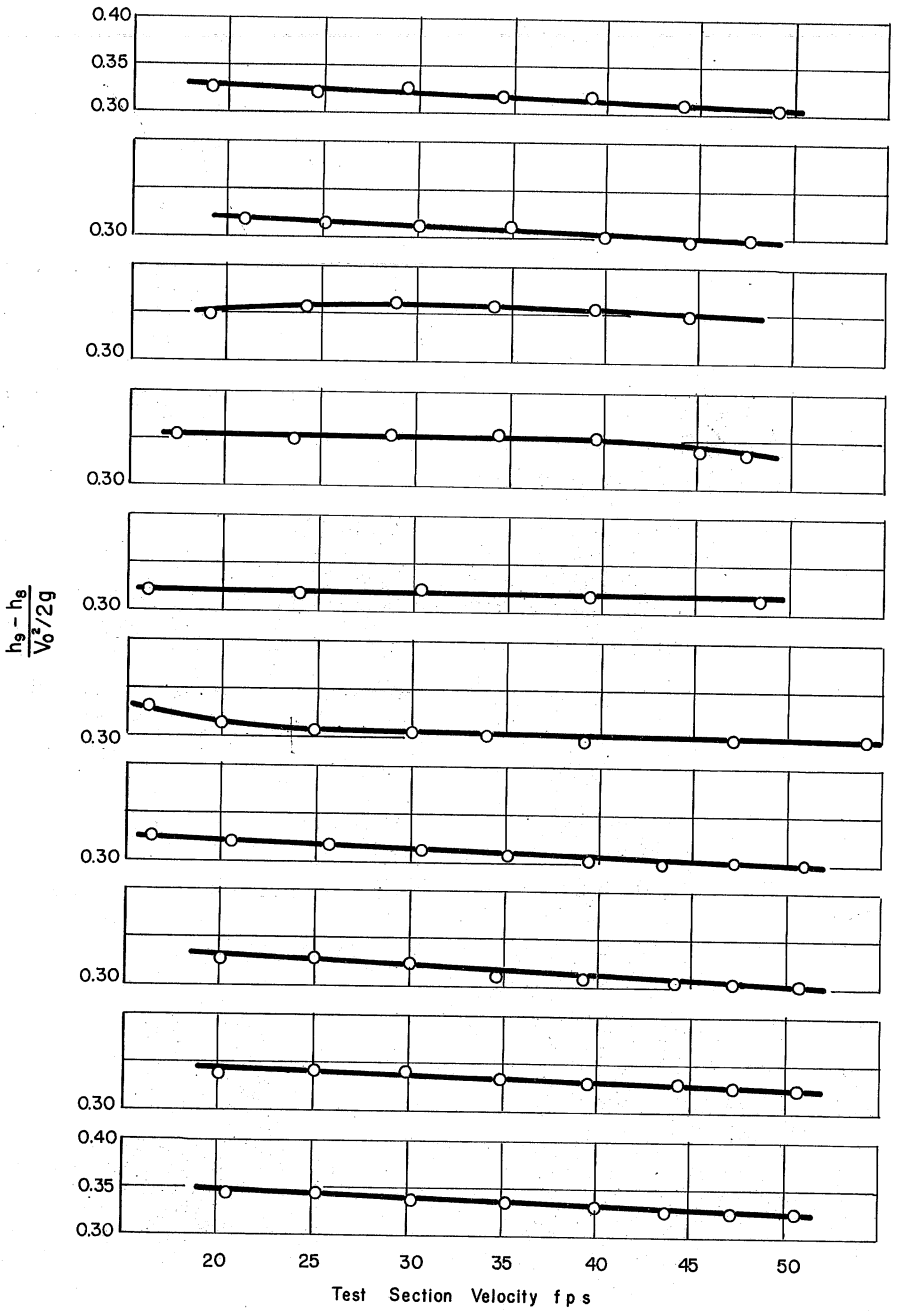

Fig. 41 – Measured Pressure Rise through Model Pump

Assembly	Type	Gap, inches
11	C	2.25
14	C-V	0.75
15	C-V	0.75
16	C-VI	0.75
17	C-VI	2.00
18	C-VI	2.00
19	C-VI	1.00
20	C-VI	1.00
22	E-VI	1.00
23	E-VI	1.00

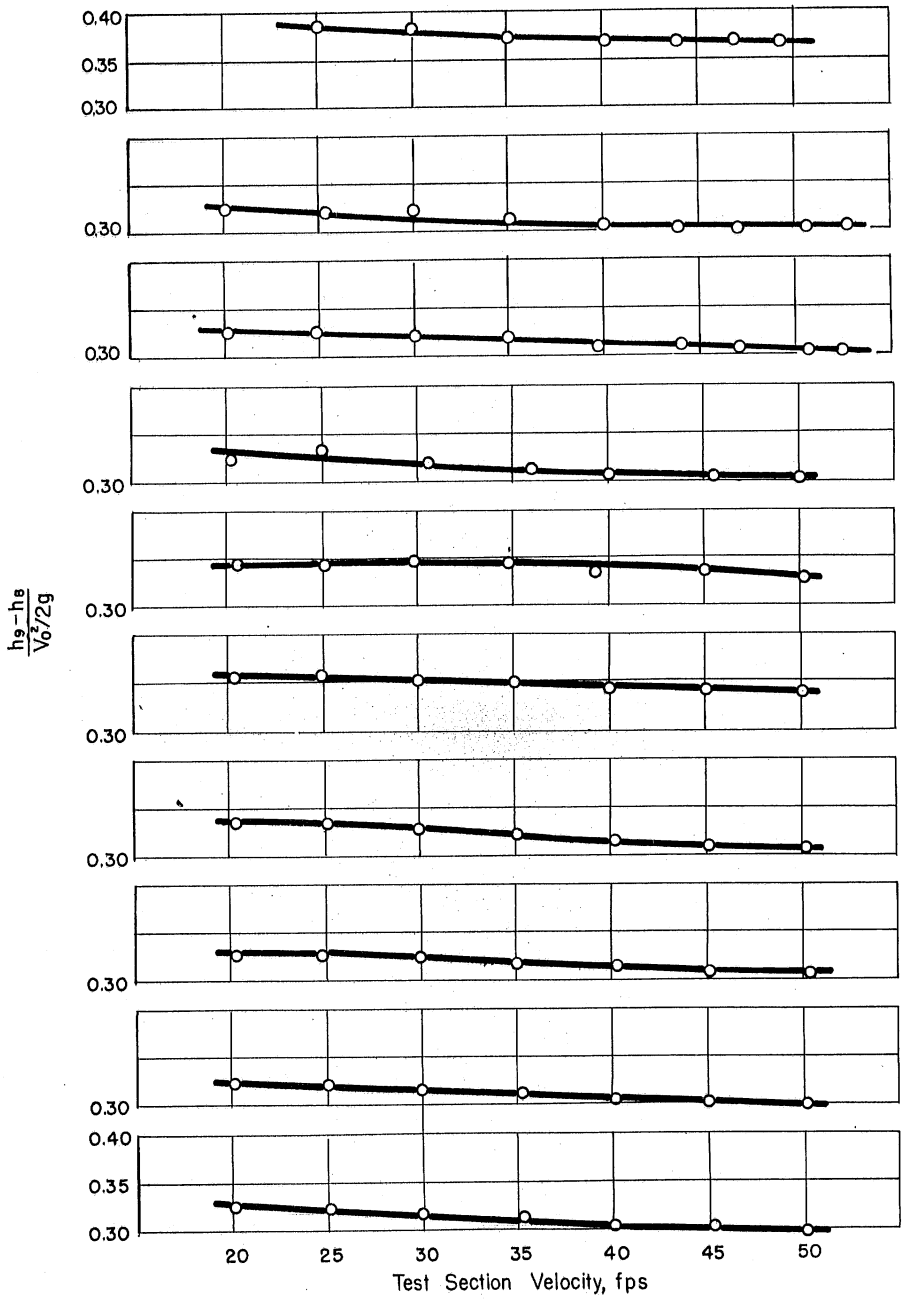

Fig. 41 (Concluded) - Measured Pressure Rise through Model Pump

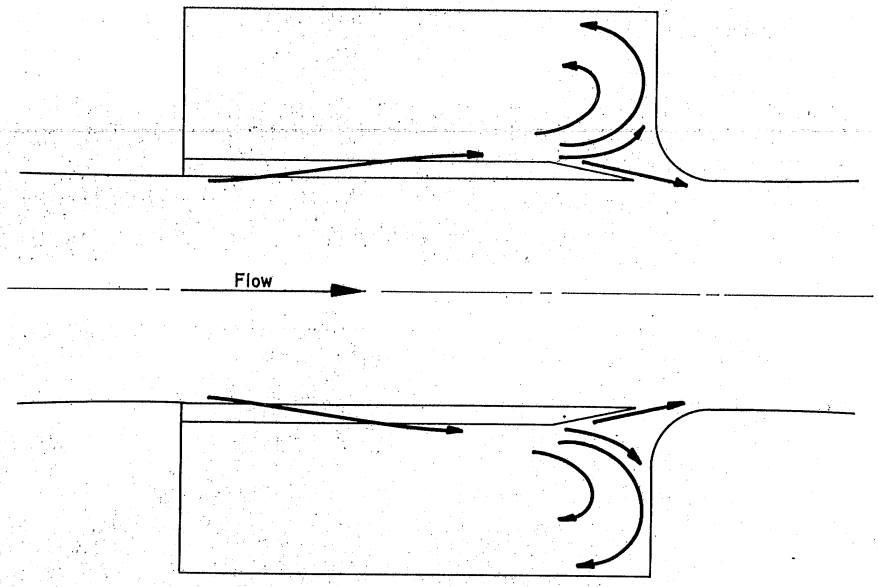

Fig. 42 - Schematic Flow Pattern in Reservoir

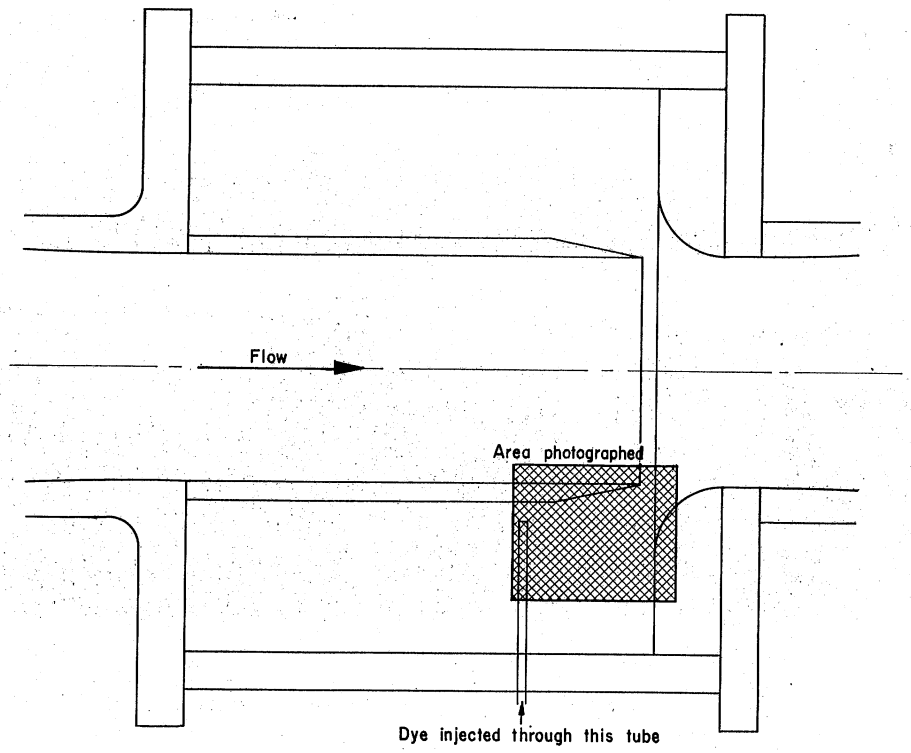

Fig. 43 - Area of Reservoir Flow Patterns Shown in Figs. 44 and 45

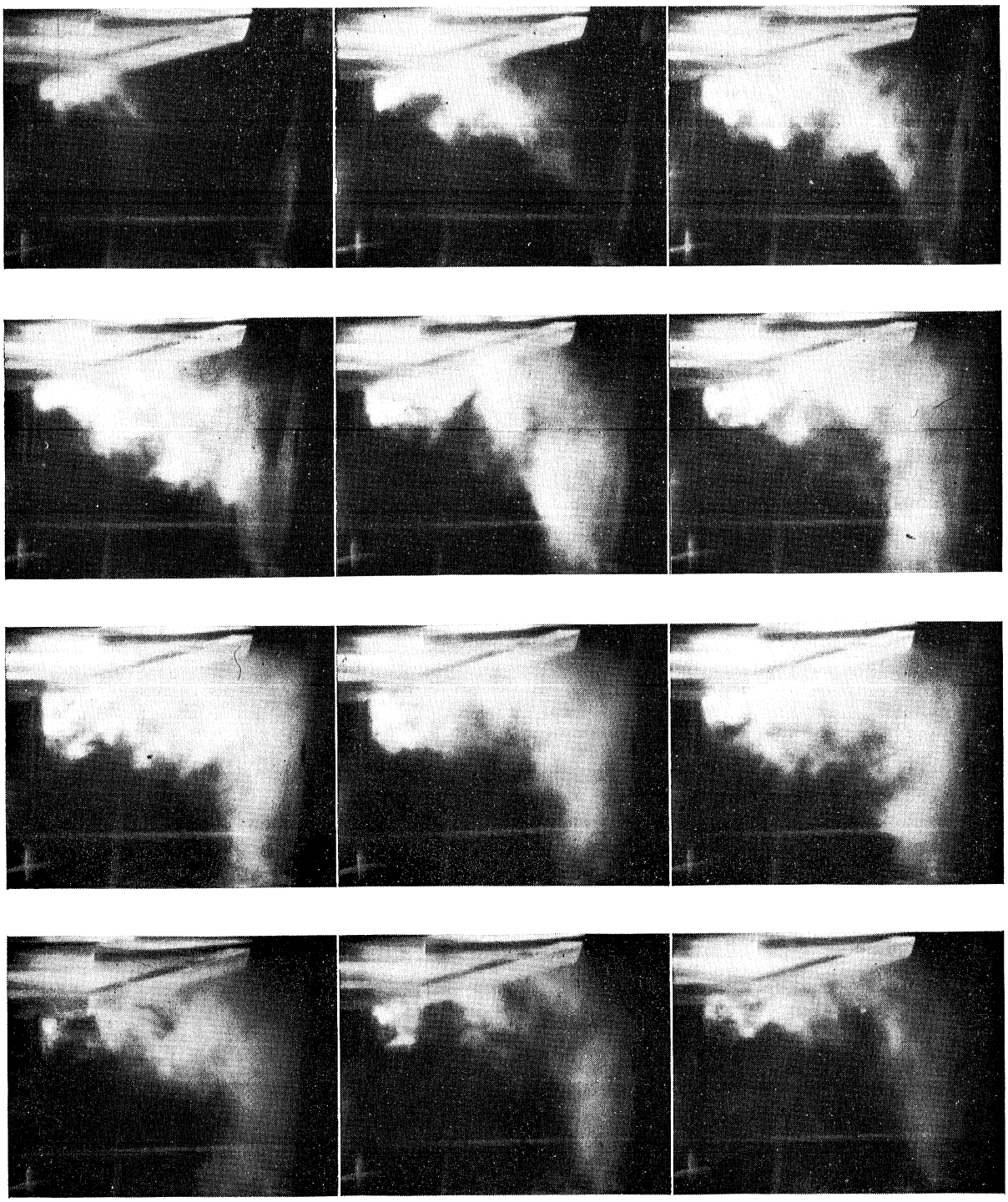

Fig. 44 - Flow Paths near Pick-up Cone, Type C-III Slotted-Wall Test Section (Assembly 9)
Dye Injected at Outer Surface of Type C Cylinder at $x/D_o = 1.5$
Photos Are at 1/80-sec Intervals

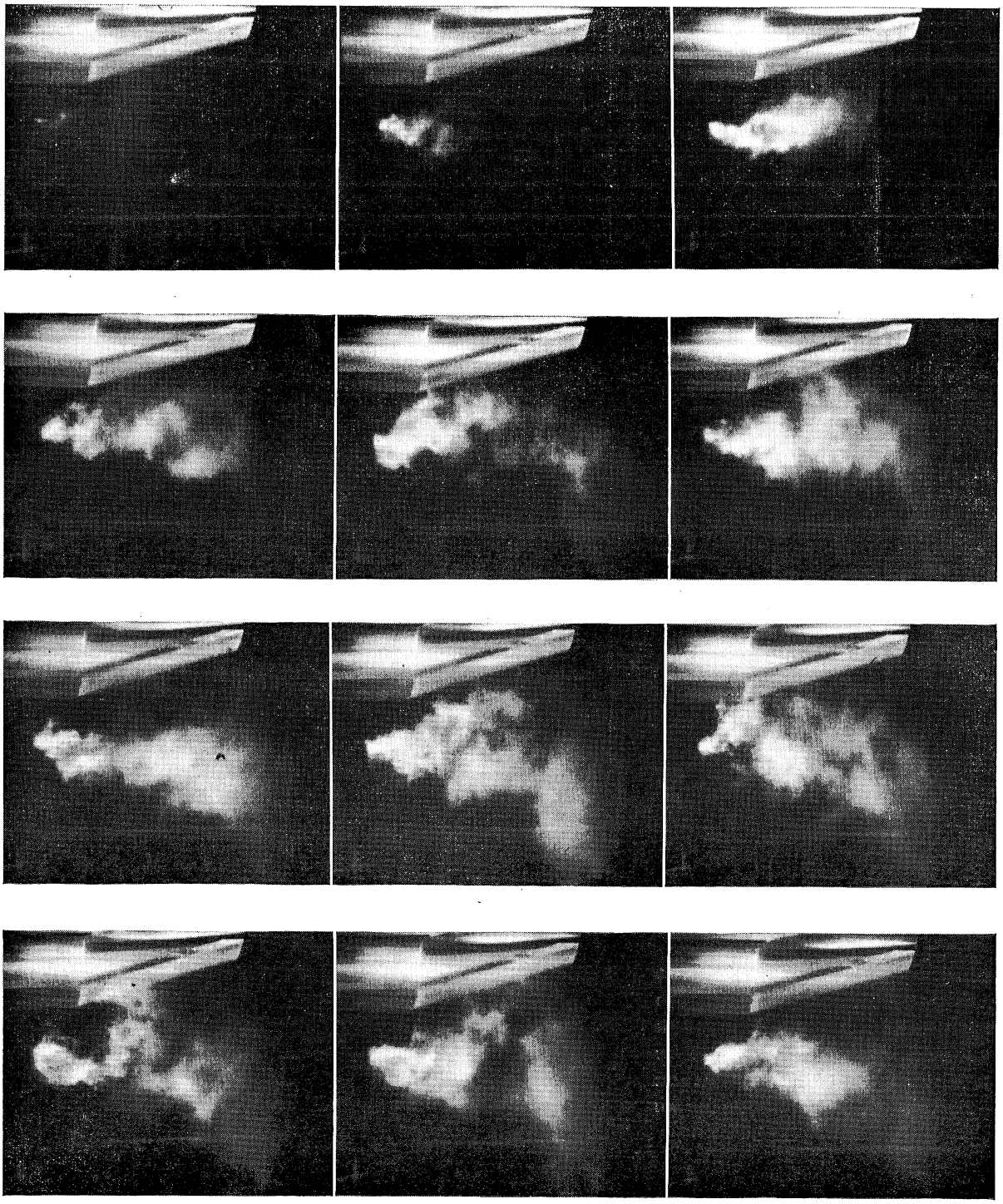

Fig. 45 - Flow Paths near Pick-up Cone, Type C-III Slotted-Wall Test Section (Assembly 9)

Dye Injected 0.5 In. from Outer Surface of Type C Cylinder at $x/D_o = 1.5$
Photos Are at 1/60-sec Intervals

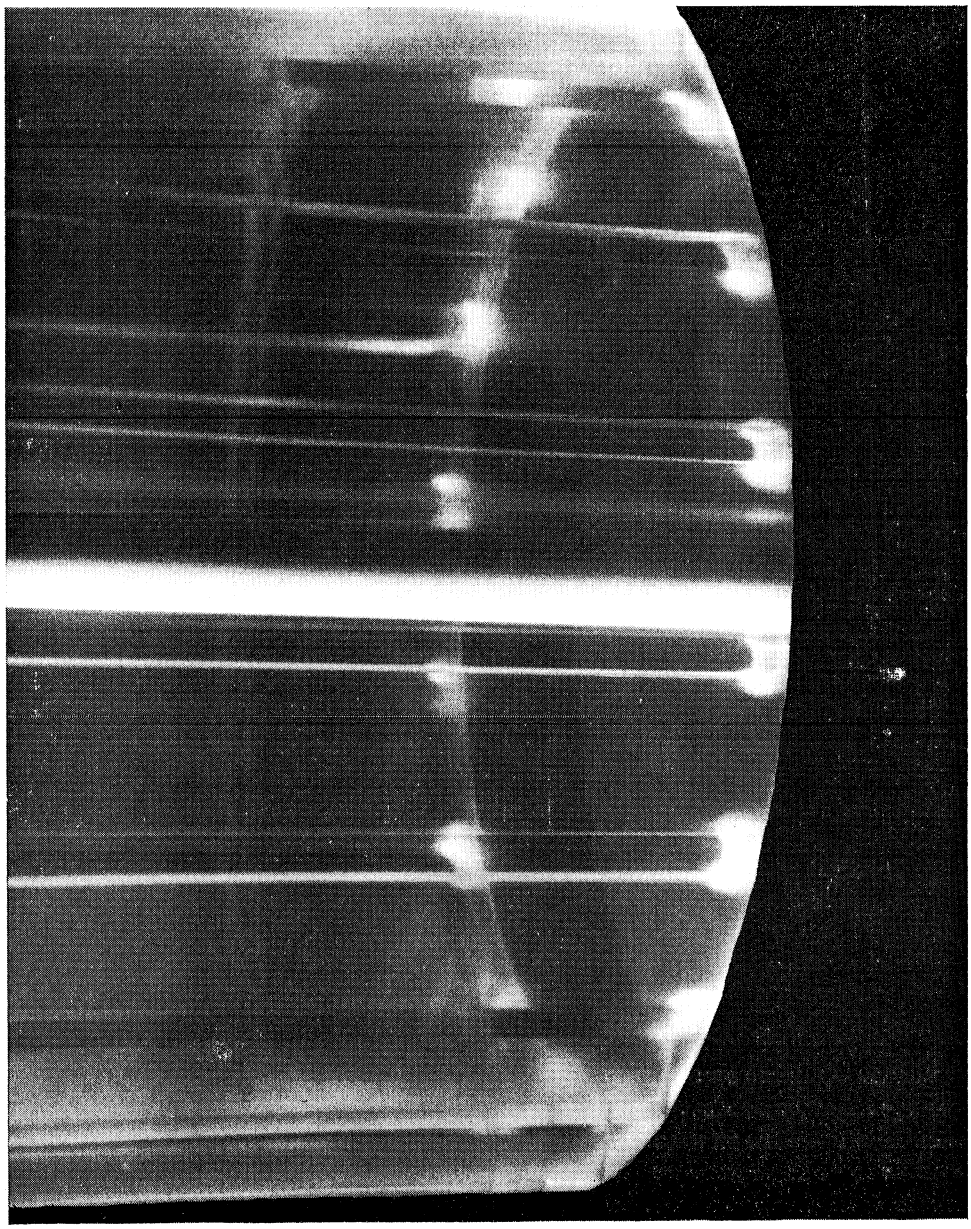

Fig. 46 - Cavitation in Type A Slotted-Wall Test Section (Assembly 1)
Flow Is from Left to Right
$\sigma_o = 1.0$

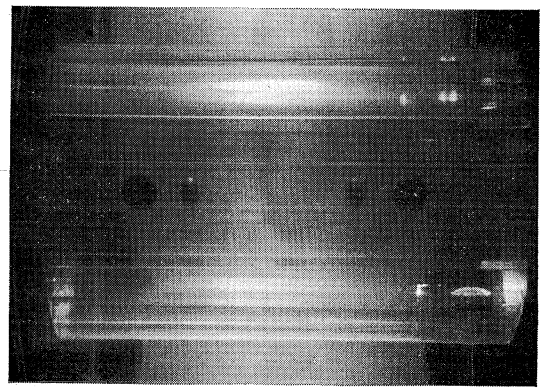

a) σ_o = 0.7

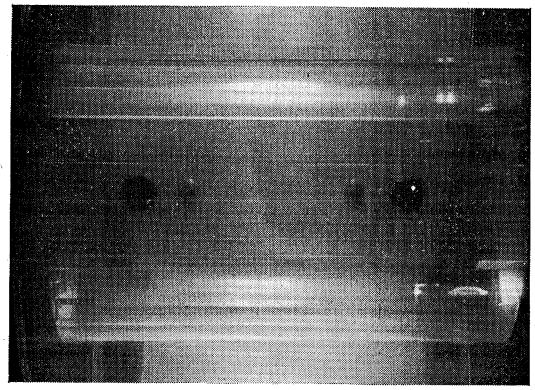

b) σ_o = 0.6

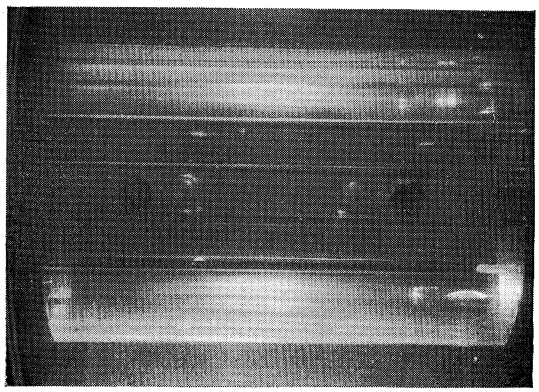

c) σ_o = 0.55

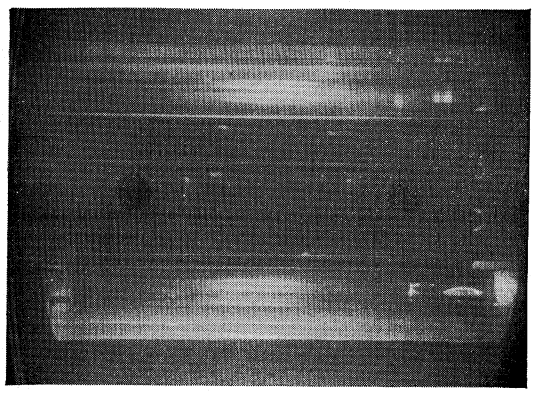

d) σ_o = 0.5

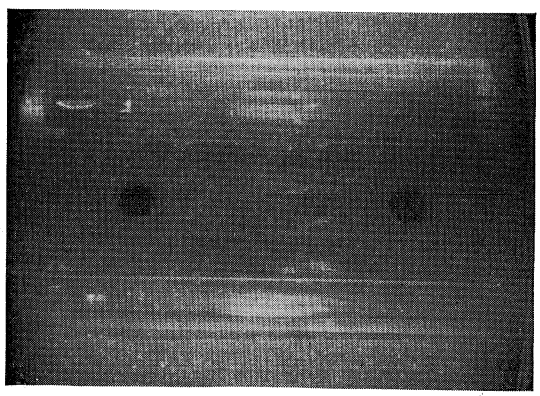

e) σ_o = 0.4

CAVITATION WAS INCIPIENT AT A CAVITATION INDEX OF σ_o = 0.7 IN SEPARATION ZONES NEAR THE RE-ENTRANT POINT AT THE DOWNSTREAM END OF THE SLOTS, SIMILAR TO THE SEMICIRCULAR CAVITATION ZONES AT THE RIGHT CENTRAL PART OF (d), AND ALONG THE SLOTS MIDWAY IN THE TEST SECTION. AT 0.6 THIS CENTRAL CAVITATION ZONE WAS EXTENDED. AT 0.5 CAVITATION AT THE BEGINNING OF THE SLOTS BECAME EVIDENT, AND THE RESERVOIR BECAME VERY CLOUDY.

Fig. 47 - Cavitation in Type D Slotted-Wall Test Section (Assembly 21)

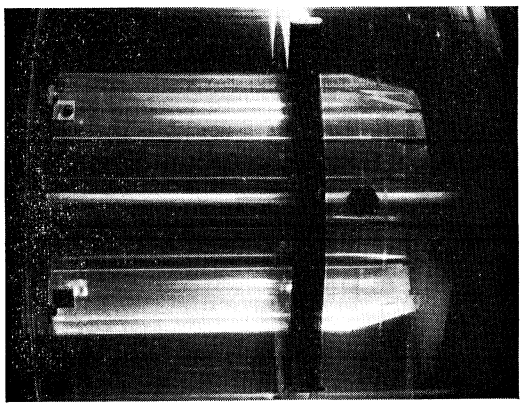

a) σ_o = 0.7

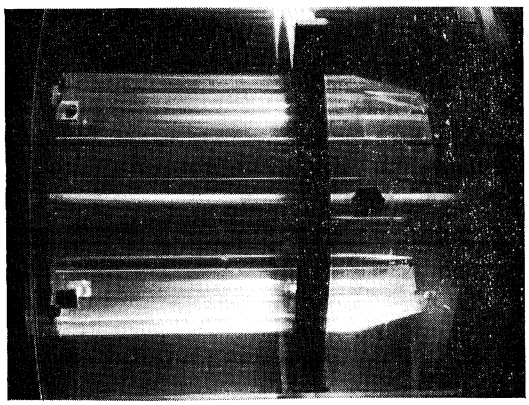

b) σ_o = 0.6

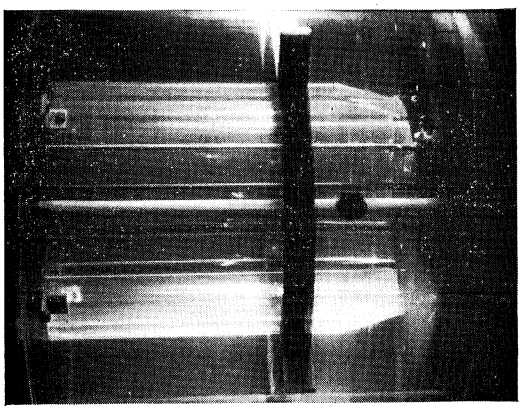

c) σ_o = 0.5

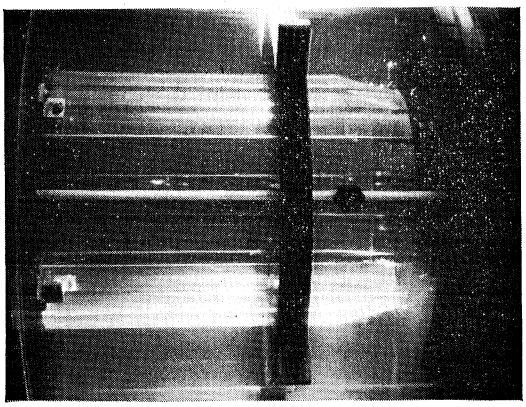

d) σ_o = 0.4

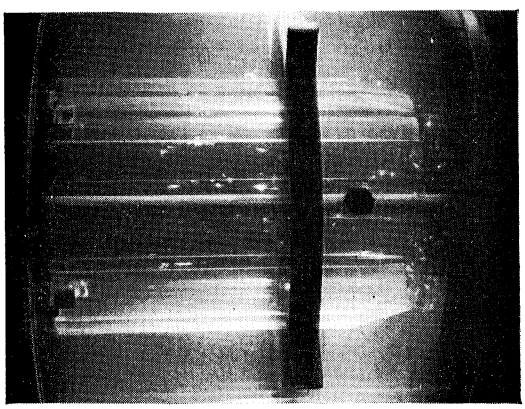

e) σ_o = 0.35

CAVITATION WAS INCIPIENT AT A CAVITATION INDEX OF σ_o = 0.70 AS VORTEX CAVITIES IN THE WAKES OF THE ENDS OF THE GUIDE BARS. CAVITATION FURTHER UPSTREAM NEARER THE CENTER OF THE TEST SECTION BEGAN AT A CAVITATION INDEX OF ABOUT 0.50. BELOW THAT THE RESERVOIR BECAME CLOUDED.

Fig. 48 - Cavitation in Type C-III Slotted-Wall Test Section (Assembly 9)

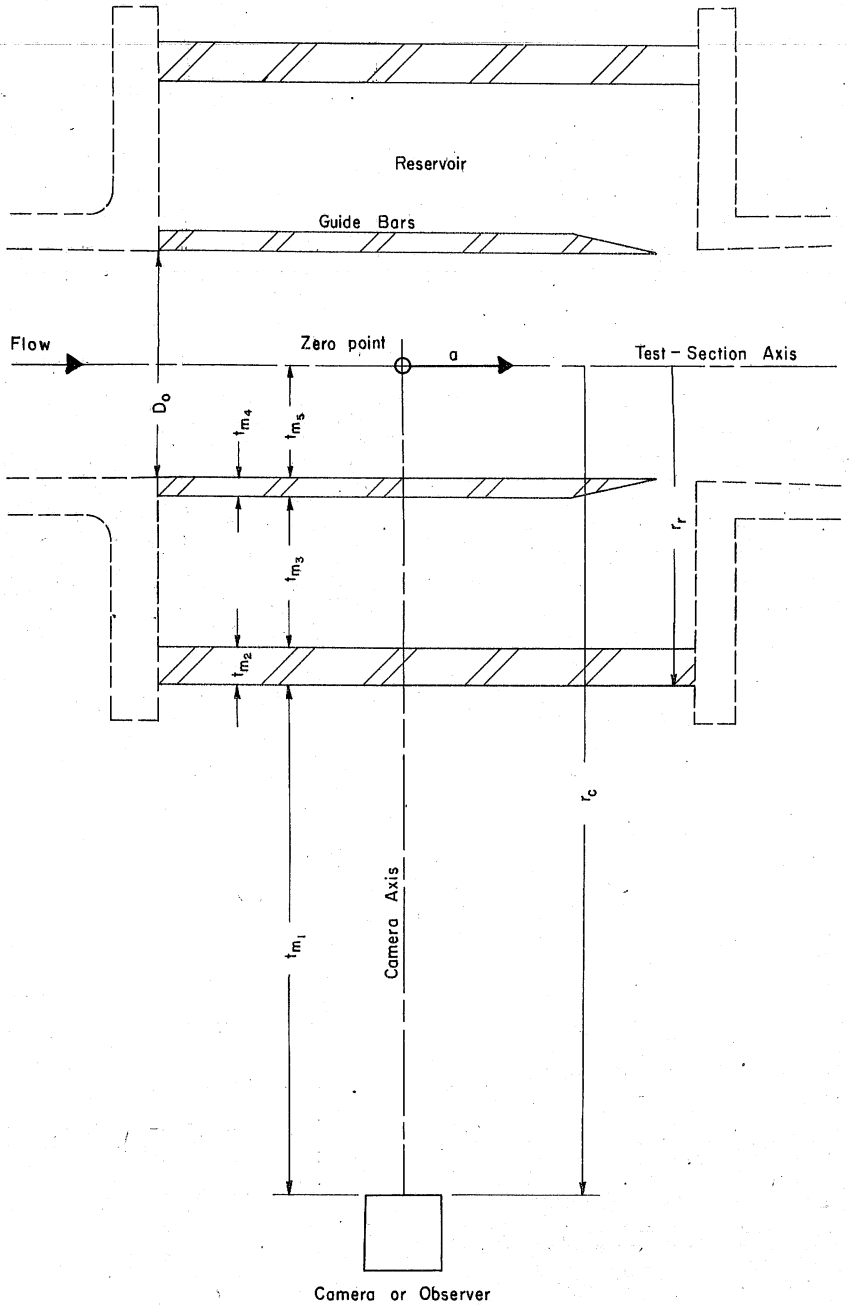

Fig. 49 – Definition Sketch for Optical Analysis of Distortion

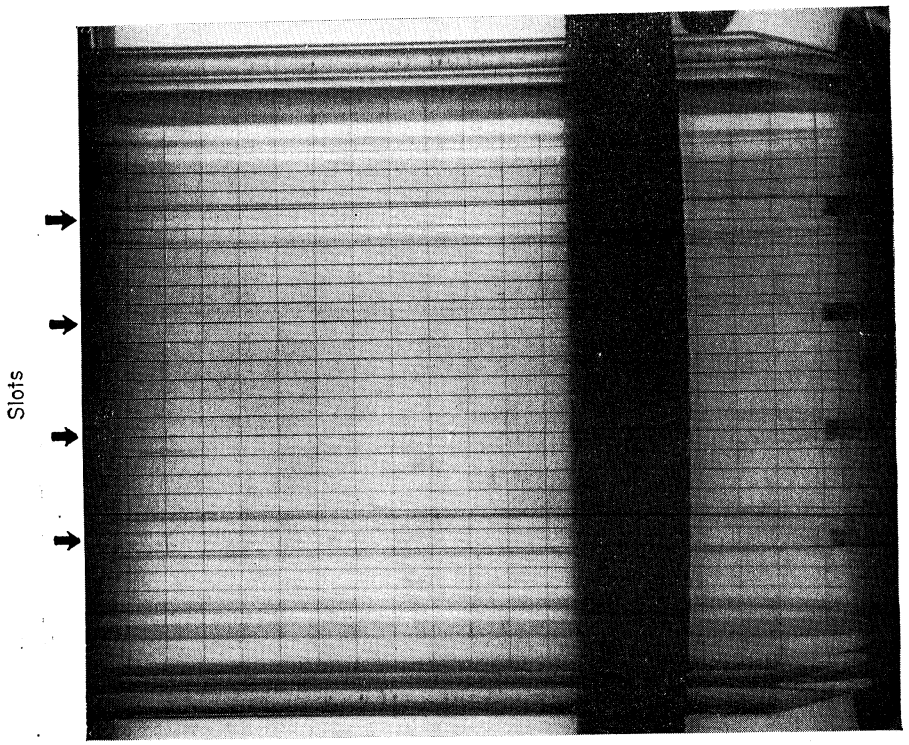

Fig. 50 - Rectangular Grid in Type C Slotted-Wall Test Section Viewed along Plane of Slots

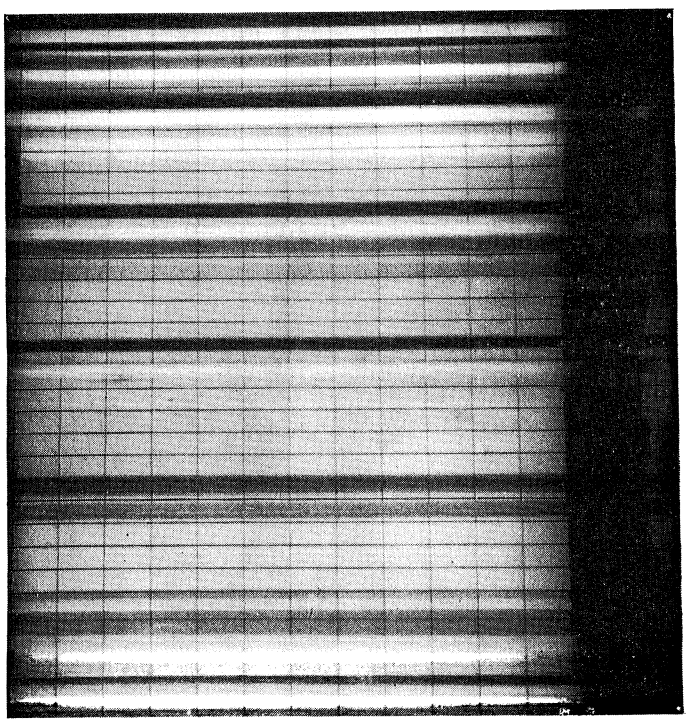

Fig. 51 - Rectangular Grid in Type C Slotted-Wall Test Section Viewed 10^{o} from Plane of Slots

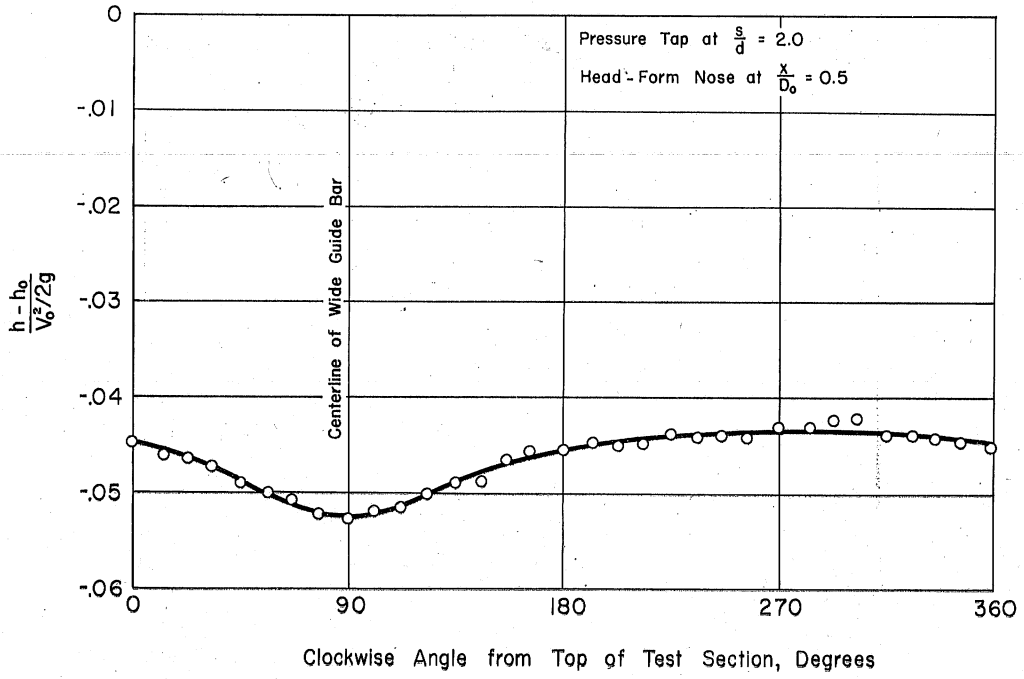

Fig. 52 – Peripheral Pressure Variation around Hemispherical Head Form in Type E-VI Slotted-Wall Test Section (Assembly 22)

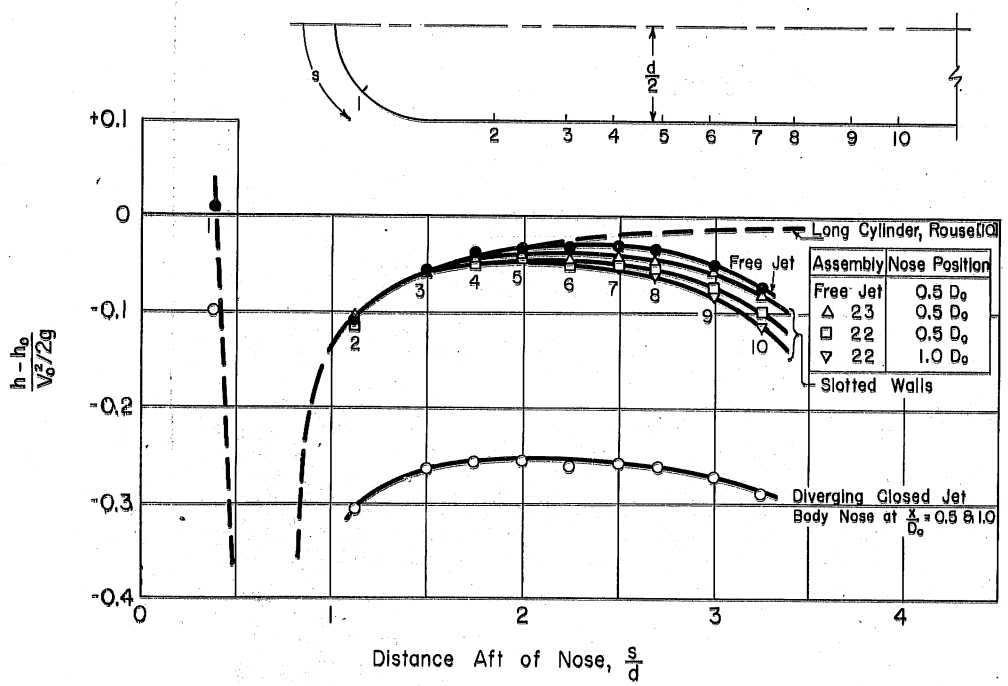

Fig. 53 – Pressure Distribution along Short Cylindrical Body with a Hemispherical Head Form Measured in Various Test Sections

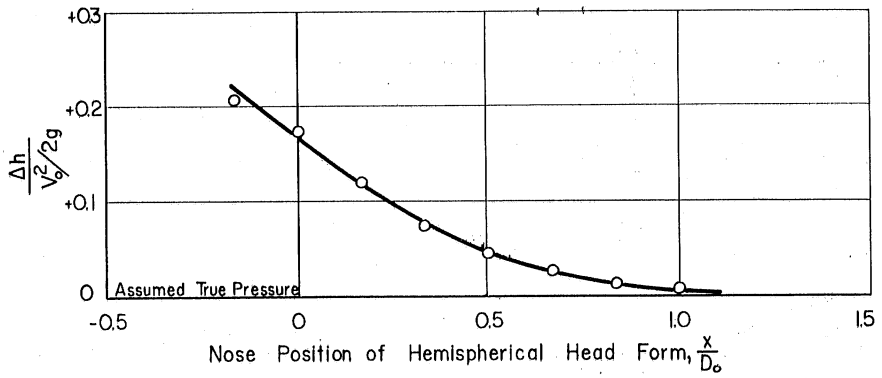

Fig. 54 - Effect of Nose Position of Hemispherical Head Form on Boundary Pressure 0.5 Diameter Upstream of Test Section into Contraction

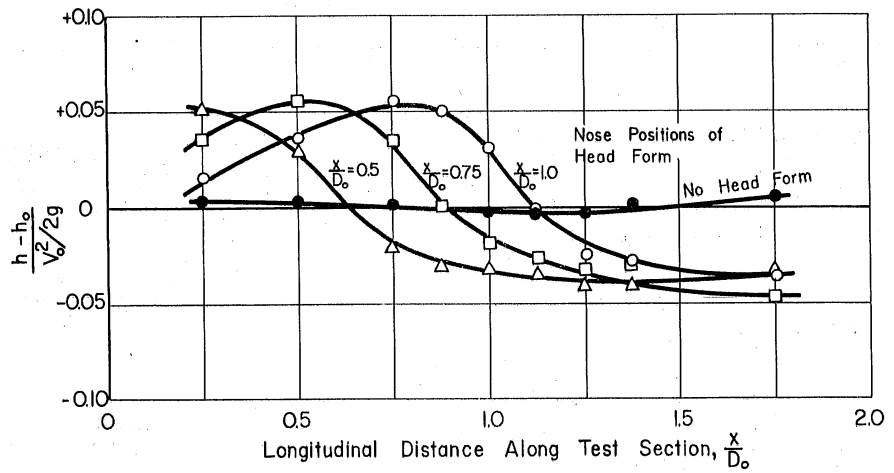

Fig. 55 - Measured Guide-Bar Pressures with 1/3 D_o Hemispherical Head Form at Various Locations along Test-Section Axis (Assembly 22)